

This is an Open Access document downloaded from ORCA, Cardiff University's institutional repository: <https://orca.cardiff.ac.uk/id/eprint/157120/>

This is the author's version of a work that was submitted to / accepted for publication.

Citation for final published version:

Stringer Martin, Mercedes, Zeng, Ziming, Zhang, Xiaoyan, Chai, Yanyan, Li, Wen, Zhang, Jikai, Ong, Huiling, Liang, Dongfang, Dong, Jing, Li, Yiming, Fu, Yongqing and Yang, Xin 2023. Methodologies, technologies and strategies for acoustic streaming based Acoustofluidics. *Applied Physics Reviews* 10 , 011315.

Publishers page: <https://doi.org/10.1063/5.0134646>

Please note:

Changes made as a result of publishing processes such as copy-editing, formatting and page numbers may not be reflected in this version. For the definitive version of this publication, please refer to the published source. You are advised to consult the publisher's version if you wish to cite this paper.

This version is being made available in accordance with publisher policies. See <http://orca.cf.ac.uk/policies.html> for usage policies. Copyright and moral rights for publications made available in ORCA are retained by the copyright holders.



Methodologies, technologies and strategies for acoustic streaming based Acoustofluidics

Mercedes Stringer¹, Ziming Zeng¹, Xiaoyan Zhang¹, Yanyan Chai¹, Wen Li¹, Jikai Zhang², Huiling Ong², Dongfang Liang³, Jing Dong³, Yiming Li³, Yongqing Fu², * Xin Yang^{1,*}

¹ Department of Electrical and Electronic Engineering, School of Engineering, Cardiff University, Cardiff CF24 3AA, UK

² Faculty of Engineering and Environment, Northumbria University, Newcastle Upon Tyne, Newcastle NE1 8ST, UK

³ Department of Engineering, University of Cambridge, Cambridge, CB2 1PZ, UK

Corresponding authors: Dr. Xin Yang (YangX26@cardiff.ac.uk), Prof. Yongqing (Richard) Fu (Richard.fu@northumbria.ac.uk)

Contents

Abstract.....	2
1. Introduction.....	2
2. Fundamental of surface acoustic waves.....	5
3. Mechanisms of acoustic streaming and Acoustofluidics	7
3.1. Governing equations and related forces.....	8
3.1.1. Streaming Analysis with different flow velocity regimes.....	9
3.1.2. Forces in acoustic streaming	10
3.2. Fundamentals and mechanisms of acoustic streaming.....	11
4. Acoustofluidic transduction technologies for acoustic streaming and acoustofluidics.....	15
4.1. Design and manufacture of electrodes	15
4.1.1. Design criteria.....	15
4.1.2. Transducer materials	17
4.1.3. Fabrication techniques	18
4.2. Advances of Interdigital Transducers	20
4.2.1. Conventional IDT structures	20
4.2.2. Unconventional IDT structures	22
4.2.3. IDTs embedded into multi-layer structures.....	25
5. Acoustofluidic streaming applications using transducer designs.....	26
5.1. TSAWs based streaming and acoustofluidics	27
5.1.1. Mixing, concentration, and splitting of sessile droplets in digital acoustofluidics	28
5.1.2. Pumping, jetting, nebulization/atomization, and droplet generation in digital acoustofluidics	32
5.1.3. Mixing, concentration, and rotation of liquid in chamber/channel for continuous acoustofluidics	38
5.2. SSAWs based streaming and acoustofluidics	43
5.2.1. SSAW induced droplet streaming in digital acoustofluidics	44
5.2.2. SSAW induced streaming in microchannel for acoustic tweezers in continuous acoustofluidics	45

41 6. Summary and future prospects.....48
42 7. References..... 51

43

44 **Abstract**

45 Acoustofluidics offers contact-free manipulation of particles and fluids, enabling their uses in
46 various life sciences, such as for biological and medical applications. Recently there have been
47 extensive studies on acoustic streaming based acoustofluidics, which are formed inside a liquid
48 agitated by leaky surface acoustic waves (SAWs) through applying radio-frequency signals to
49 interdigital transducers (IDTs) on a piezoelectric substrate. This paper aims to describe acoustic
50 streaming based acoustofluidics and provide readers with an unbiased perspective to determine
51 which IDT structural designs and techniques are most suitable for their research. This review
52 firstly qualitatively and quantitatively introduces underlying physics of acoustic streaming.
53 Then it comprehensively discusses the fundamental designs of IDT technology for generating
54 various types of acoustic streaming phenomena. Acoustic streaming related methodologies and
55 the corresponding biomedical applications are highlighted and discussed, according to either
56 standing surface acoustic waves or travelling surface acoustic waves generated, and also sessile
57 droplets or continuous fluids used. Travelling SAW based acoustofluidics generate various
58 physical phenomena including mixing, concentration, rotation, pumping, jetting,
59 nebulization/atomization, and droplet generation, as well as mixing and concentration of liquid
60 in a channel/chamber. Standing SAWs induces streaming for digital and continuous
61 acoustofluidics, which can be used for mixing, sorting, and trapping in a channel/chamber. Key
62 challenges, future developments and directions for acoustic streaming based acoustofluidics
63 are finally discussed.

64

65 Keywords: Acoustic Streaming, Surface Acoustic Wave, Interdigital Transducer,
66 Acoustofluidics

67 **1. Introduction**

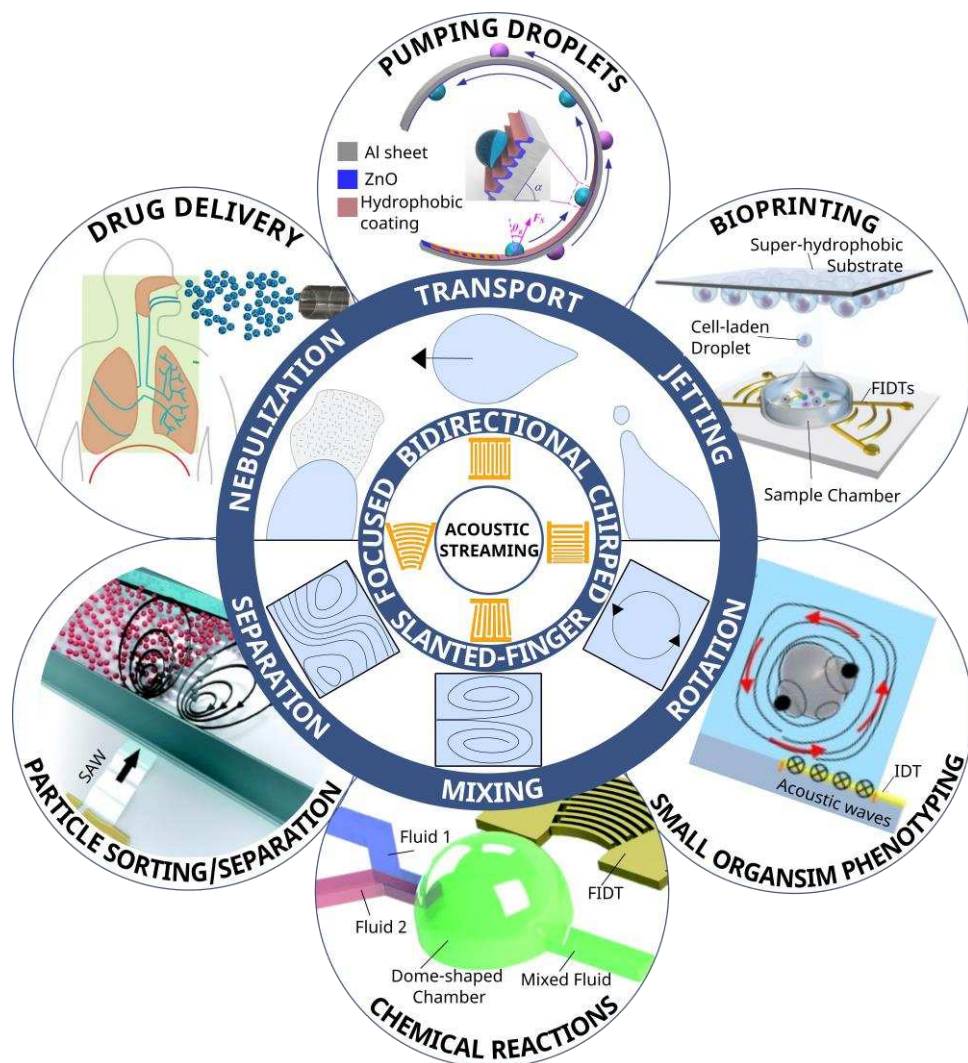
68 Interactions between acoustics and fluids have been well known for thousands of years. For
69 example, the ancient Chinese spouting bowl (or called resonance bowl) was employed
70 spiritually for meditation to promote healing ¹. It used the vibrations generated from rubbing
71 the handles to form standing waves which cause water droplets to be ejected above the water
72 surface and form various fascinating patterns ². However, it was until year 1866 that research

73 on acoustic streaming was emerged when Kundt's tube experiment was designed to measure
74 the speed of sound in a fluid ³. By rubbing a metal rod resonator at the end of a tube in which
75 the fluid contained small particles, these particles were periodically patterned and clustered
76 over time at the nodes of the vibration due to the formation of standing waves ³. Acoustic
77 streaming was firstly reported by Dvorak in 1876 using the Kundt's tube ⁴. He observed that
78 the air was flowing from the node towards the antinodes along the axis of the tube, while the
79 flow of the air near the wall was directed in the opposite direction ⁵. This observation led to the
80 first theoretical model derived by Rayleigh in 1884 ⁶, and was further studied almost a century
81 later by various scientists including Schlichting (1932) ⁷ (who solved the incompressible
82 streaming mechanisms near the wall), Westervelt (1953) ⁸ and Nyborg (1953) ⁹ (both of whom
83 extended the methodology for a compressible fluid at its first-order perturbation).

84 Acoustic streaming frequently occurs in fluidics, and it generates regions of recirculation,
85 pressure gradients, both of which can be used for particle manipulation such as patterning ¹⁰,
86 concentration ^{11,12}, and separation ^{13,14}. Particle manipulation is a widely studied topic which
87 is related to the precise control of the dynamics of particles, for example, in biological samples.
88 It can be realized by various passive methods, such as deterministic lateral displacement,
89 pinched flow fractionation, crossflow filtration, hydrodynamic filtration, and inertial
90 microfluidics ¹⁵. Although these methods are often advantageous owing to their simplicity and
91 low costs, they do not always offer precise and on-demand control in comparison to many
92 active methods involving external forces or fields, such as magnetic ¹⁶, electrical (e.g., based
93 on electrokinetic ¹⁷ effects such as free-flow electrophoresis ¹⁸ and dielectrophoresis ¹⁹), optical
94 ^{20 21}, and ultrasonics or acoustic wave forces. Among these active methods, acoustic wave
95 based ones have the advantage of manipulating various bioparticles, from nanometer-sized
96 extracellular vesicles to micrometer-sized circulating tumor cells (CTCs), with considerable
97 throughputs and high compatibility ²²⁻²⁶. These devices are not only non-invasive, label-free,
98 and contactless, but also convenient to be integrated with other systems for multifunctionality
99 ^{25,27,28}.

100 Acoustic streaming can also generate acoustic pressure or force to perform operations such as
101 deformation, transportation and manipulation of bulk fluid, namely jetting ^{29,30}, nebulization or
102 atomization ³¹⁻³⁴, microscale streaming ³⁵, object rotation ^{36,37}. All of these have established a
103 myriad of emerging medical applications. Figure 1 schematically illustrates examples of
104 generation of acoustic streaming by using IDT techniques, and its methodologies and
105 applications. A handful of popular IDT designs (bidirectional IDT, chirped IDT, slanted-finger

106 IDT, and focused IDT) are shown in the center. Figure 1 also include examples of acoustic
 107 streaming based acoustofluidic applications (drug delivery³⁸, bioprinting³⁹, pumping droplets
 108 ⁴⁰, small organism phenotyping³⁶, chemical reactions⁴¹, particle sorting/separation¹¹) and their
 109 respective methodology (nebulization, jetting, transport, rotation, mixing, separation,
 110 trapping). Overall, Figure 1 displays a glimpse of the possibilities that acoustic streaming based
 111 acoustofluidics could offer. Although this phenomenon is well known and widely studied for
 112 decades, it has only recently been attracted for microfluidic applications as it overcomes a lot
 113 of challenges, which are caused by low Reynolds numbers of micro- or nanoscale liquids, either
 114 in sessile droplet format or a continuous fluid within microchannels or microchambers⁴²⁻⁴⁵.



115
 116 Figure 1. The generation of acoustic streaming by using IDT techniques, and its methodologies
 117 and applications. Popular IDT designs (Bidirectional IDT, Chirped IDT, Slanted-Finger IDT,
 118 and Focused IDT) are shown in the center. Example methodologies generated by IDTs
 119 (nebulization, jetting, transport, rotation, mixing, separation) are illustrated in the middle circle,
 120 and relevant acoustic streaming applications based on the respective methodology (drug
 121 delivery³⁸, bioprinting³⁹, pumping droplets⁴⁰, small organism phenotyping³⁶, chemical
 122 reactions⁴¹, particle sorting/separation¹¹) are shown on the outer circle.

123 In-depth reviews of these ultrasonic or acoustic wave methods for particle manipulation and
124 acoustofluidic functions have previously been given by many researchers ^{2,27,46-51}. Although
125 these reviews have covered most critical information on fundamental mechanisms and
126 chemical, biomedical, biological applications of acoustofluidics, acoustic sensors and lab-on-
127 a-chip, none of them are focused on the advances in methodology and techniques based on
128 acoustic streaming for both liquid droplets and continuous flow liquids. Therefore, this paper
129 aims to focus on fundamental designs, techniques, and key applications of acoustic streaming,
130 providing qualitative and quantitative discussions of its mechanisms, and highlight its key
131 biological and medical applications (which can be revealed from Figure 1).

132 **2. Fundamental of surface acoustic waves**

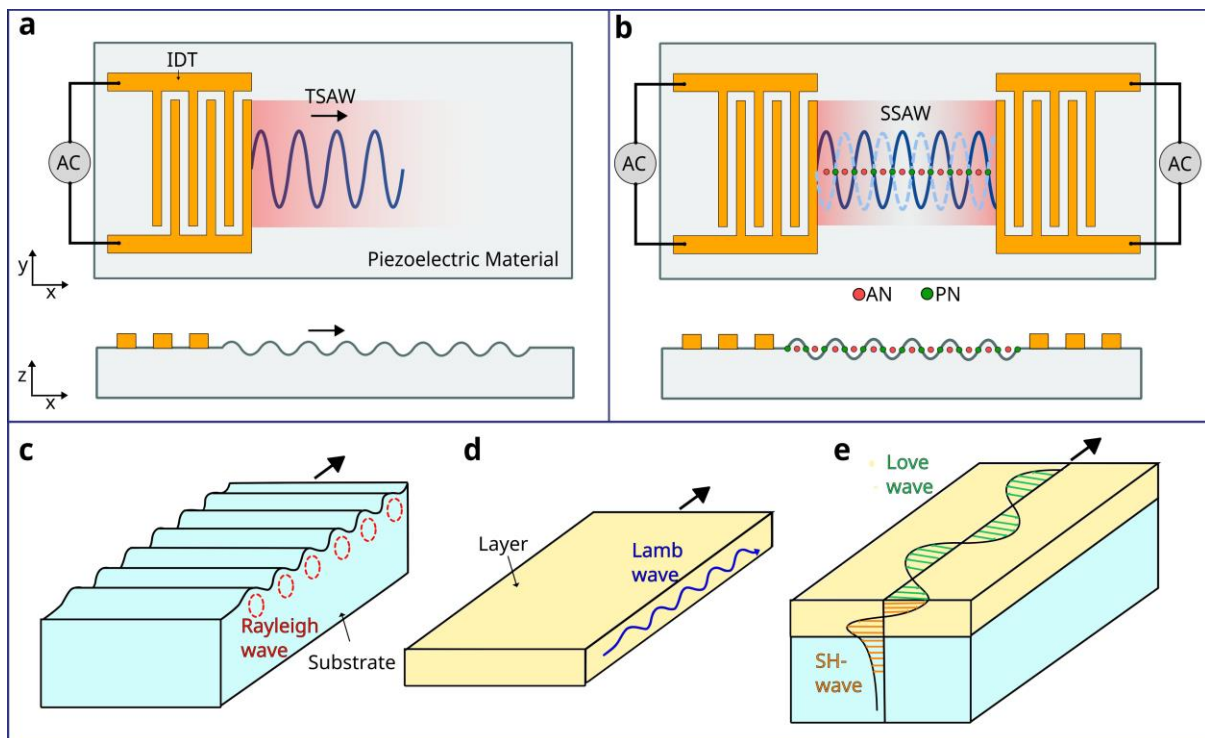
133 Acoustic waves are generated by applying radio-frequency (RF) signals to electrodes which
134 are commonly patterned onto a piezoelectric substrate, such as quartz or lithium niobate
135 (LiNbO_3) or lithium tantalate (LiTaO_3). The resulted acoustic waves propagate either in the
136 direction perpendicular to the surface of the material into the bulk medium (bulk acoustic wave
137 or BAW), or along the surface of the material (surface acoustic wave or SAW). This review
138 mainly discusses SAWs, whose electrodes are consisted of two metallic interlocking comb-
139 shaped arrays called interdigital electrodes (IDEs) or interdigital transducers (IDTs), which
140 convert electrical energy into acoustic waves through the reversed piezoelectric effect. When
141 an RF voltage is applied to the IDTs, it causes alternating regions of tensile and compressive
142 strains between the fingers of the electrode, thus producing mechanical waves which can
143 propagate on the surface. IDTs have been extensively investigated in the past fifty years for
144 usages in RF communications or filters applications ^{52,53}, and radio-frequency identification
145 (RFID) ^{52,54,55}. However, for acoustofluidic applications, this is a relatively new and an exciting
146 area to be explored ^{53,56}.

147
148 SAW devices can produce different types of surface wave modes to target various applications
149 ²⁸. Most SAW devices are designed to generate Rayleigh waves which propagate along the
150 surface of the substrate, with both longitudinal and vertical shear components. In Rayleigh
151 waves, particles on the surfaces have elliptical trajectory, and show a rapid decay of particle
152 oscillation with depth ⁵⁷. There are strong interactions of Rayleigh waves with the liquid (also
153 the particles inside), which enable them suitable for microfluidic applications. The velocity of
154 the waves is dependent on the material of the substrate and the orientation of the crystals. A
155 conventional Rayleigh SAW device typically consists of an IDT to create travelling surface

156 acoustic waves (TSAWs) as shown in Figure 2(a). If a pair of these identical IDTs are used and
 157 placed opposite to each other, two oppositely propagating TSAWs will interfere each other,
 158 creating a standing surface acoustic wave (SSAW), illustrated in Figure 2(b). These SSAWs
 159 produce pressure nodes (PNs) and antinodes (ANs) between two IDTs, which are often used
 160 for particle manipulation^{58,59}.

161
 162 Apart from the fundamental Rayleigh waves (illustrated in Figure 2(c)), higher wave modes of
 163 SAWs in a layered SAW device are called Sezawa waves, which mainly propagate through the
 164 boundary or interlayers at a higher velocity than that at the top layer⁵⁷. Lamb waves (Figure
 165 3(c)), which are often generated in thin plate or membranes, are similar to Rayleigh waves.
 166 However, they travel along the whole plate structure (i.e., along both upper and lower surfaces)
 167 and hence have two free surfaces as guiding boundaries, rather than just one free surface⁶⁰.
 168 Shear horizontal SAWs (SH-SAWs, Figure 2(d)) propagate on the substrate surface as well as
 169 on many piezoelectric thin films, all of which have in-plane crystal textures⁶¹. Love waves
 170 occur in SH-SAWs (Figure 2(e)) whose surface is covered with a thin wave guide layer. The
 171 SH-SAWs and Love mode waves are mainly used for biosensing rather than microfluidic
 172 applications, due to their less damping effects or weak coupling with the liquid, compared with
 173 those of the Rayleigh ones⁵⁷.

174



175

176 Figure 2. Schematic illustrations of SAW devices⁶² and types of wave propagation by means
177 of the distribution of displacements⁶¹. (a) Top and side views of SAW generated by a single
178 IDT producing TSAW. (b) Top and side views of SAW generated by a pair of opposite IDTs
179 producing SSAW, demonstrating regions of PNs and ANs.. (c) Rayleigh wave⁶³ (d) Lamb
180 waves⁶⁴ (e) Shear horizontal waves and Love waves⁵⁷.

181

182 A typical SAW IDTs (using an SAW resonator as an example) include the electrode fingers,
183 bus bars and electrode pad, and in many cases, the reflectors. For biosensing or medical
184 diagnosis applications, these SAW devices are required to achieve higher SAW frequencies,
185 larger amplitude, smaller width (higher quality factor), reduced noises, and precise IDT
186 dimensions. SAW devices with frequencies from tens of MHz up to tens of GHz with high
187 quality factor and low noise have been extensively reported⁶⁴⁻⁶⁷. Whereas for microfluidics
188 applications, these SAW devices are required to generate multiple microfluidic functions which
189 often require higher output powers, higher vibration amplitudes, various types of wave modes,
190 possible wider range frequencies (e.g., from low frequency of a few MHz up to a few hundred
191 MHz). Some high frequency SAW devices (e.g., a few hundreds of MHz) were explored for
192 manipulating nanoscale droplet, single cells or sub-micron particles^{68,69}.

193

194 When designing SAW IDTs, there are different issues to be considered, e.g.,
195 geometry/thickness, electrode materials selections, mass loading, piezoelectric shorting,
196 electrical regeneration and geometric discontinuity, strength of electromechanical constant and
197 metallization patterns^{70,71}. Recently many studies have been done on the design and patterning
198 of various types of electrodes for lab-on-a-chip applications (including bio-samples functions
199 and precise sensing functions), and more importantly, to improve microfluidic functions^{53,56}.
200 However, currently available IDT designs are purposely developed for RF communication or
201 various sensing applications, and not specifically focused on their designs for the optimum
202 acoustofluidics functions²⁵. Therefore, in this paper, we will firstly introduce the mechanisms
203 of acoustic streaming and acoustofluidics, and then discuss various IDT designs and their
204 relevant application to acoustofluidics.

205 **3. Mechanisms of acoustic streaming and Acoustofluidics**

206 Acoustic streaming is a phenomenon that occurs in different forms due to its sensitivity to
207 various geometries and boundary conditions. It is observed in Newtonian fluids, superfluid and
208 non-Newtonian viscoelastic liquids, thus have found various applications⁷². This section aims

209 to provide the key information about generation mechanisms of acoustic streaming and
 210 describe the fundamental theories given its ubiquitous appearance.

211 **3.1. Governing equations and related forces**

212 Acoustic streaming can be analyzed quantitatively using fluid dynamics' well-known continuity
 213 and momentum equations, assuming the fluid is homogeneous and isotropic, i.e.,²

$$\frac{\partial \rho}{\partial t} + \nabla \cdot (\rho \mathbf{v}) = 0 \quad 1a$$

$$\rho \frac{\partial \mathbf{v}}{\partial t} + \rho (\mathbf{v} \cdot \nabla) \mathbf{v} = -\nabla p + \mu \nabla^2 \mathbf{v} + \left(\mu_b + \frac{\mu}{3} \right) \nabla \nabla \cdot \mathbf{v} \quad 1b$$

214 where \mathbf{v} is the flow velocity, t is time, p is the pressure of a fluid, μ_b and μ are the bulk and
 215 the shear viscosities of the fluid, respectively. The bold represent vectors, and the normal are
 216 the scalars. For simplicity, all the external fields such as gravity, buoyance, and
 217 electromagnetism have not been considered. As only the isothermal case has been considered
 218 in many cases, the heat transfer equation is normally not required⁷³. The left side of equation
 219 1 is the inertia force per unit volume of fluid. The first term is the unsteady acceleration, and
 220 the second term is the convective acceleration. Convective acceleration is associated with the
 221 Reynolds stress². The net forces per unit volume on the right side include pressure gradient
 222 and viscosity gradients⁷⁴. These equations can be used with the boundary conditions and the
 223 linear relationship between pressure p and mass density ρ to predict the motion of the fluid⁷⁵.

$$p = c_0^2 \rho \quad 2$$

224 where c_0 is the speed of sound in the fluid. Nevertheless, these equations are difficult to solve
 225 analytically. The only concept with a thorough foundation is perturbation theory which can
 226 only be used for slow streaming²⁷. The liquid flow has two components, i.e., the fluids acoustic
 227 motion and the streaming motion. Slow streaming is generated when the velocity of the
 228 acoustic component is greater than the steaming component and only encounters resistance
 229 from viscosity²⁷. It is often called linear streaming as the second-order governing differential
 230 equations in the perturbation expansion are linear, and the convective acceleration is thus
 231 disregarded. Although being called linear streaming, it should be noted that this streaming is
 232 still caused by many nonlinear effects⁷⁶. Whereas fast streaming is generated when the
 233 streaming velocity is in the same order or larger than the acoustic component. The nonlinear
 234 component is included such that convective acceleration needs to be considered. This paper is
 235 mostly focused on the theory of slow streaming.

236 Reynolds number (R_e) is a parameter used to describe the characteristics of the flow. It is the
 237 ratio of inertia to viscous terms. The flow is laminar when the viscous force dominates or
 238 turbulent when the inertia forces dominate. For slow streaming, the effect of inertia on the
 239 streaming motion is neglected by comparison to viscous effects and hence slow streaming
 240 occurs when the flow is laminar. Whereas, for fast streaming, the effect of inertia cannot be
 241 neglected hence $R_e > 1$. Reynolds number is dependent on the flow velocity and the fluid
 242 mechanical system⁷⁷. It is defined as,

$$R_e \equiv \rho U_0 \mathcal{L} / \mu \quad 3$$

243 where \mathcal{L} is the characteristic length, $U_0 \equiv |\mathbf{U}|$ is the characteristic flow velocity, which
 244 includes both the velocity of the fluid \mathbf{v}_0 and the effect of the acoustic propagation $|\mathbf{U}| = \mathbf{v}_0 +$
 245 $\langle \rho_1 \mathbf{v}_1 \rangle / \rho_0$. Reynolds number for each streaming form uses a different length scale: Schlichting
 246 $\mathcal{L} = \delta_v$, Rayleigh $\mathcal{L} = \lambda$ and Eckart $\mathcal{L} = L$. δ_v is viscous penetration depth, and L is a
 247 characteristic length scale much larger than the acoustic wavelength λ ².

248 R_e is usually low in most of microfluidics due to their small dimensions. The flow is usually
 249 laminar, and no turbulence occurs. Using perturbation theory, the slow streaming can be
 250 modelled in a predictable linear manner. However, R_e can become quite high in cases of fast
 251 streaming, where the flow turns more unstable, and the nonlinear term needs to be considered
 252 in the analysis^{2,75}.

253 3.1.1. Streaming Analysis with different flow velocity regimes

254 Perturbation theory is a method to find approximate solutions for a continuity and momentum,
 255 as shown in Eq. 3. A linearized form of these equations can be obtained by considering minor
 256 disturbances in density, pressure, and velocity;

$$p = p_0 + \varepsilon p_1 + \varepsilon p_2 + \dots \quad 4a$$

$$\rho = \rho_0 + \varepsilon \rho_1 + \varepsilon \rho_2 + \dots \quad 4b$$

$$\mathbf{v} = \mathbf{v}_0 + \varepsilon \mathbf{v}_1 + \varepsilon \mathbf{v}_2 + \dots \quad 4c$$

257 where subscripts 0, 1, and 2 represent static (absence of sound), first-order, and second-order
 258 quantities, respectively. In the absence of sound, the undisturbed state, \mathbf{v}_0 , is 0 as the fluid is
 259 quiescent. The Mach number $\varepsilon = v_1/c_0$ is used as the smallness parameter². It is defined as
 260 the ratio of fluid velocity to the speed of sound. This method assumes that the successive
 261 approximations converge, hence ε is sufficiently small and can only be used for slow streaming

262 analysis ². The successive approximations do not converge for fast streaming, and thus the
263 perturbation approach cannot be used.

264 The continuity and momentum equations can be solved for each order component of the
265 acoustic field by substituting the perturbation expansions. The first order acoustic field solution
266 describes acoustic wave motions in the system that contains oscillatory motions, where \mathbf{v}_1 is
267 the acoustic velocity and p_1 is the acoustic pressure field. The first-order solutions can be
268 substituted into second-order equations and time-averaged to find the solution for acoustic
269 streaming, which contains both harmonic and steady components²⁷. Physically, the second-
270 order time-averaged velocity $\langle \mathbf{v}_2 \rangle$ is the acoustic streaming, and the second-order time-
271 averaged pressure $\langle p_2 \rangle$ produces the acoustic radiation force that occurs when the acoustic
272 waves are scattered on the particles, causing them to move⁷³.

273 Zaremba ⁷⁸ used a different approach which overcomes the perturbation method limitation,
274 allowing the acoustic streaming velocities to be larger than the particle velocities (e.g., in the
275 case of fast streaming). It can be done by decomposing the dependent variables in the fluid to
276 time-averaged streaming flow component and instantaneous first-order component. The
277 streaming motion can be solved by substituting into the continuity and momentum equations
278 and time averaging over the excitation period ².

279

280 3.1.2. Forces in acoustic streaming

281 The forces on particles exposed to an acoustic wave are those due to direct irradiation by the
282 acoustic field and indirect irradiation from scattering of the acoustic field from other objects ².
283 Primary acoustic radiation pressure (F^{ARF}) describes the force applied on a single particle in a
284 fluid due to the SAW²⁷. Whereas secondary acoustic radiation pressure is the force due to the
285 acoustic interactions with other particles in the fluid²⁷. Depending on the particle's mechanical
286 properties, the particle moves towards the PNs or ANs due to the primary and secondary
287 acoustic radiation forces ^{27,79}.

288 Acoustic radiation force F^{ARF} is determined by the surface integral of the time-averaged
289 second-order pressure p_2 and momentum flux tensor $\rho_0 \langle \mathbf{v}_1 \mathbf{v}_1 \rangle$ at a fixed surface just beyond
290 the oscillating sphere^{80,81}. Hence, the generalized equation can be written as:

$$\mathbf{F}^{\text{ARF}} = - \int_{\partial\Omega} da \{ \langle p_2 \rangle \mathbf{n} + \rho_0 \langle (\mathbf{n} \cdot \mathbf{v}_1) \mathbf{v}_1 \rangle \} \quad 5$$

291 where \mathbf{n} is the unit normal vector of the particle surface directed into the fluid.

292 Overall, the particles in a fluid are exposed to the net acoustic radiation force and the SAW
 293 acoustic streaming induced Stokes drag force \mathbf{F}^{drag} ⁸². The dominant force depends on the
 294 particles size. As a result, particles larger than a given threshold size will have their motion
 295 dictated by the acoustic radiation force.²⁷ The size threshold is dependent on factors such as
 296 actuation frequency, acoustic contrast factor, and kinematic viscosity⁸³.

297 The Stokes drag force, \mathbf{F}^{drag} , is dependent on particle size and shape, the fluid flow field, and
 298 the fluid viscosity⁸⁴. Hence on a spherical particle of radius r , with medium viscosity η and
 299 relative velocity v , \mathbf{F}^{drag} it is given by^{84,85}

$$\mathbf{F}^{\text{drag}} = 6\pi\eta r v \quad 6$$

300 Compared to traditional fluid mechanics, microfluidics has a number of significant forces
 301 which would otherwise be insignificant in larger scales². For a small scale, the fluid physics is
 302 dominated by surface tension and viscosity, whereas at a larger scale, body forces such as
 303 gravity are important². Other particle-particle interaction forces also exist, such as *van der*
 304 *Waals* interactions, electrostatic interactions and hydrophobic/hydrophilic effects⁸⁶.

305 **3.2. Fundamentals and mechanisms of acoustic streaming**

306 Acoustic streaming is a liquid flow phenomenon generated by forces arising from the presence
 307 of a gradient in the time-averaged acoustic momentum flux in a fluid^{86,87}. In a simple term, it
 308 is the fluid flow generated by the attenuation of an acoustic wave in the fluid, classified into
 309 two common types; boundary-driven streaming and bulk-driven streaming (also named Eckart
 310 streaming or quartz wind)⁸⁶.

311 Firstly, the acoustic wave is attenuated by the boundary interaction with the container walls,
 312 resulting in boundary-driven streaming. When an acoustic wave propagates parallel to a solid
 313 boundary, the non-slip boundary creates a high-velocity gradient perpendicular to the solid
 314 surface. This creates a steady boundary layer vorticity, called inner boundary streaming (or
 315 Schlichting streaming) which is confined within the thin viscous boundary layer (called shear-
 316 wave layer or stokes layer) of thickness given by $\delta_v = \sqrt{2\nu/\omega}$, where ν is the kinematic

317 viscosity, and ω is the angular frequency of the acoustic wave ⁷⁵. The strong inner boundary
 318 streaming flow generates counter-rotating streaming vortices within the fluid, called outer
 319 boundary streaming, or Rayleigh streaming ⁷⁵. Boundary-driven streaming can appear as (1) a
 320 wave travelling down a waveguide, (2) a standing wave in a resonant chamber, or (3) a wave
 321 scattering off a solid object ⁷⁵. For example, for a standing wave, boundary streaming consists
 322 of a vortex-antivortex pair per half wavelength along the direction of acoustic propagation ⁸⁶.
 323 It typically occurs in smaller acoustofluidic channels where the characteristic length scale of
 324 the fluid chamber is less than the acoustic wavelength such that,

$$\lambda \gg h \gg \delta_v \quad 7$$

325 where λ is the acoustic wavelength, h is the characteristic length scale of the fluid chamber and
 326 δ_v is the viscous penetration depth.

327 In comparison, bulk-driven streaming (Eckart streaming) is due to the viscous attenuation in
 328 the bulk of the fluid ⁸⁶. Stoke's Law of sound attenuation states that the dissipation rate is
 329 proportional to the square of the sound frequency ⁸⁶. The acoustic pressure amplitude decreases
 330 with distance from the acoustic source as the wave's amplitude diminishes. This energy loss
 331 causes a steady momentum flow, which generates a fluid jet in the acoustic propagation
 332 direction. Due to the pressure difference, fluid from the chamber's sides replaces the fluid
 333 propelled away by the streaming jet, resulting in a vortex-like flow ⁸⁸. It is more pronounced
 334 when the length of the fluid chamber L_E is greater than the acoustic wavelength, and hence
 335 typically occurs in larger devices ⁸⁹.

$$L_E \gg \lambda \quad 8$$

336 For BAW systems, the streaming is typically driven by the boundary layer streaming (i.e.,
 337 Schlichting streaming and Rayleigh streaming), whereas streaming fields within SAW systems
 338 are typically driven by the velocity gradient resulting from the attenuation within the fluid (i.e.,
 339 bulk driven streaming) ⁹⁰. This is because in a BAW field, the sound propagation is parallel to
 340 the edge of the fluid chamber giving rise to strong boundary effects, whilst these are lessened
 341 in a SAW field in which the sound propagates at an angle to the boundary ⁹⁰. For a droplet,
 342 when the SAW contacts the liquid, part of the SAW refracts into the liquid as a longitudinal
 343 wave at an angle known as the Rayleigh angle θ_R ^{27,91}, given by the following equation,

$$\theta_R = \sin^{-1} \frac{v_l}{v_s} \quad 9$$

344 where v_s is the SAW velocity on the surface material, and v_1 is the acoustic velocity in the
 345 liquid ⁹². For example, a Rayleigh angle of about 22° is obtained when using a 128° Y-cut
 346 LiNbO₃ piezoelectric substrate at room temperature, where the SAW velocity is about 3,990
 347 m/s, and the speed of sound in water is 1,490 m/s ²⁷. Whereas this value can be as large as 41°
 348 for a ZnO/Al plate SAW based device, as the SAW velocity in the aluminum substrate is about
 349 1,835 m/s ⁹³. The SAW changes modes into a leaky SAW in the fluid that decays exponentially
 350 with distance from the source due to the attenuation by viscosity along its transmission through
 351 the medium ⁹⁴. This decay length is the attenuation length, α^{-1} ⁹⁵:

$$\alpha^{-1} = \frac{\rho_s v_s^2}{f \rho_1 v_1} \quad 10$$

352 where ρ_1 and ρ_s are the densities of the fluid and the solid, respectively. In contrast, SAW
 353 propagates in the liquid medium along the Rayleigh angle with a distinctly higher attenuation
 354 length, β^{-1} ⁸⁷:

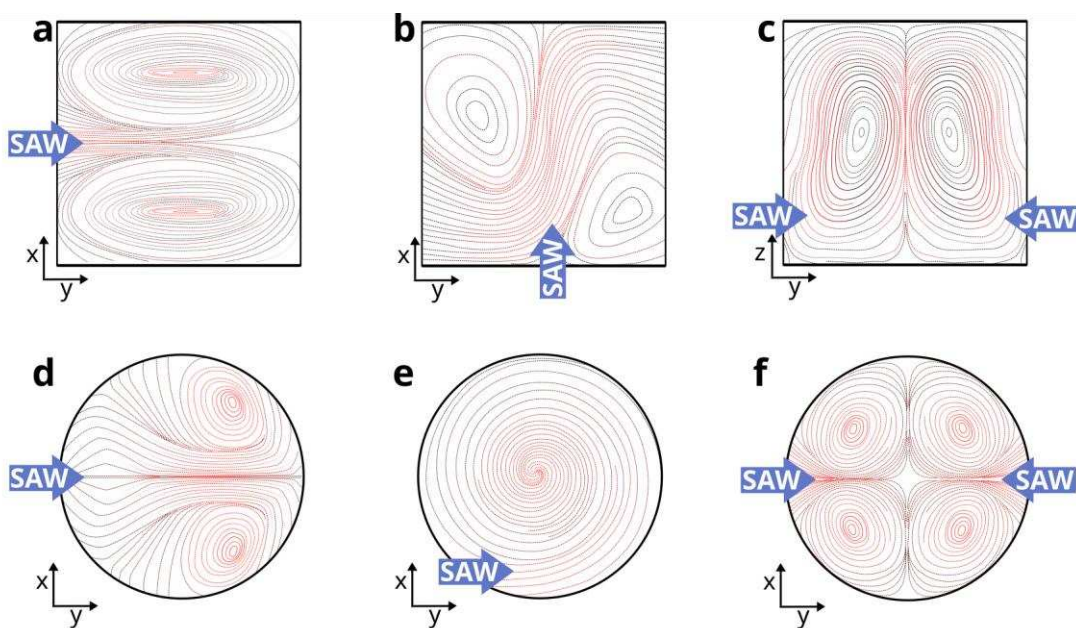
$$\beta^{-1} = \frac{\rho_1 v_1^3}{4\pi^2 f^2 (\frac{4}{3}\mu + \mu')} \quad 11$$

355 where μ and μ' are the shear and bulk viscosities of the fluid, respectively.

356 Bulk driven acoustic streaming force is formed in the fluid due to the non-zero and temporally
 357 phase-shifted distribution of the pressure and velocity [50], [51]. Inner boundary streaming
 358 may also arise due to the transmission of shear from the substrate to the fluid, which is confined
 359 in the viscous boundary layer ⁹⁶. Consequently, this could drive outer boundary streaming in
 360 the bulk of the fluid. However, boundary layer streaming is not frequently reported in SAWs
 361 ⁹⁸, and is often negligible compared to bulk streaming if the fluid container size and SAW
 362 attenuation length are much greater than the SAW wavelength ⁹⁹.

363 The SAW induced streaming pattern varies dramatically with the shape of the confined liquid,
 364 the type of IDT configuration used, and the incident position, angle, operating frequency and
 365 power of the SAW ²⁷. Typical SAW streaming patterns that may occur for droplets and
 366 channels are displayed in Figure 3. Figure 3(a-c) and figure 3(d-e) illustrate streaming patterns
 367 in channels and droplets, respectively, demonstrating the varying streaming patterns with
 368 different SAW propagation positions and directions (blue arrow). Figure 3(a) and figure 3(b)
 369 show the fluid being driven by the propagating SAWs (coming from the left of the channel,
 370 and the bottom of the channel, respectively), generating two vortex-like flows (top and bottom,

371 and left and right, respectively). These types of streaming patterns can be used for methods
 372 such as mixing, concentration and rotation as outlined in Section 5.1.3. Figure 3(c) illustrates
 373 an example of SSAW streaming¹⁰⁰ in front view, revealing two vortexes. SSAW streaming
 374 applications are discussed in Section 5.2. SAW propagation. Figure 3(d) displays a droplet
 375 streaming pattern, where the SAW propagation enters from the left and forms two vortexes.
 376 Figure 3(e) demonstrates streaming when the SAW propagates laterally offset to the droplet,
 377 creating one vortex. Figure 3(f) shows SSAW propagation where four vortexes are created. As
 378 discussed in Sections 5.1.1 and 5.1.2, these types of streaming can be used for mixing,
 379 concentration, and pumping.



380

381 Figure 3. Illustration of two-dimensional fundamental streaming patterns for (a-c) channels and
 382 (d-f) droplets, with different SAW propagation positions as shown by the blue arrows.
 383 (a) and (b) show streaming patterns in the top view, where the SAW propagation enters from
 384 the left, and the bottom, respectively. (c) displays streaming patterns in the front view, where
 385 SAW propagation comes from both the left and the right producing SSAW streaming. SAW
 386 propagation enters the droplets (top view) from (a) the left, (b) laterally offset, and (c) both left
 387 and right (SSAW).

388 The input power applied to an IDT for actuating a droplet can considerably vary the streaming
 389 patterns. At low input powers (in the order of mW), preliminary acoustic streaming on the free
 390 surface is generated, which can be used for vibration, mixing and driving applications. Higher
 391 input power (e.g., above a few watts) leads to a breakup of the stabilizing interface and allows
 392 for techniques such as jetting, atomization or nebulization¹⁰¹.

393 Two types of acoustofluidics have often been defined. The first one is called digital
 394 acoustofluidics, which is about sessile droplet under the acoustic field. Droplets act as sample

395 carriers that can be systematically sorted, trapped, mixed, pipetted, and split. They offer many
396 advantages such as low sample consumption, high throughput, flexible manipulation, and
397 elimination of cross-contamination and channel fabrication ¹⁰². Parameters including the
398 droplet's shape, volume, contact angle and evaporation determine acoustic streaming patterns
399 that consequently lead to variations in particles' concentration behavior ^{101,103}.

400 Another acoustofluidic field is called continuous flow acoustofluidics, e.g., studying the liquid
401 within microchannels or chambers interacting with the acoustic waves. Channels and
402 chambers have advantages as they often contain larger volumes of liquid, incorporate flow, and
403 modify their boundary conditions to allow versatile applications. It is important to note that the
404 channel/chamber boundary has a large impact on its applications. It could consist of different
405 materials (e.g., glass capillary, polydimethylsiloxane (PDMS)), interfaces (e.g., liquid-air,
406 liquid-glass) or geometries (e.g., different dimension/shape tubes or chambers).

407 For both these acoustofluidics, the methods to generate various liquid streaming in a SAW
408 device are crucial. This can be effectively realized using IDTs and this will be introduced and
409 discussed in detail in the next section.

410 **4. Acoustofluidic transduction technologies for acoustic streaming and acoustofluidics**

411 **4.1. Design and manufacture of electrodes**

412 **4.1.1. Design criteria**

413 The key design parameters for the IDTs of SAWs include: center (or resonant) frequency ω_f ,
414 frequency spectrum, bandwidth, power output density, choice of electrode materials,
415 shape/dimensions (including thickness), positions, substrate isotropic/anisotropic properties,
416 and number of reflective electrodes ¹⁰⁴, dispersion, substrate, reflection/transmission functions,
417 electrode types, weighting functions, resistance, electrode length and aperture, electrode phase,
418 electrode positions or delay effect, and wave direction or directivity (e.g., bidirectionality or
419 unidirectionality). The main objectives for improving electrode designs include: (i) increasing
420 the generation efficiency of acoustic waves; (ii) improving spurious signal suppressions; (iii)
421 decreasing insertion loss; and (iv) reducing signal distortion.

422

423 Depending on the different applications (e.g., biosensing or acoustofluidics), the key issues
424 about IDT designs are: ¹⁰⁵

425 **(1) Beam divergence or wave diffraction**⁶³. Due to the beam steering effects, or due to the
426 anisotropic effect of piezoelectric materials, the waves will not propagate in a direction
427 perfectly normal to the wavefront. **Acoustic aperture**¹⁰⁶ (i.e., the overlapping length of
428 electrode) needs to be designed precisely to avoid diffraction of the acoustic beam, and a
429 narrow aperture will cause beam steering and wave spreading when propagating. IDT
430 impedance is also dependent on this aperture. Normally it is recommended to be at least 50
431 times of the wavelengths to achieve an effective function.

432 **(2) Bragg reflection**¹⁰⁶. This is the wave reflections due to the electrode interactions causing
433 in phase scattered waves which have a much stronger reflection. This often happens when the
434 wavelength λ is equal to the periodicity, P . This can be solved by using different electrode
435 designs, such as double electrode (or split electrode) IDTs, which is discussed in the following
436 section.

437 **(3) Numbers of fingers** N ^{63,107}. Increasing this number, the bandwidth will become
438 narrowed, which is useful for achieving a better-quality factor of the resonant peaks. The
439 bandwidth (equals to $2f_0/N$) is also inversely proportional to the number of fingers in the IDTs,
440 and increasing the finger numbers can minimize spurious responses. However, too many finger
441 numbers will cause mass loading and scattering effects from the electrodes (which might
442 degrade the IDT's performance), as well as a much larger size or area of the electrode.

443 **(4) Triple transit signals**¹⁰⁶. This is often caused by the output IDTs producing reflected
444 waves, which are reflected from the opposite IDTs and then reflected second time by the input
445 IDTs. This is also called triple-transit-interference (TTI), or the multiple path effects generated
446 by non-matched output of IDTs as ripples with periodicity in the frequency responses.

447 **(5) Impedance mismatch**^{63,108}. This is one of the key reason for the complexity of surface
448 acoustic wave fields used for microfluidic applications¹⁰⁸. The impedance matching is critical,
449 otherwise, much of the acoustic wave energy will be dissipated within the IDTs. Electrical
450 dissipation in other forms should be avoided, such as electrical shielding and conductive short
451 connections. This can be solved by using a matching network or adjusting the IDT designs.

452 **(6) Bidirectional effect**⁶³. A straight conventional IDT has waves propagating in two
453 directions; thus, the wave energy will be wasted if one of the wave directions is not used. This
454 can be resolved using different designs such as single-phase unidirectional transducer which is
455 discussed later.

456 (7) **Heating effect**⁵⁷. The propagating wave produces atomic vibrations that causes heating
457 effects. Heating effects can be increased by defects, degradation, or malfunction of the device
458 causing internal dissipations of energy, or from reflections from the power supply.

459

460 In the following sections, we will separate the IDT topics into transducer materials, fabrication
461 techniques, and advances in IDT for acoustic streaming and acoustofluidics applications.

462

463 **4.1.2. Transducer materials**

464 IDT's materials influence the performance and electromechanical coupling coefficient of the
465 SAW devices^{109–111}. The IDTs are generally required to have a low mass to minimize wave
466 damping. They also need to have a high acoustic impedance to confine the acoustic waves
467 within the piezoelectric layer, and have a high conductivity to minimize the series resistance in
468 the transmission of the excitation signals. The different electrode materials have been discussed
469 by Fu et al.⁵⁷, based on their acoustic impedances ($Z = \rho \cdot v$, in which ρ and v are the density
470 of material and velocity of the waves) and ξ is resistivity of the materials.

471

472 For fabricating SAW devices, Al and Au/Cr (or Au/Ti) are the most frequently used electrode
473 materials. Al is the 3rd most abundant element on earth (after O and Si). Al electrode has its
474 advantages of low cost, a low resistivity, and low acoustic impedance, as well as a high Q factor
475 used as SAW IDTs, thus it is often used for delay lines and transversal filters. However, it has
476 some critical issues such as low mechanical strength, low melting points and poor electro-
477 corrosion resistance. Normally it requires enough thickness (commonly 100 to 200 nm) to
478 present a low electrical resistance but should not be too thick to cause problem with mass
479 loading effect and significantly increased acoustic impedance. Au electrodes have its
480 advantages at high power or with liquid, or in corrosive environments. However, at higher
481 frequency, gold IDTs show large mechanical losses, relatively large mass loading and
482 reflection, whereas aluminum IDTs show high reflection coefficients and high Q factors at
483 higher frequencies¹¹².

484

485 Some conducting and transparent oxides, such as aluminum doped zinc oxide and indium tin
486 oxide, have also been applied as electrode materials for transparent SAW devices^{113,114}.
487 Graphene^{115,116} and its derivatives, with their theoretically high conductivity and being an
488 extremely thin and light material which would cause insignificant mass loading¹¹⁷, has been

489 applied as the IDTs of SAW devices ^{118,119}. Multilayer graphene with a sheet resistance of a
490 few tens of Ω/sq could improve the transmission properties ¹²⁰.

491

492 When choosing the substrate materials to place the IDTs on, various factors should be
493 considered, including cost, temperature dependence, attenuation, and propagation velocity. For
494 example, the anisotropic properties of the substrates will cause significant direction-dependent
495 electromechanical coupling effects, therefore, their orientation and cut will determine the
496 efficiency of the device's electrical energy transduction from the SAWs. Anisotropy effect of
497 the substrate will affect which type of waves are generated: e.g., SH-SAW, leaky SAW, or
498 pseudo-SAW ²⁷. The anisotropic wave propagation velocities within the planes are critical
499 issues for effective IDT layout designs along various crystal-cut directions ¹²¹.

500

501 LiNbO_3 is commonly used in SAW fabrication for acoustofluidics due to its outstanding
502 electromechanical coupling coefficient ¹⁰⁷. However, due to LiNbO_3 's rigidity, brittleness, and
503 anisotropic nature, many other substrates have also been explored. Piezoelectric thin films
504 including zinc oxide (ZnO) ^{122–124} and aluminum nitride (AlN) can be deposited onto various
505 substrates such as silicon (Si), glass, ceramics, diamond, quartz, glass, and more recently also
506 polymer, metallic foils and bendable glass/silicon for making flexible devices ^{57,123}. Using
507 piezoelectric films would allow for fabrication of integrated, disposable, or bendable devices.
508 Due to the isotropic nature of thin film materials deposited onto a planar substrate, flexible
509 designs of electrodes or IDTs, such as focused, curved, circular/annular, or randomly shaped
510 patterns are readily achievable on thin film acoustic wave devices ⁵⁷. Additionally, bulk
511 ceramic substrate such as LiNbO_3 has a low thermal conductivity and poor fracture toughness
512 which becomes a challenge when a high power is needed. Thin films such as aluminum nitride
513 or gallium nitride (GaN) could be a novel piezoelectric films that, although piezoelectric
514 performance is compromised, allow for higher input power and superior thermal stability ^{125,126}.

515

516 **4.1.3. Fabrication techniques**

517 Cleanroom manufacturing techniques involve photolithography, evaporation and sputtering,
518 lift off or etching. These techniques allow for the fabrication of high efficiency, small-scale,
519 precise, and reproducible IDTs. Standard patterning techniques are either subtractive or
520 additive patterning, e.g., one method involving etching and the other lift-off, respectively. The
521 main steps for subtractive patterning are deposition, lithography, and etching. Firstly, the wafer

522 is cleaned before any IDE material is deposited to ensure the metal adheres successfully.
523 Deposition can be done by either sputtering, thermal evaporation, or chemical vapor deposition.
524 Lithography is performed by patterning photoresist using ultraviolet light exposure through a
525 mask to create a positive image of the IDEs after developing. Wet or dry etching can be used
526 to etch the IDE material. Lastly, the photoresist is removed to complete the process. The
527 additive method involves using lithography to pattern photoresist such that it creates a negative
528 image of IDTs after being developed. The IDE material is deposited on top of the patterned
529 photoresist. Then, the photoresist and the excess IDE material is removed using a lift-off
530 process.

531

532 Apart from the above conventional photolithography processes, new techniques such as
533 electron beam lithography, focused ion beam milling, or nanoimprinting, have been used for
534 making sub-micron wavelengths, thus super-high frequency SAW devices can be obtained. For
535 example, SAW devices with super-high frequencies (from 20 to 44 GHz) based on LiNbO₃,
536 ZnO/SiO₂/Si, or LiNbO₃/SiO₂/SiC heterostructures were reported using an e-beam lithography
537 method^{127–129}.

538

539 Clean room technique however can be expensive. Brittle piezoelectric substrates such as
540 LiNbO₃ are often used for making the IDTs. Not only can it be problematic to make
541 modifications, but also it is difficult to repair any mistakes or damages once the patterns have
542 been processed. To overcome this, IDEs can be manufactured separately from the piezoelectric
543 material, and then pressed onto the piezoelectric substrates to generate SAWs, for example,
544 using a printed circuit board (PCB), which is especially useful for prototyping. This method
545 consists of mechanically clamping electrodes made using PCB or even flexible PCB with a
546 piezoelectric substrate^{130–132}, thus the waves can be generated by simply applying RF
547 frequency to the pressed IDEs on the piezoelectric substrates.

548

549 Additional methods of creating electrodes have also been explored, such as by pouring low-
550 melting-point metal into a mold by PDMS¹³³, stacking aluminum foil strings onto substrate¹³⁴
551 and using superstrates on conventional SAW devices to allow their reusages for different
552 applications¹³⁵. 3D printing can be used to produce various shapes of electrodes and electrode
553 arrays with specially designed reflectivity and directionally (e.g.,
554 bidirectionality/unidirectionality) and varied frequency spectra, although the IDTs' resolution
555 might not be as good as those from lithography ones.

4.2. Advances of Interdigital Transducers

4.2.1. Conventional IDT structures

As mentioned in Section 4.1, the **standard bidirectional IDTs** have a simple design (as shown in Figure 4(a)), which has two electrode fingers, bus bars and electrode pad. However, it has issues such as internally mechanical edge reflections and loss of wave energy at two sides therefore half of the energy could be wasted in one direction. Various IDT designs have been studied to solve the critical issues, including straight or curved (focused or plane waves) types of IDTs, standing waves or propagating waves, and aligned or shifted waves. It should be noted that some of these IDTs are designed for sensing purposes, but not best for acoustic streaming applications.

(1) **Split IDTs (Figure 4(b))**. This is used to reflect some of the waves, thus reduce reflections. It is also used to minimize the spurious response due to the finger reflections.

(2) **Single phase unidirectional transducer (SPUDTs, Figure 4(c))**. SPUDTs have been commonly used to reflect or cancel regenerated waves using the internally tuned reflectors within the IDTs to form unidirectional SAW propagations from the IDTs. It can minimize the triple transmission effect (TTE), reduce the noise/insertion loss, and reduce the passband ripples.^{136,137} There are different designs for the SPUDTs. (1) Split finger pair by simply using $1/16 \lambda$, in which all the gaps are equal to $1/8 \lambda$. (2) Fixed split finger pair and varied widths to obtain a required directivity, e.g., different-width split finger SPUDT¹³⁸, in which the gap width between sections of opposite directivities as $1/16 \lambda$ and the distance between the two adjacent reflection center is $1/4 \lambda$. (3) Triple electrode section SPUDT, in which all the gaps and fingers are designed as $3\lambda/8$, which will generate a third harmonic response stronger than its fundamental response. (4) Special designs such as with finger widths of $1/5$, $2/5$, $1/5$, and $1/5 \lambda$. The problems for these SPUDTs are that the small electrodes size limits the fabrication of super high frequency devices. There is a reduction in total SAW energy meaning that the SAW generation efficiency is much lower, and its insertion loss is higher.

(3) **Distributed acoustic reflecting transducer (DART, Figure 4(d))**. This includes a sequence of identical cells with a length equal to wavelength λ , and each cell has two electrodes width of $1/8 \lambda$, and one electrode of width $1/4 \lambda$, the inter-electrode space is $1/8 \lambda$. Variable reflection can be achieved to cancel the net reflection and transmission effects. By segmenting

589 the reflecting electrodes, a variable reflectivity can be achieved, thus providing design
590 flexibility. They might be beneficial for SAW microfluidics and sensors as it not only improves
591 the performance, but also maintains the SAW devices at the best operating conditions.

592

593 **(4) Floating electrode unidirectional transducers (FEUDTs, Figure 4(e)).** One (or more)
594 electrodes is/are not connected to others and are floating. In the FEUDTs, the shorted or open
595 electrode configuration changes the transducer/reflector interaction and promote forward
596 transmissions.

597

598 **(5) Apodised IDTs (Figure 4(f)).** This is achieved by varying or setting the non-uniform
599 beam profiles for weighting a SAW transducer. In this design, the IDTs have different lengths
600 and different positions, and they generate impulse response/pre-patterned pulse waves. The
601 overlaps of the electrodes are varied along the length of the transducer, which can generate a
602 specific frequency response. In apodization technique, the top electrode is designed with non-
603 parallel edges which increases the resonant path and leads to more attenuated modes, thus
604 degrading the strength of spurious lateral modes. This pattern is generally used for wave
605 shaping and manipulation of frequency response of the IDTs. It can also be used for minimizing
606 heating effects, and avoiding bulk wave interferences, diffraction, and IDT end-effects, or
607 optimizing the output signal profile.

608

609 **(6) Focused or curved IDTs (FIDT, Figure 4(g)).** These IDTs can generate strong and
610 focused acoustic force or energy, which can be used to concentrate the acoustic energy to a
611 focal point. It has been utilized for improving pumping and mixing efficiency in
612 acoustofluidics, and for enhancing sensitivity and resolution in sensing applications. The
613 curved IDTs have been utilized for enhanced pumping and mixing functions with a strong
614 concentration effect.¹³⁹ However, due to the anisotropic nature of many crystal cuts of bulk
615 piezoelectric materials, it is recommended to modify the IDTs into a concentric elliptic shape,
616 whose curvature might be smaller than that of the wave surface^{139,140}.

617

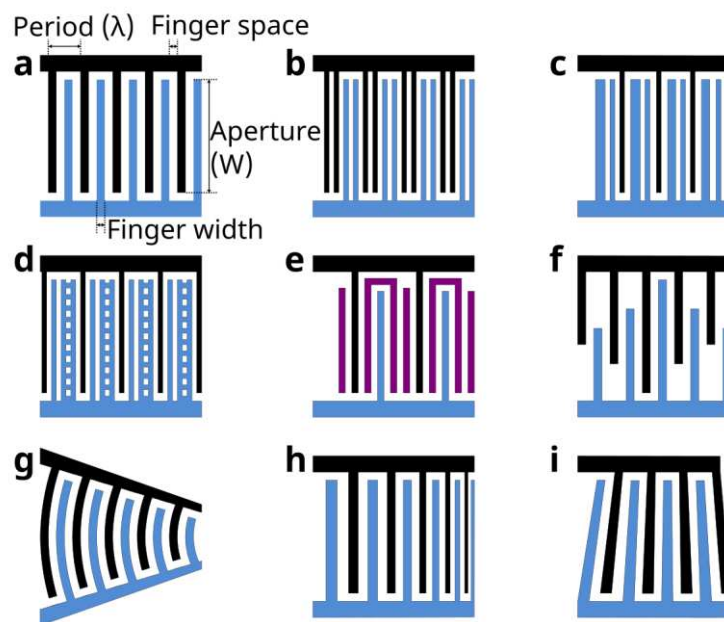
618 **(7) Chirped IDTs or dispersive delay lines (Figure 4(h)).** These are achieved by varying
619 the width and frequency of IDTs to control wave modes and reflectivity, to linearly modulate
620 the wave pitch or frequency. The bandwidth can be relatively large, and the frequency can be
621 changed gradually by decreasing the electrode spacing and increasing the electrode spacing. It
622 can be designed into an expander (from large width to smaller width) or a compressor (from

623 small width to larger width). Chirped IDTs are useful for manipulating droplets in different
 624 directions and for focused acoustic energy propagation. They are able to manipulate or change
 625 the moving direction of a droplet by changing and tuning the operating frequency continuously,
 626 thus used for manipulation of single microparticles, cells and organisms^{141–143}.

627

628 **(8) Slanted finger IDTs or tapered or tilted IDTs (SF-IDT, Figure 4(i)).**^{144,145} They have
 629 varied frequencies in the IDT section by changing the electrode's periodicity. They have broad
 630 bandwidths, which can change the moving direction of a droplet by changing the operating
 631 frequency continuously^{27,146,147}.

632



633

634 Figure 4. Conventional IDT designs. **(a)** Standard bidirectional IDTs **(b)** Split IDTs **(c)** Single
 635 phase unidirectional transducer (SPUDT) **(d)** Distributed acoustic reflecting transducer
 636 (DART) **(e)** Floating electrode unidirectional transducer (FEUDT) **(f)** Apodised IDT **(g)**
 637 Focused or curved IDT **(h)** Chirped IDT or dispersive delay lines **(i)** Slanted finger IDT or
 638 tapered or tilted IDTs (SF-IDT).

639

640 4.2.2. Unconventional IDT structures

641 Apart from the above commonly used IDT structures, there are many different types of
 642 uncommonly used IDT patterns.

643

644 **(1) Circular or annular IDT (Figure 5(a)).** Focused IDTs can be extended to create circular
 645 IDTs^{148,149}. Circular IDTs have a large focused acoustic force or energy, and have been utilized
 646 for improved pumping, mixing, and jetting of droplets. However, they have the same problem

647 as FIDTs of the anisotropic properties of the substrates of $128^\circ\text{Y LiNbO}_3$ is, e.g., there is
648 anisotropic effect for the velocities of waves along different directions. This can be improved
649 by designing a slowness curve deviating from the circular shape, or using a concentric elliptic
650 shape, which causes the beam direction no longer to parallel to the propagation direction ¹⁵⁰.
651 Also, for these circular IDT devices, the angle dependent coupling coefficient in a device of
652 $128^\circ\text{Y LiNbO}_3$ is significant. Therefore, the key issue for such a circular IDT device is to
653 achieve uniform waves from different directions. As we mentioned before, for piezoelectric
654 thin film based SAW devices, such an issue is often insignificant due to the isotropic wave
655 propagation on the planar surfaces of thin film SAW devices.

656

657 **(2) Dual wavelength IDTs.** Two different wavelength designs in one IDT can be applied,
658 which can generate two different SAWs after applying different frequencies. Although both
659 IDT designs consist of the same aperture, the dual-wavelength SAWs can be generated
660 separately or simultaneously, which can be spatially superimposed along the propagating path
661 within the microchamber or the microfluidic channel. The generated complex acoustic pressure
662 field can be applied to separate or mix particles of different sizes.

663

664 **(3) Spiral IDT designs** ^{151,152} or **anisotropic swirling SAWs** (see Figure 5(b) to 5(d)). These
665 can be used to tailor acoustical vortices, or for 3-D particle manipulation and vorticity control.
666 Spiral electrode designs can generate in-plane torsional vibrations. Spiral IDTs can be difficult
667 to design when consider the anisotropic wave velocity in different plans and directions for
668 many bulk piezoelectric crystals. Three types of design structures are proposed. (1) Swirling
669 IDT designs (Figure 5(b)), which can generate varied acoustic wave fields by simply changing
670 the applied signals; (2) Constant electrode spiral angle (Figure 5(c)), which provides a uniform
671 spiral angle for electric field but varied intensity ^{13,151}; (3) Constant pitch (distance) between
672 adjacent electrodes (Figure 5(d)), which can provide a uniform intensity of electrode fields but
673 various spiral angles, hence this design has a better in-plane torsional displacement and
674 vibrations than the previous one ^{153,154}. The last one is also called Ring waveguide resonator
675 IDTs ¹⁵⁵, which was reported to have a high-quality factor due to its regularity of electrode
676 structure, and the electrical admittance does not have any sidelobes. Thus, it can be suitable for
677 sensor applications. This design has a “slow” electrode region with a “fast” surrounding region,
678 with the acoustic fields concentrated in the electrode region. Additionally, circular slanted
679 finger IDTs with angularly varying finger widths and spacing can introduce frequency-

680 multiplexing ¹⁵⁶. Practically, these complex wave fields generated using spiral SAW acoustical
681 vortices can be used for particle tweezing, liquid twisting and swirling on a single functional
682 platform. This design can generate focused waves which are varied constantly by adjusting
683 different focusing points in arbitrary positions ^{157,158}. This has been used to demonstrate for a
684 variety of biological applications, including droplet transportation separation, fusion, and
685 nebulization ^{157,158}.

686

687 **(4) Holographic IDTs (Figure 5(e))** ^{159,160}. These can be used to produce waves by
688 designing specially metallic electrodes with equi-phase lines of the targeted wavefield at the
689 surface of a piezoelectric substrate, showing laterally focused (cylindrical) and 3D focused
690 (spherical) acoustical vortices. The SAW based holographic IDTs ^{159,160} have advantages of (i)
691 high working frequency, allowing resolutions down to micrometric scales; (ii) easy fabrication
692 with standard lithography techniques; and (iii) simple integration in a standard microscope
693 since they are flat, transparent and miniaturized ^{159,160}.

694

695 **(5) Ball shaped IDTs (Figure 5(f))**. The wave propagates around the equator of a large
696 sphere in multiple roundtrips, where the number of the SAW circulations around the ball equals
697 the SAW's propagation length. This can be used as a good sensor or acoustofluidic device on
698 a ball-shaped device. Due to the collimation of the SAWs, the energy loss from diffraction is
699 avoided. Therefore this is beneficial for sensors as the SAW propagation path can be much
700 longer and the sensitivity could be higher ¹⁶¹.

701

702 **(6) Inter-digitated IDT (IIDT, Figure 5(g))**. It uses the interweaved input and output
703 transducers to eliminate the inner transducer's bidirectional insertion losses and suppress the
704 sidelobes of the spectrum.

705

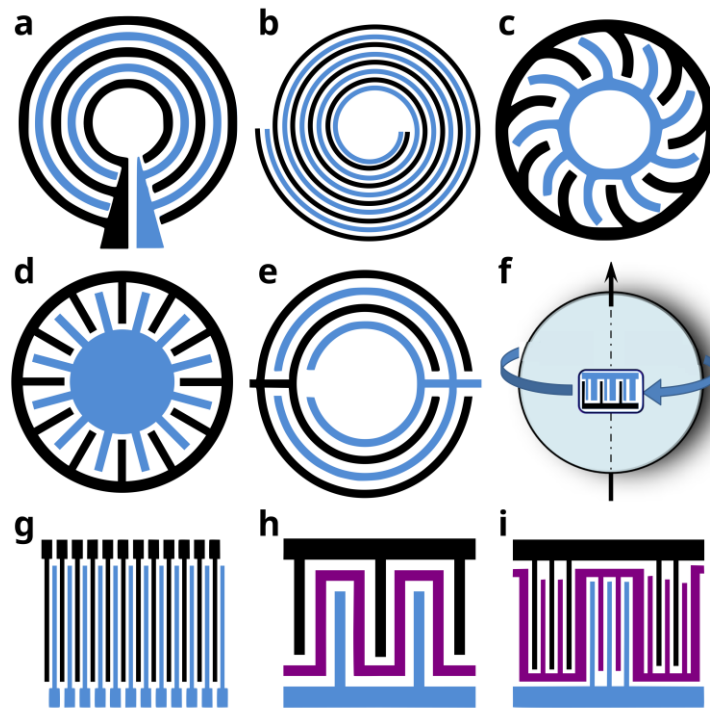
706 **(7) Tunable IDT (Figure 5(h) and multiphase IDTs (Figure 5(i))**. Conventional IDTs with
707 fixed pitch comb electrodes can be replaced by a series of densely distributed electrodes to
708 form a tunable IDT ¹⁶². Different wavelengths can be formed by connecting them in various
709 configurations, without changing the electrode layout. Other tunable IDTs could be consisted
710 of several IDTs arranged in an in-line configuration with different center frequencies and
711 bandwidths ¹⁶³.

712

713 **(8) Embedded IDTs**. IDTs are normally made on top of the piezoelectric substrates, which

714 have potential problems of reflection and scattering effects of these IDTs. One potential method
 715 to solve this is to use the IDTs fingers embedded inside the substrates ¹⁶⁴. However, this needs
 716 extra fabrication steps such as etching into substrates and post-polishing or other procedures
 717 ¹⁶⁴. This type of design is important for focused IDTs, which can minimize the finger grating
 718 effects on the angular dependence of the phase velocity ¹⁶⁵. For thin film-based SAW devices,
 719 this becomes easier as the IDTs can be deposited firstly onto the surface, or filling in the
 720 grooves to eliminate technological imperfections for burying electrodes ^{166,167}.

721



722

723 Figure 5. Unconventional IDT designs. (a) Circular or annular IDT (b) Swirling IDT (c)
 724 Electrode spiral angle IDT (d) Ring waveguide resonator IDT (e) Holographic IDT (f) Ball
 725 shaped IDT (g) Inter-digitated IDT (IIDT) (h) Tunable IDT (i) Multiphase IDT.

726

727

4.2.3. IDTs embedded into multi-layer structures

728

729 As explained before, due to the isotropic nature of thin film materials deposited onto a planar
 730 substrate, flexible designs of electrodes or IDTs, such as focused, curved, circular/annular, or
 731 randomly shaped patterns, are readily achievable on thin-film acoustic wave devices ¹²¹. Due
 732 to the thin film deposition process, the IDTs do not always need to be on top of the piezoelectric
 733 materials. For example, a “liquid needle” has been the early demonstration in which a circular
 734 self-focused bulk wave acoustic transducer with circular IDTs (on both top and bottom of the
 735 thin-film piezoelectric material) are used to generate a focused acoustic wave and produce a
 736 needle-shape liquid column on the free liquid surface ^{168–170}. As different layers have been used

737 in thin-film acoustic wave devices to improve temperature stability, phase velocity and
738 electromechanical coupling coefficient, the position of the IDTs can be designed in different
739 ways ¹⁷¹. As explained in Ref. ⁵⁷, there are variations of such designs. (1) the IDTs can be on
740 top of the substrate, and either the substrate or the intermediate layer must be piezoelectric; (2)
741 the IDTs can be on top of the intermediate layer, and either the intermediate or the top layer
742 must be piezoelectric; (3) the IDTs can be on the top layer, and in this case, the top layer must
743 be piezoelectric to excite the acoustic waves. (4) two same types of IDTs on both intermediate
744 and top layers to enhance the acoustic wave generation; (5) the IDTs can be located on top of
745 the piezoelectric film with a short-circuiting plane underneath; (6) The IDTs can be located
746 under the piezoelectric layer with a short-circuiting plane on top.

747

748 The IDTs can be either on the piezoelectric layer or beneath the piezoelectric layer to generate
749 the acoustic waves. Adding a piezoelectric layer or dielectric layer with a high permittivity
750 above the IDTs increases the electromechanical coupling, allowing the fabrication of devices
751 with reduced insertion loss or smaller size ¹⁷². A hard insulating top layer can shield the IDTs
752 of the piezoelectric film or sub-layers and the substrate from harsh environments or liquids,
753 thus enhancing the long-term stability of the devices ¹⁷³.

754

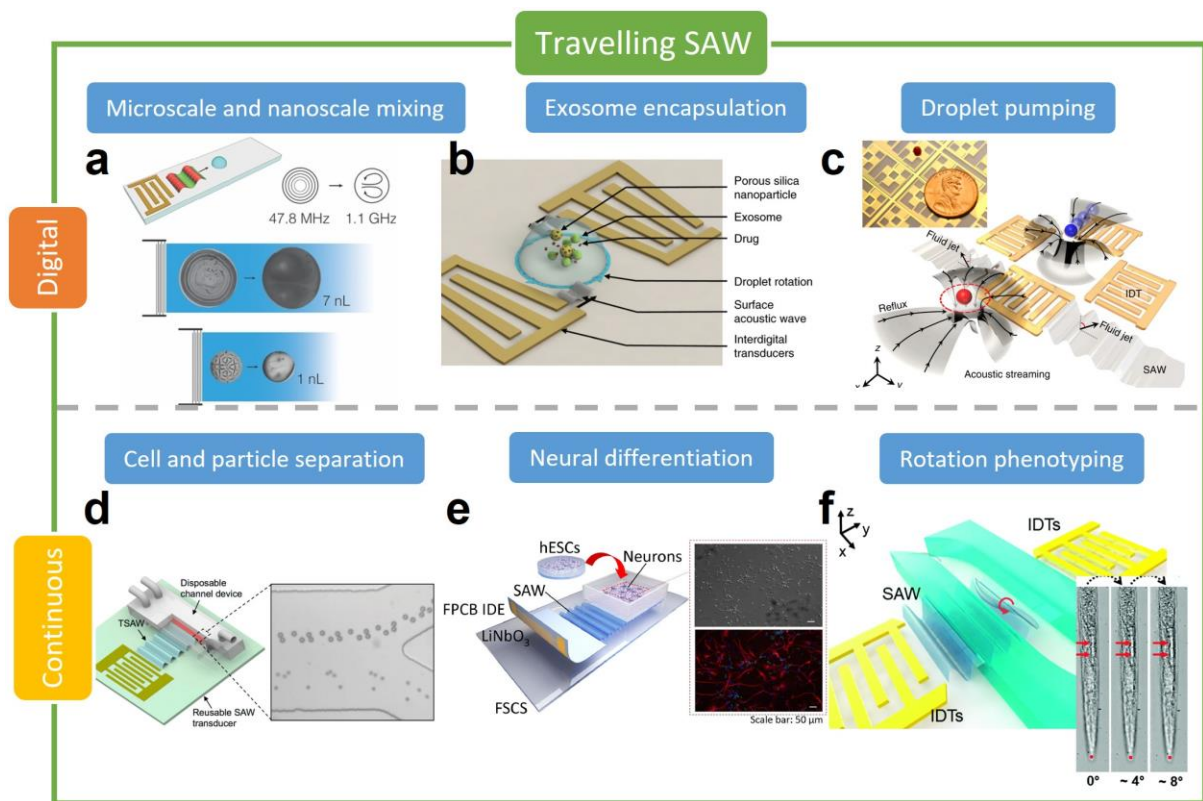
755 In brief, IDT designs and fabrications are critical in generating streaming patterns using SAW
756 devices. Different IDT designs and configurations can generate a variety of sensing functions
757 and distinct streaming patterns. Adjusting the IDT design, configuration, and input parameters
758 (such as applied power, amplitude and frequency) makes it possible to improve sensitivity, or
759 manipulate the acoustic streaming patterns for the desired applications, as discussed in the next
760 section.

761 **5. Acoustofluidic streaming applications using transducer designs**

762 SAW devices are increasingly used in biomedical applications as they are simple but meet most
763 of point-of-care requirements. Numerous actuation techniques with different applications can
764 be achieved depending on factors such as the boundary conditions (sessile droplet, open or
765 closed channel or chamber), static liquid or flowing liquid, the power delivered to the device
766 (ranging from mWatts to Watts) and the IDT designs (for example conventional IDT, FIDT).
767 The following sections will discuss various applications based on travelling SAWs (TSAWs)
768 and standing SAW (SSAWs) based acoustic streaming and acoustofluidics.

769 **5.1. TSAWs based streaming and acoustofluidics**

770 TSAWs generates physical phenomena of streaming driven particle behavior and the drifting
 771 of particles due to acoustic radiation forces, under propagating acoustic waves into the substrate
 772 and liquid ¹⁷⁴. An overview of typical medical applications using TSAW based streaming are
 773 shown in Figure 6. TSAW typically propagate in one direction²⁷ and can produce streaming
 774 vortices and particle movement. Hence depending on the IDT configuration, TSAW streaming
 775 can be used to generate various methodologies such as mixing, concentration, pumping, jetting,
 776 and rotation. In turn, these methodologies can be used for specific digital and continuous
 777 acoustofluidic real-life medical applications such as nanoscale mixing (Figure 6(a)), exosome
 778 encapsulation (Figure 6(b)), droplet pumping on different orientations (Figure 6(c)), cell and
 779 particle separation (Figure 6(d)), neural differentiation of cells (Figure 6(e)) and rotation of
 780 large vertebrates for phenotyping (Figure 6(f)). We will discuss various IDT configurations,
 781 their corresponding methodologies, and relevant medical applications in the following sections.



782

783 Figure 6. Examples of real-life medical applications of TSAW streaming, for both
 784 digital and continuous acoustofluidics. **TSAW digital ones:** (a) A gigahertz SAW device for
 785 nanoscale droplet mixing.¹⁷⁵ R.J. Shilton, M. Travagliati, F. Beltram, and M. Cecchini,
 786 *Advanced Materials* 26, 4941, 2014; licensed under a Creative Commons Attribution (CC BY
 787 NC ND) license. (b) A SAW device with a pair of slanted IDTs that induce droplet rotation as
 788 well as vortex streaming, which allows to concentration and fusion of the porous silica
 789 nanoparticles, exosomes, and drug within the droplet.¹⁷⁶ Z. Wang, J. Rich, N. Hao, Y. Gu, C.

790 Chen, S. Yang, P. Zhang, and T.J. Huang, *Microsyst Nanoeng* 8, 45, 2022; licensed under
791 Creative Commons Attribution (CC BY) license. (c) A digital acoustofluidics consisting of
792 four IDTs (one pixel) for contactless and programmable droplet manipulation.¹⁷⁷ Zhang, S.P.,
793 Lata, J., Chen, C. et al. *Nat Commun*, 9, 2928, 2018; licensed under Creative Commons
794 Attribution (CC BY) license. **TSAW continuous ones:** (d) A detachable device with a reusable
795 IDT and a disposable microchannel, for size selective PS microparticle separation.¹⁷⁸ Reprinted
796 with permission from Zhichao Ma, David J. Collins, and Ye Ai, *Analytical Chemistry*, 2016,
797 88 (10), 5316-5323. Copyright 2016 American Chemical Society. (e) A detachable FPCB
798 device for neural differentiation of human embryonic stem cells. Reproduced with
799 permission.¹⁷⁹ Sun, C., Dong, Y., Wei, J., Cai, M., Liang, D., Fu, Y., Zhou, Y., Sui, Y., Wu,
800 F., Mikhaylov, R., Wang, H., Fan, F., Xie, Z., Stringer Martin, M., Yang, Z., Wu, Z., Tian, L.,
801 & Yang, X. *Acta Biomaterialia*, 151, 333-345, 2022; licensed under Creative Commons
802 Attribution (CC BY) license. (f) SAW device using a streaming vortex distribution for rotation
803 of *Caenorhabditis elegans*.³⁷ Reproduced from *Lab Chip* 19, 984 (2019) with the permission
804 of The Royal Society of Chemistry.

805

806 **5.1.1. Mixing, concentration, and splitting of sessile droplets in digital acoustofluidics**

807 **Mixing**

808 Microfluidic applications involving sessile droplets are hampered by diffusion-limited mixing
809 due to their small dimensions. SAW devices can be used as a mixer to overcome this issue. It
810 is effective to use TSAW induced streaming to mix sessile droplets¹⁸⁰ and nanoliter order
811 droplets¹⁷⁵ by placing a singular straight IDT directly opposite to it (Figure 7(a)). This droplet
812 mixing can be used in applications such as size tunable nanoparticle fabrication using droplet
813 fusion¹⁸¹, or particle sampling device for the collection of airborne micro-particles¹⁸². TSAW
814 streaming can be utilized for cleaning biological sensors, by removing fouling caused by
815 nonspecific binding proteins on the surface, to allow more accurate determination and reuse of
816 the devices¹⁸³. The TSAW induced mixing can be combined with a metal enhanced
817 fluorescence¹⁸⁴ or surface plasmon resonance system³⁵, to improve mass transfer for
818 biosensing capabilities. Moreover, combining a singular straight IDT device and electrowetting
819 on dielectric (EWOD) can precisely guide and position microdroplets, for example, EWOD
820 assisted SAW particle streaming and concentration, SAW assisted EWOD splitting, and
821 EWOD assisted SH-SAW sensing¹⁸⁵. The addition of an electric field can also increase the
822 streaming velocity in a droplet by a factor of about 2-3 and change the flow pattern compared
823 to that without the electric field¹⁸⁶.

824 As a result of the mixing and hence inhomogeneously acoustic streaming in a droplet, cells
825 within the liquid droplet will experience a shear force¹⁸⁷. This shear force may interact with
826 cells through biological pathways, including the cell membrane, extracellular matrix, and

827 cytoskeleton, instead of simply displacing cells ¹⁸⁸. The shear forces can induce action
828 potentials ¹⁸⁹ and calcium responses ¹⁹⁰ in neurons, and affect cell adhesion and survival rate
829 in cell culture ^{188,191,192}. For example, an actuated straight IDT can result in the collision
830 between cells and magnetic Ag-nanowires in a cell droplet, leading to 97% lysis efficiency
831 with a power of just 1 Watt ¹⁹³. Similarly, by using a 17.1 MHz electrode of width controlled
832 SPUDT to ensure that the acoustic energy is directed solely in the forward direction, HEK 293
833 cells can be effectively detached and sorted from A7r5 cells based on differences in adhesion
834 strength within minutes ¹⁹⁴. In Ref. ¹⁹¹, an FIDT has been used for characterization of adhesive
835 properties of red blood cells (RBCs) in a 9 μm droplet within just 30 s. This method can be
836 used to perform rapid diagnostics and disease monitoring in a small fluid volume, which is
837 attractive as it requires no external rising agents such as trypsin, typically used for cell
838 dissociation from the solid substrate.

839 When mixing particles with a high rate of mass transfer, it is necessary to consider the size of
840 the particles. Large particles are affected mainly by radiation forces, while small particles will
841 flow along with the vortices of acoustic streaming ¹⁹⁵. The uses of both the acoustic radiation
842 force and the acoustic streaming generated by a 20 MHz straight IDT can be used
843 simultaneously concentrate and separate two microparticle sizes (e.g., 6 and 31 μm
844 polystyrene-PS particles ¹⁹⁶) in a sessile droplet. The smaller particles are dispersed in the bulk
845 of the droplet due to drag force, whereas the larger particles are concentrated on the free surface
846 of the droplet due to the radiation force. This demonstrates the existence of frequency-
847 dependent crossover particle size that can affect species partitioning.

848 **Concentration**

849 The key for the concentration of an object within a droplet is the asymmetric distribution of
850 SAW radiation along the width of the droplet. It is possible to achieve this by different schemes
851 of symmetry breaking of SAW propagation to generate an azimuthal liquid recirculation as
852 shown in Figure 7(b-d). The concentration effect can also be generated by placing the droplet
853 along one side of the IDTs with a reflector (Figure 7(b)). Shielding off one half of an open
854 reflector using a damp material allows control over the SAW that is reflected (Figure 7(c))¹⁹⁷.
855 Additionally, cutting the edge opposite to the input IDT at an angle to the propagation axis can
856 effectively reflect the SAW radiation at an angle, resulting in symmetry breaking (Figure 7(d)).
857 Using this method, it is possible to efficiently concentrate micrometer sized objects, such as
858 PS microspheres (1 to 45 μm) and living yeast cells (10-20 μm) using low powers from 120 to

859 510 mW¹⁹⁷. The concentration of particles can increase analyte detection sensitivity and
860 overcomes the diffusion limitation without particle damage, allowing a range of sensor
861 technologies.

862 Four distinct regimes (R1-R4) of particle concentration that are mostly available at higher
863 frequencies can be produced by placing a singular straight IDT offset to a droplet as shown in
864 Figure 7(e)¹². In R1, the particles are concentrated at the center of the droplet in the form of a
865 bead. In R2, the particles are around the periphery of the droplet in the form of a ring. In R3,
866 at the side of the droplet, an isolated island is formed. Finally in R4, a smaller ring is formed
867 at the center of the droplet¹². The different regimes are due to the various forces generated
868 (acoustic streaming-based drag force, travelling or standing SAW-based acoustic radiation
869 force and the centrifugal force)¹². The regimes of particle's aggregation depend on the κ -factor
870 (defined by $\kappa = \pi d_p / \lambda_f$, where d_p is the diameter of the particle and λ_f is the wavelength of the
871 acoustic wave in the fluid), the acoustic wavefield (travelling or standing), the acoustic waves
872 attenuation length (x_s) and droplet volume where r_d is the radius of the droplet. The attenuation
873 of the sound wave in the fluid (x_f) is negligible as it attenuates at a much longer distance, and
874 hence the focus is on the rapidly attenuating SAW wave¹².

875 A focused SAW can generate concentric surface acoustic waves which have high intensity,
876 high beam width compression ratio and small localized area. Hence, the focused SAWs can be
877 used to enhance streaming force up to 480% of the conventional SAWs¹⁹⁸. Circular and
878 focused SPUDT have an increased wave intensity and asymmetry of the waves, and therefore
879 they can also be effectively used to concentrate particles, which is one order of magnitude
880 faster than straight SPUDT and several orders of magnitude faster than the conventional
881 microscale devices¹⁹⁹. When comparing the different SPUDT devices, the circular SPUDT has
882 been shown effective at a given input power since it can generate the largest azimuthal velocity
883 gradient within the fluid to drive particle shear migration. On the other hand, the focused
884 SPUDT (Figure 7(f)) can generate the highest mixing intensity due to the focused SAW
885 radiation that substantially enhances acoustic streaming in the fluid²⁰⁰.

886 **Separation**

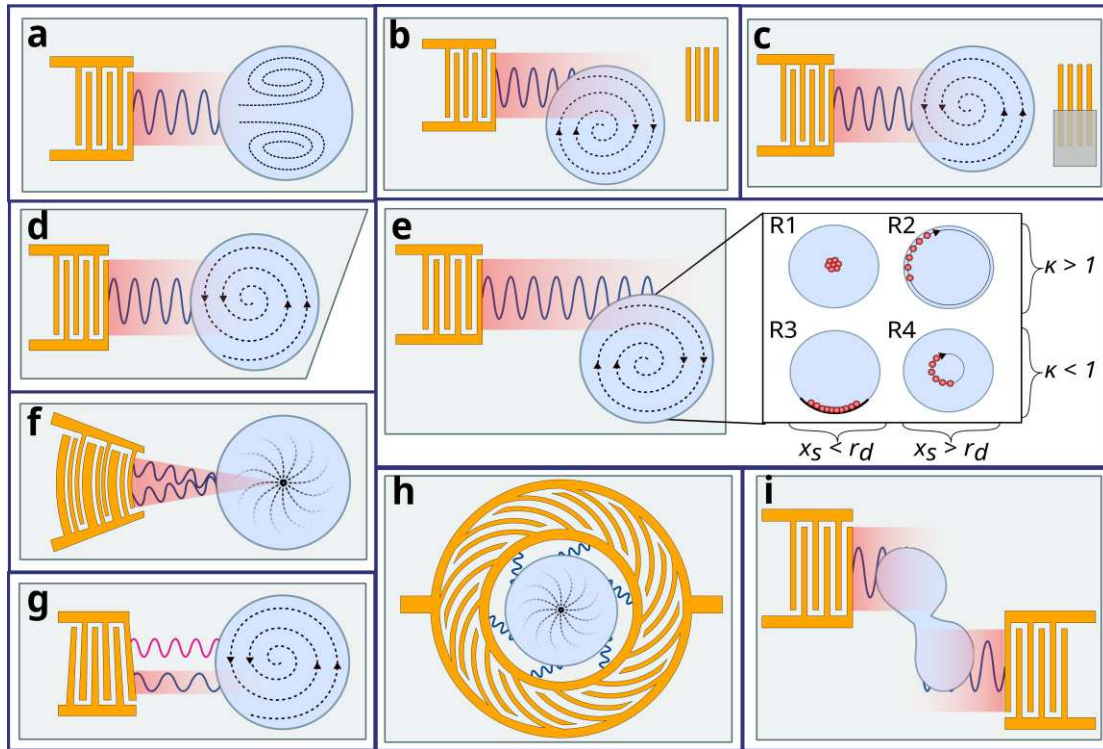
887 Another method for asymmetric actuation is to use an SF-IDT, which causes a circular rotation
888 motion inducing acoustic streaming of the cells in the droplet for their separation (Figure 7(g)).
889 Such actuation has been reported to separate malaria-infected RBC at the periphery of the
890 droplet, based on the difference in cells' densities using SAWs²⁰¹. Most acoustofluidic systems

891 that aim for nanoscale manipulation are difficult to achieve this function due to the insufficient
892 acoustic radiation force and abundance of acoustic streaming to control nanosized particles.
893 Nonetheless, this acoustic centrifuge motion can overcome such limitations. Gu *et al.*¹⁴
894 reported the use a pair of SF-IDTs and a circular PDMS containment ring to define the droplets
895 equilibrium shape. The SF-IDTs allows various frequencies to be applied, generating SAWs at
896 different positions on the piezoelectric substrate, and therefore spin can be created on altered
897 size droplets, so long as the wave enters the droplet from a position which has a slight bias
898 from its center line. By adding two spinning droplets with a microchannel for particle passage,
899 differential phenomena including concentration and separation can occur. Using this method,
900 exosome separation and transport can be achieved, where the right-side droplet contained a
901 greater distribution of the smaller nanoparticles and the left-side droplet with the larger
902 nanoparticles¹⁴. This configuration has also been used to perform both drug loading and
903 exosome encapsulation¹⁷⁶.

904 An omnidirectional spiral SAW that uses a 152° Y-rotated, can rapidly rotate a microliter
905 droplet for multi-size particles for their separations and extractions, as illustrated in Figure 7(h).
906 The rapid rotation is realized through the axisymmetric omnidirectional spiral SAW.
907 Separation and extraction of RBCs and platelets within mouse blood can be achieved with 83%
908 and 97% purity, respectively¹³. Unlike previous configurations to separate particles, this
909 method can successfully extract target particles for bio-sampling functions.

910 **Splitting**

911 Instead of particle concentration and separation of objects in a droplet, SAW can aid in merging
912 and splitting of droplets as illustrated in Figure 7(i). Two single phase transducer (SPTs)²⁰²
913 can realize this separation function. An SF-IDT²⁰³ was also used for separation of water from
914 an oil/water mixed drop. A pair of IDTs which were laterally offset modulated SAWs enabled
915 droplets with volumes of 0.5 to 6 μl to be symmetrically divided into two equal size droplets
916²⁰⁴.



917

918 Figure 7. Droplet mixing, concentration and splitting of sessile droplets in digital
 919 acoustofluidics IDT device examples. (a) Singular straight IDT directly opposite droplet for
 920 TSAW mixing. (b-d) Schemes of symmetry breaking for rotational motion such as using a (b)
 921 reflector, (c) shielding off one half of an open reflector, (d) or cutting the substrate. (e) Singular
 922 offset IDT with 4 regimes of concentration (R1) particles are concentrated at the center of the
 923 droplet, (R2) around the periphery of the droplet, (R3) at the side of the droplet, and (R4)
 924 close to the center of the droplet. (f) Focused SPUDT with focused SAW around center of the droplet.
 925 (g) SF-IDT with SAW generated at defined position asymmetrically with respect to droplet for
 926 rotation motion. (h) Omnidirectional Spiral IDT with circular streamlines in the droplet ¹³ (i)
 927 Pair of laterally offset straight IDTs for droplet splitting.

928 **5.1.2. Pumping, jetting, nebulization/atomization, and droplet generation in digital**
 929 **acoustofluidics**

930 **Transportation**

931 Discrete liquid pumping (i.e., droplet translation) can be achieved by applying SAW to a sessile
 932 droplet. If the applied SAW power is higher than a limit, the internal streaming leads to a
 933 deformation of the droplet, which eventually translates the droplet in the direction of the SAW
 934 propagation. The applied SAW power overcomes the forces stimulated by contact line pinning
 935 and contact angle hysteresis. For microfluidic applications, pumping of a sessile droplet in the
 936 scale of microliter without evaporation is challenging, hence low powers need to be used, or
 937 the droplet has to be encapsulated in oil ²⁰⁵. Other methods to avoid problems of droplet
 938 evaporation and temperature for biological activity can be accomplished by aid of a steel ball

939 medium²⁰⁶, avoiding direct radiation of SAWs on the piezoelectric substrate using a superstrate
940 idea, or by converting the microdroplets into a continuous flow²⁰⁷.

941 When using a 20 MHz straight IDT SAW device (Figure 8(a)), the maximum droplet velocity
942 happens when the diameter of droplet is equal to the attenuation length²⁰⁸. For smaller
943 diameters of droplet, the whole SAW energy is not absorbed by the droplet. However, droplets
944 with larger diameters move slower because the same amount of applied SAW energy was used
945 to move a higher mass.

946 If the droplet viscosity becomes larger, the pumping velocity significantly decreases for small
947 droplets (from 2 to 20 μl)²⁰⁹. The necessary power to deform and move a sessile droplet could
948 be reduced between 50 to 75% through vibrating the droplet. This approach is important for
949 cases for which temperature needs to be kept a constant. Another method to decrease the
950 acoustic power required to transport a droplet is using SAW inertia-capillary modes of
951 oscillation. For example a 19.5 MHz straight IDT can be used with Rayleigh-Lamb inertia-
952 capillary modes to move a droplet at a speed of 5 mm/s with the required power reduced by a
953 factor of 3²¹⁰.

954 Surface properties can affect the droplet pumping velocity with SAWs. A superhydrophobic
955 surface would minimize the contact area between liquid and solid and reduce the pinning force,
956 making the surface slippery. However, this minimized interaction area limits the amount of the
957 energy which can be transferred by the SAW to the liquid medium. Droplets with lower
958 volumes at higher applied RF voltages are transported with higher velocity on hydrophobically
959 treated surfaces²¹¹. Pumping of droplets with volumes up to 10 μl can be achieved using a
960 straight IDT on a thin-film piezoelectric material treated with a hydrophobic self-assembled
961 monolayer of octadecyl trichlorosilane (OTS)²¹¹. A slippery layer of lubricating oil-filled
962 hydrophobic surface can also be used, and the threshold power to pump the droplet on a ZnO/Si
963 SAW device can be significantly reduced (up to 85%)²¹². Surface behavior of droplet
964 manipulation in microfluidics has further been discussed in detail by Wu *et al.*²¹³.

965 Droplet acoustofluidic devices typically need a flat surface to operate correctly. However,
966 changing the surface treatment and using thin-film SAW devices, such as ZnO/Si, ZnO/glass,
967 AlN/Si²¹⁴ or ZnO/Al, can achieve droplet transportation across a wide range of substrates and
968 their geometries, including inclined, curved, vertical, inverted, and lateral positioned surfaces⁴⁰
969 (Figure 8(b)).

970 Transporting droplets across different piezoelectric substrates could be helpful if each separate
971 substrate has a different function, such as mixing and separating, rather than a substrate with
972 all the operating units. For example, it is possible to use three 128° Y-X LiNbO_3 substrates
973 each with their own 27.5 MHz IDT and reflector, where one is an interface chip and two are
974 working chips 1 and 2²¹⁶. The interface chip can be adjusted to be the same height as working
975 chip 2 with a gap as small as possible so that the SAW can transport the droplet across.
976 Similarly, the droplet can be transported to working chip 1 by adjusting the height. It should
977 be noted that although many of these methods for droplet translation do not use a FIDT, if a
978 droplet is placed on the focal distance of an 13 MHz FIDT, it can move approximately five
979 times faster than a straight IDT when compared to a straight IDT of the same frequency and
980 dimension²¹⁷.

981 Small-scale programmable microfluidic processing can be accomplished by using SAW
982 streaming to actuate and transport droplets along predetermined trajectories. Chemical
983 modifications of the chip surface can be used to design the paths to create virtual wells and
984 tubes (hydrophilic and hydrophobic regions) which confine small droplets. Depending on the
985 actual layout of the chip/IDTs, the droplets can be split into smaller ones, merged, mixed, and
986 processed²¹⁸. Instead of predetermined trajectories, acoustic streaming induced hydrodynamic
987 traps can be used for contactless droplet transport and manipulation of droplets within volumes
988 between 1 nL to 100 μL along any planar axis. For example, using four straight IDTs to create
989 an 8 by 8 array Figure 8(c)), the streaming effect pushes fluid out along one direction, and
990 pumps the fluid (with fluorinated oil as carrier layer) along the vertical directions¹⁷⁷. The
991 acoustic streamlines converge at two horizontal stagnation points above the two symmetric
992 sides of the IDT, hence the water droplets floating on the oil can be trapped²¹⁹. The re-
993 programmable digital multi-path platform can achieve various droplet manipulation (transport,
994 merge, mix and split) and can be scaled to perform massive interaction matrices within a single
995 device.

996 IDT arrays inside a layer of oil can generate acoustic streaming vortices for rewritable digital
997 acoustofluidics, contact-free routing and active/passive gating⁴⁵. Droplets over the transducer
998 are guided to the center hydrodynamic equilibrium position between barrel-like acoustic
999 streaming vortices. The vortices are extended to the adjacent transducers when multiple
1000 transducers are sequentially activated using multi-toned electrical signals. Hence a long virtual
1001 channel for unidirectional transportation and gating can be produced⁴⁵. These programmable
1002 microfluidic processing techniques offer basic functional units that mimic electronic

1003 functionality for biomedical and biochemical applications such as on-chip bioassays, high
1004 throughput compound screening, biochemical synthesis, and droplet processing strategies that
1005 follow digital logic rules ⁴⁵.

1006 **Jetting**

1007 Jetting can be generated by concentrating the wave energy into a small, focused area and
1008 maximize the mechanical displacements into sessile droplet. A nozzleless method to jet liquid
1009 can be beneficial in 2D and 3D bioprinting, needle-free fluid injection or single-molecule
1010 detection. It offers the advantages of being low cost, simple manufacturing, and the ability for
1011 miniaturization. Jetting can be achieved with a standard SAW devices such as on a substrate
1012 of 128° Y-X LiNbO₃ (Figure 8(d)) surface-treated with hydrophobic layer, so long as the SAW
1013 streaming force is large and strong enough to expel a droplet from the substrate ¹⁰⁴. Jetting can
1014 even be generated along inclined or bent surfaces using thin-film materials such as AlN/Si
1015 Rayleigh SAW device ²¹⁴.

1016 With a single IDT, the droplet is generally ejected along the Rayleigh angle (e.g., 23° on a 128°
1017 Y-X LiNbO₃ substrate) in the SAW propagation direction. Vertical jetting phenomena can be
1018 generated from an SH-SAW device with a single straight IDT made on a 36° Y-X LiTaO₃
1019 substrate, which is drastically different from those from the conventional Rayleigh SAWs
1020 ^{220,221}. The SH-SAW propagates with a relatively shallow energy penetration into the droplet.
1021 The energy and pressure are distributed randomly between the droplet and the surface in the
1022 whole contact area. The wave energy/pressure is mainly concentrated at the center of the
1023 droplet and vertically dissipated, causing vertical jetting ²²¹.

1024 Focused IDTs can generate increased concentration for droplet jetting and ejecting applications
1025 ²⁹, which can be significantly affected by the substrate's wettability ¹²¹. A pair of FIDTs can
1026 extend a pendulous droplet to form a liquid bridge with a second substrate underneath it. This
1027 straightforward method makes it possible to build capillary bridges for the low viscosity
1028 liquids, such as water, to investigate their capillary-thinning behavior ²²².

1029 Single droplets can be ejected into the air by also using a pair FIDTs (Figure 8(e)), where the
1030 droplet size can be adjusted by the pulse width duration, and on-demand repetitive droplet
1031 ejection can be managed by continuously resupplying a parent drop reservoir ²²³. Such device
1032 can also be used to enable the encapsulation of single CTCs ²²⁴⁻²²⁶ and rare cryopreserved cells
1033 ²²⁷, as well as an acoustic droplet-based printing of tumor organoids ³⁹ and tumor
1034 microenvironment ²²⁸. Acoustic single-cell printing provides the ability to study cell

1035 heterogeneity toward the development of personalized cancer medicine and predicting the
1036 responses of tumors to therapy ³⁹. Such a nozzle-free, contact-free, and low cell-damage
1037 method will surely advance the bioprinting technology. However, it should be noted that there
1038 is a significant temperature increase of an FIDT device in water, and thus issues about high-
1039 temperature sensitivity of biological tissues and cells should be considered ²²⁹. Single straight
1040 IDTs can also be patterned on the underside of a chip and generate surface reflected bulk waves
1041 (SRBWs) on a hybrid resonant acoustic (HYDRA) platform (Figure 8(f)) ²³⁰. This specially
1042 designed droplet ejecting method can protect the device as the liquid does not need to contact
1043 directly with the IDT or piezoelectric substrate ²³¹, and thus enables a modular and
1044 reconfigurable platform with individual chips in a 96 well plate.

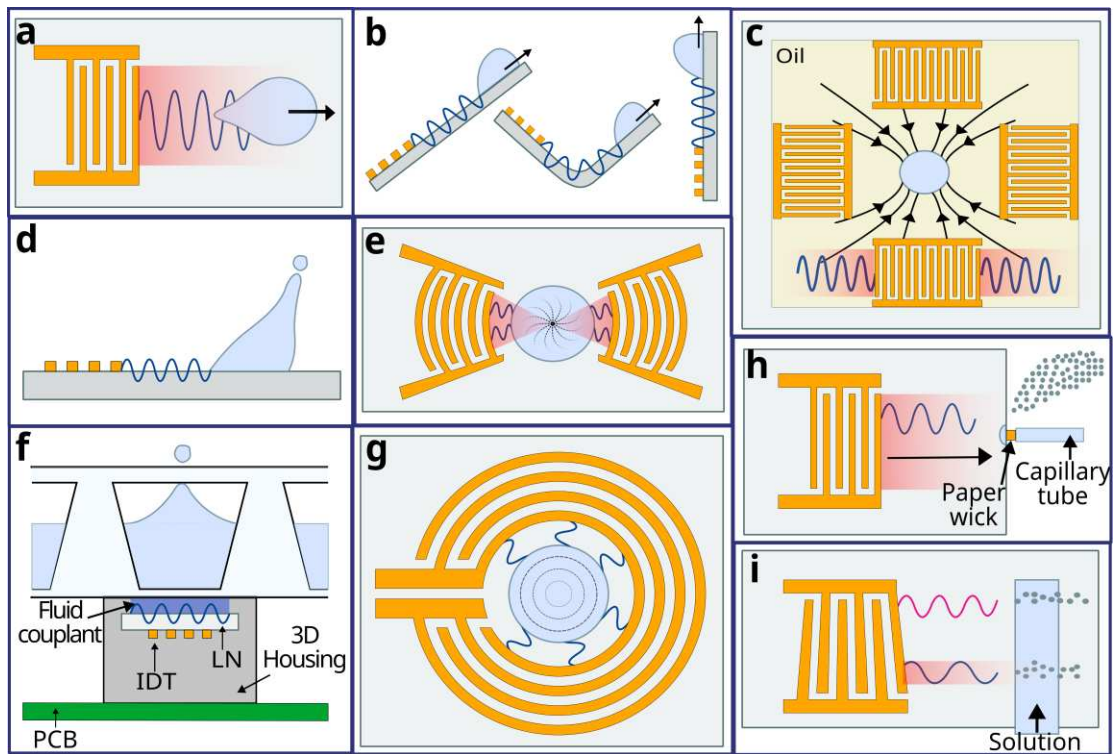
1045 Focused SAWs induced jetting can be easily generated using the annular pattern IDTs (Figure
1046 8(g)). For example, a sample reservoir on top of a piezoelectric substrate with an AIDT can
1047 form picolitre (24 pL) droplets within 10 ms and encapsulate a single cells ²³². Multiple AIDTs
1048 can be combined to create a 4×4 two-dimensional ejector array which can generate drop-on-
1049 demand and continuous mode of operation 28 μm diameter droplets ²³³. This open pool and
1050 nozzleless reservoir means that droplet directionality is easily controllable with reliable
1051 ejection outcomes. Nevertheless, as mentioned previously, due to the significant anisotropic
1052 effect of such piezoelectric materials, unique designs are needed to correct the differences in
1053 acoustic velocities for an efficient or focused effect, leading to more complex modelling and
1054 mask designs ²³⁴.

1055 Thin-film SAW devices such as using ZnO or AlN ²³⁵ not only have isotropic wave velocities
1056 but offer higher power handling capability. In-plane isotropic ZnO/Si circular SAW with an
1057 AIDT can produce vertical droplet jetting. Compared with 128° Y-X LiNbO₃ AIDT, ZnO
1058 annular SAW shows controllable, concentrated, thin liquid generated, whereas LiNbO₃ does
1059 not result in a highly concentrated thin liquid column ³⁰. However, the electro-mechanical
1060 coupling coefficient of ZnO SAW device is much lower than that of 128° Y-X LiNbO₃, thus
1061 the jetting could be relatively weak ²³⁶. The jetting efficiency can be improved by introducing
1062 an ultra-smooth nanocrystalline diamond (UNCD) interlayer to a ZnO/Si device ²³⁷, which can
1063 help to increase the amount of the SAW energy transferred from the solid surface to the liquid
1064 medium.

1065 **Nebulization**

1066 Atomization and nebulization are methods to generate fine aerosol droplets important for
1067 numerous applications where small, similar-sized droplets are needed, such as spray cooling,
1068 inhalation therapy for drug delivery, mass spectrometry and bioprinting. Compared to other
1069 methods, they can generate monodispersed microdroplets with minimal shear and cavitation,
1070 preventing biomolecule damage due to their high frequencies and low powers. Nebulization
1071 can be carried out directly from the substrate using a single IDT (Figure 8(h))^{238–241}. For
1072 example, such a device has been demonstrated to nebulize epidermal growth factor receptor
1073 monoclonal antibodies into a fine aerosol mist for pulmonary delivery, which is beneficial for
1074 lung cancer treatment³². Moreover, a single IDT can use a SRBWs to achieve higher output,
1075 greater efficiency and efficacy. This type of wave propagates along and through the substrate,
1076 therefore it can draw the solution from a vial through the needle in contact with the substrate,
1077 and then nebulize the liquid²⁴². Therefore *in vitro* pulmonary delivery of antibiotic alternatives
1078 can be successfully achieved against *Staphylococcus aureus*³⁸ as well as *in vivo* human lung
1079 deposition²⁴².

1080 The droplet size of mist generated by atomization can be controlled by adjusting the physical
1081 properties of the liquid and the input power to the device³². For example, thin-film liquid
1082 geometries can lead to smaller droplets and higher atomization rates, mainly due to the higher
1083 frequency used and much concentrated effects on the surfaces³¹. A thin graphene film
1084 deposited on 128° Y-X LiNbO₃ combined with an focused SPUDT can have up to 55%
1085 enhancement in the rate of fluid atomization²⁴³. Based on a comparison of SAW atomization
1086 for spray cooling with a focused SPUDT versus a SF-IDT, the focused SPUDT achieves higher
1087 efficiency. However, the SF-IDT allows placement of atomization at a specific location within
1088 the SAW device (Figure 8(i))²⁴⁴. By using a pair of FIDTs on a ZnO/Si device with a relatively
1089 large arc angle (90°) of the IDT, it is possible to achieve an increased nebulization rate, reduced
1090 critical powers required to initialize nebulization, and concentration of the nebulized plume
1091 into a narrower size of spray³⁴.



1092

1093 Figure 8. Pumping, jetting and nebulization for digital acoustofluidics IDT device examples.
 1094 (a) Singular straight IDT on a horizontal surface and (b) inclined, curved, vertical, inverted and
 1095 lateral surface for TSAW droplet transport ⁴⁰. (c) One unit consisting of a four straight IDT
 1096 array (one pixel) for digital microfluidics ¹⁷⁷. (d) Singular straight IDT and (e) pair of FIDT
 1097 for TSAW droplet jetting. (f) Singular Straight IDT on the underside of a chip for SRBW
 1098 HYDRA Platform droplet ejecting ²³⁰. (g) An annular IDT for TSAW droplet jetting ²³². (h)
 1099 Singular straight IDT and (i) SF-IDT for TSAW nebulization.

1100 **5.1.3. Mixing, concentration, and rotation of liquid in chamber/channel for continuous**
 1101 **acoustofluidics**

1102 **Mixing**

1103 When mixing in a microchannel or a chamber, it is convenient to use a straight IDT to overcome
 1104 diffusion limitations in the microscale liquid. It can support nanoparticle production ²⁴⁵ or
 1105 increase reaction yield in the microchannel for biosensing applications ²⁴⁶. When this
 1106 configuration is combined with a surface plasmon resonance microfluidic sensor, SAW mixing
 1107 can aid in alternative applications such as surface chemical and biochemical functionalization
 1108 by improving functionalization efficiency up to 5 times with respect to that without using
 1109 SAWs ²⁴⁷. The key parameters to control acoustic mixing in microchannels are the SAW
 1110 power, flow rate and fluid viscosity ^{245,248}. A SAW device with a thick PDMS channel can lead
 1111 to acoustic wave attenuation and hence much SAW power could be lost. A single IDT can also
 1112 be used directly underneath a PDMS microchannel to generate strong acoustic streaming for
 1113 fluid mixing, and using this method, a total flow rate of 50 $\mu\text{l}/\text{min}$ at a low power consumption

1114 (e.g., 12 V_{pp}) can be achieved²⁴⁹. To control mixing speed and flow patterns, an SF-IDT was
1115 used to optimize SAW amplitude and frequency due to the narrow SAW beam and variable
1116 launching point^{144,250,251}.

1117 When comparing FIDTs with the straight IDTs, the focused acoustic radiation creates a high
1118 acoustic wave intensity that enhances mixing performance in a specific microchannel region
1119 (Figure 9(a))²⁵². For example, a 100.4 MHz single FIDT device can apply considerable
1120 pressure to a small region that can be focused on a water droplet on an ultrasonic couplet
1121 between a SAW device and a cell culture dish, which can facilitate the local removal of cells
1122 from a culture surface⁴². A singular FIDT can be used with a dome-shaped chamber, and can
1123 achieve mixing ratio higher than 0.9 at a total flow rate of 300 μl/min at 20 V⁴¹. The chamber
1124 acts as a more stabilized droplet that maximizes the effect of SAW transmitted at a refraction
1125 angle of roughly 22° with a contact angle of 68°.

1126 To enhance mixing effects, one could consider the addition of bubbles in the channel^{253–257}. If
1127 these trapped air bubbles are excited by acoustic waves at their resonance frequency, acoustic
1128 streaming is induced and the fluid mixing is improved by disrupting the laminar flow. For
1129 example, this method can mix highly viscous fluids within 50 milliseconds²⁵⁵. Nevertheless,
1130 there are concerns of bubble instability, heat generation, and inconvenient bubble trapping
1131 processes; hence other methods to enhance streaming based mixing should be considered. The
1132 geometry of the channel plays a crucial role in acoustic streaming vortices and mixing. For
1133 example, using a sharp edge^{258–267} a large Reynolds body force can be generated if compared
1134 to using a non-sharp edge²⁵⁸, and this has proven effective in mixing²⁶⁵, cell lysis²⁶⁸, pumping
1135²⁶⁹ and rotation^{270,271}. Such acoustic streaming enhancement is not limited to sharp edges, and
1136 other microstructures^{272,273} such as microcylinders^{274–276}, micro square pillars²⁷⁷, and micro
1137 parallelepipeds^{273,278} can also be applied.

1138 The mixing efficiency could also be improved using three-dimensional dual SAWs generated
1139 from two focused SPUDT devices. Each of them was patterned on a piezoelectric substrate,
1140 thus achieving 100% mixing efficiency at a flow rate of 50 μl/min for 14 V or 95.6% efficiency
1141 at a flow rate of 120 μl/min for 18 V²⁷⁹. Hence, two focused acoustic waves were introduced
1142 from the top and bottom substrates in diagonally opposite directions, and induced micro
1143 swirling with the same rotational direction, which enhanced mixing performance²⁷⁹. It should
1144 be noted that although the techniques mentioned above contain the typical solid metal

1145 electrodes, other materials such as a conductive liquid-based FIDT can be used, which achieved
1146 a mixing efficiency higher than 90% at a flow rate lower than 120 $\mu\text{L}/\text{min}$ and 21 V ²⁸⁰.

1147 SAW can induce vibrational mixing by using SAW devices with high frequencies and lower
1148 continuous powers, compared to lower frequencies or with short but very intense pulses. Low
1149 frequencies have longer attenuation path lengths that can produce strong reflections, hence
1150 creating dominant SSAWs that suppresses the acoustic streaming. Unlike using short but very
1151 intense pulses, using low power by continuous signals is beneficial for applications which need
1152 mechanical stimulations, yet ensure that both cavitation and heating are negligible. For
1153 example, low power and single 100 MHz SAW device was used for vibration enhanced cell
1154 growth ²⁸¹. A 20 MHz device was used for accelerated neural differentiation of human
1155 embryonic stem cells ¹⁷⁹. Another 30 MHz FIDT device at 20% duty cycle was used to trigger
1156 intracellular calcium responses in HEK293T ²⁸². Due to the absence of cavitation generated at
1157 such a low power and high frequency, the 30 MHz focused SPUDT can effectively enhance
1158 the uptake of difficult-to-transfect nonadherent cell lines such as suspension T cells in just 10
1159 min of exposure while maintaining high cell viabilities (>91%). This is much better if compared
1160 to other methods such as conventional nucleofection of 76%, which is one of the most widely
1161 used intracellular delivery methods ²⁸³.

1162 **Concentration and separation**

1163 Concentration of particles and cells within a channel and then separation have been typically
1164 realized using acoustic radiation forces ¹⁰² with SSAWs, where the objects migrate toward
1165 minimum PNs or ANs. This methods allows for concentrating and separating extracellular
1166 vesicles ^{284 285} and CTCs ^{286 287}. Nevertheless, there was also reports that a single IDT with a
1167 designed frequency of 49.5 MHz can be used to generate TSAW for separation of 10 and 25
1168 μm particles in a microchannel ¹⁷⁸. A combination of acoustic radiation force and acoustic
1169 streaming force can also be realized in multi-stage acoustic devices (Figure 9(b)). For example,
1170 Wang *et al.* uses a pair of straight IDTs to generate SSAW to focus CTCs and RBCs at the
1171 pressure nodes without the requirement of the sheath flow, and the pulsed focused TSAW uses
1172 acoustic streaming to push the CTCs away from RBC for CTC isolation ²⁸⁸. If a pair of
1173 opposing straight IDTs are of different frequencies, two counterpropagating decaying TSAWs
1174 would be produced which can be used for particle sorting. This method allows a much longer-
1175 range force field, in which migration takes place across multiple wavelengths, and causes
1176 particles to be gathered together in a single trapping site ²⁸⁹.

1177 Large amplitude and high frequency FSAWs cause strong acoustic streaming to generate fluid
1178 streamlines and vortices. This allows for functions such as size selective aggregation down to
1179 300 nm in a closed channel ²⁹⁰, selective capture of 2 μm particles from mixing suspension of
1180 1 μm particles in a continuous flow ²⁹¹, and constant differential focusing of nanometer
1181 particles in a continuous channel (see Figure 9(c)) ¹¹. This configuration can be combined with
1182 hybrid microfluidic cell sorting techniques such as using a reverse wavy ²⁹² or spiral ²⁸⁷
1183 microchannel for passive inertial cell enrichment and as well as active TSAW single cell
1184 sorting. It could be a promising solution for practical biomedical applications as it provides
1185 high throughput and high accuracy isolation of rare cell populations.

1186 **Rotation**

1187 The same approach, by which IDTs can generate an acoustic streaming vortex in a channel,
1188 enables contactless rotation of small veritable models ^{37,270}. Such rotational tweezing enables
1189 high-speed, 3D multispectral imaging and digital reconstruction, which yields accurate 3D
1190 models for quantitative evaluation of morphological characteristics and advanced
1191 combinations metrics useful for small organism phenotyping, screening, and microsurgery. For
1192 example, rotation of *Caenorhabditis elegans* can be achieved by simply using a pair of straight
1193 IDTs with a frequency 19.32 MHz and activating one at a time to create a single vortex and
1194 hence rotate along the corresponding acoustic streaming direction ³⁷. However, the vortex size
1195 is limited and insufficient to rotate large organisms in the millimeter scale. Rotating larger
1196 organisms, such as zebrafish larvae are commonly used in rapid drug screening and disease
1197 evaluation, hence it is vital to develop functional platforms for clear visualization and accurate
1198 analysis for high throughput phenotypic evaluations. Quantification and 3D reconstruction can
1199 be achieved by rotating the zebrafish larvae using a straight IDT and a patterned fluidic channel
1200 aligned on and parallel to the lateral side of the IDT with half of its width on the IDT ³⁶ (Figure
1201 9(d)). The fluid above the IDT forms a strong, stable, and consistent single unidirectional
1202 vortex pattern ³⁶.

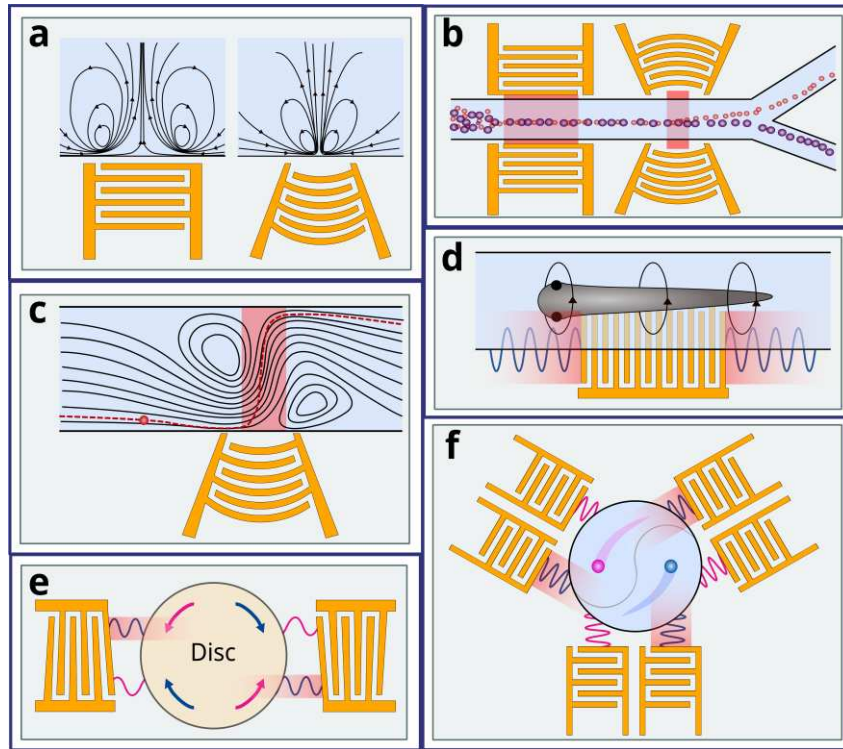
1203 The designed rotation mechanism can be used to manipulate and drive objects, such as a
1204 centrifugal microfluidic platform. For example, a miniaturized lab-on-a-disc (miniLOAD)
1205 SAW device with two offset FIDTs was reported in Ref. ²⁹³. The acoustic streaming drove the
1206 rotation of thin millimeter discs atop of a fluid coupling layer, on which microchannels was
1207 fabricated so that operations can be achieved. By adding a second pair of opposing offset
1208 FIDTs, the rotational velocity and direction of the disc can be controlled by altering the input

1209 frequency to the transducer ²⁹⁴. Moreover, a pair of opposite SF-IDTs can be used for the
1210 miniLOAD device to alter the frequency when a disc of a different size needs to be used (Figure
1211 9(e)) ²⁹⁴.

1212 Compared to these large-scale structures, precise rotation and manipulation of microparticles
1213 in a channel need precisely controlled. For example, using six IDTs (divided into two sets) and
1214 symmetrically distributed around an annular shaped changer at an angle of 120° can lead to tri-
1215 directional symmetrical acoustic tweezer ²⁹⁵ as shown in Figure 9(f). Here the TSAWs are
1216 generated to precisely control microparticle movements which allows programmable motion
1217 control by switching the excitation combinations of IDTs, producing linear, clockwise, and
1218 anticlockwise trajectories. An array of IDTs, designed in relation to the anisotropic properties
1219 of the substrate, can also produce similar swirling acoustic vortices for fluid actuation and
1220 particle manipulation ¹⁵⁸. Similarly, an array of piezoelectric transducer plates can produce
1221 stable and symmetric pairs of vortices to create hydrodynamic traps for object manipulation²⁹⁶.
1222 In fact, acoustic tweezers can be achieved without a complex transducer array and yet
1223 manipulate a wide range of particle sizes. With a single transducer, the acoustic radiation force
1224 in two dimensions is combined with an acoustic streaming vortex for levitation in the third
1225 dimension²⁹⁷.

1226 **Droplet manipulation**

1227 Fluid in a droplet form in another liquid within a microchannel can be controlled through
1228 acoustic streaming. For example, an SF-IDT in an H-shaped junction for the regulated flow
1229 switching between two fluid streams ⁴³. Likewise, liquid droplets in a microchannel can be
1230 precisely controlled for applications such as isolated microenvironments without cross-
1231 contamination ²⁹⁸. It was reported that droplets can be selectively merged using an SF-IDT to
1232 trigger the biochemical reactions ^{299 298}, encapsulate samples ³⁰⁰, or using an FIDT to
1233 selectively dispense based on their volumes ³⁰¹. Nanoslit channels have also been created and
1234 combined with the TSAW streaming to perform notoriously difficult nanoscale manipulation
1235 due to the dominance of surface and viscous forces ^{302,303}. Using a straight IDT, controllable
1236 manipulation of 200 fl ³⁰² and 10 fl ³⁰³ droplets in a nanofluidic channels have also been
1237 achieved. The ability to manipulate droplets in these nanostructures makes it useful for
1238 increasing the sensitivity of analytical tools for applications such as medical diagnostics and
1239 personalized treatments.



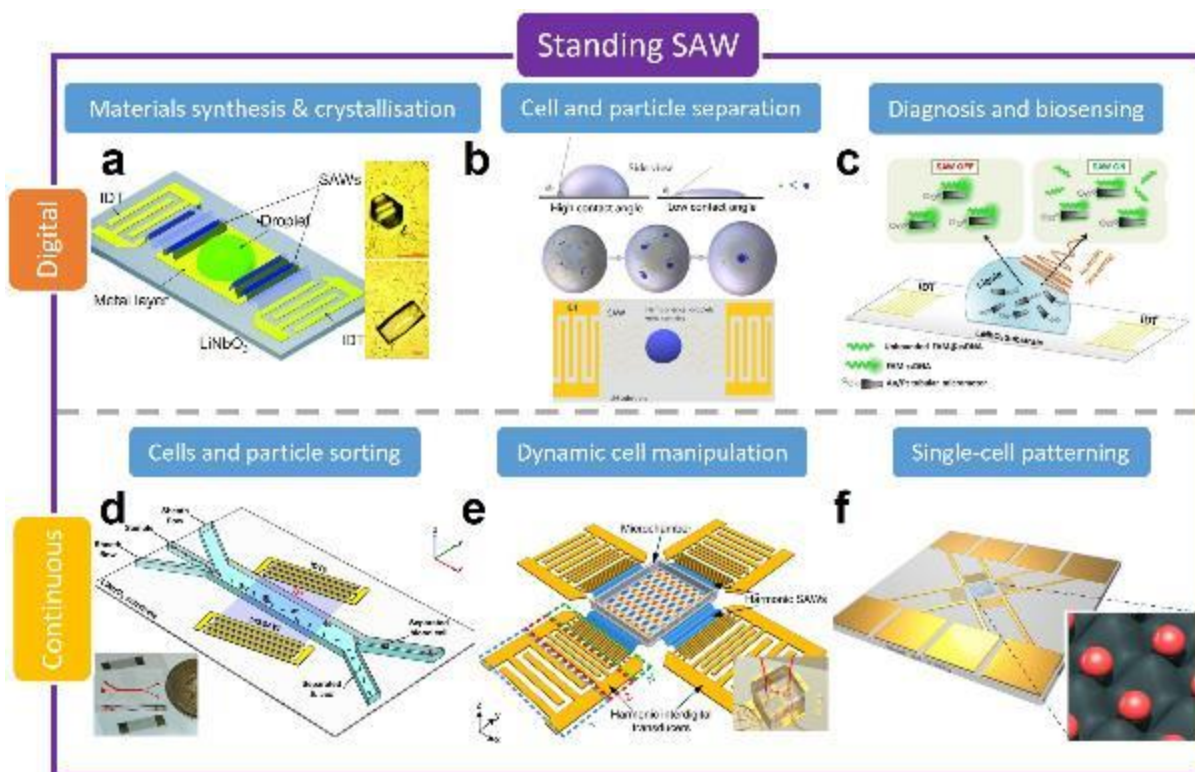
1240

1241 Figure 9. Mixing, concentration, and rotation of liquid in chamber/channel IDT device
 1242 examples. **(a)** The acoustic streaming generated by straight vs. focused IDT in a closed channel.
 1243 **(b)** Multistage device for tumor cell isolation. The device consists of pair of straight IDTs for
 1244 SSAW concentration and a pair of FIDT for TSAW isolation. **(c)** The acoustic streaming of a
 1245 focused IDT in a continuous flow, acting to direct particle laterally **(d)** Rotational manipulation
 1246 of zebrafish larvae ³⁶. The device consists of a straight IDT and a patterned fluidic channel
 1247 aligned on and parallel to the lateral side of the IDT with half its width on the IDT. **(e)** A pair
 1248 of SF-IDT for bidirectional rotating of a thin disc over of fluid coupling layer. **(f)** Tri-directional
 1249 symmetrical acoustic tweezers for programmable trajectory manipulation ²⁹⁵. The device
 1250 comprises six IDTs (divided into two sets) and is symmetrically distributed around an annular-
 1251 shaped changer at an angle of 120°.

1252

1253 5.2. SSAWs based streaming and acoustofluidics

1254 As mentioned previously in Section 2, when two oppositely propagating TSAWs interfere each
 1255 other, SSAWs are created. These SSAWs produce PN and ANs between two IDTs, which are
 1256 often used for particle manipulation, separating, sorting, and patterning. Additionally, SSAW
 1257 can produce acoustic streaming in the fluid which can be used for mixing. Examples of typical
 1258 medical SSAW applications for digital and continuous acoustofluidics are shown in Figure 10.
 1259 These are consisted of materials synthesis and crystallization (Figure 10(a)), cell and particle
 1260 separation (Figure 10(b)), diagnosis and sensing (Figure 10(c)), cells and particle sorting
 1261 (Figure 10(d)), dynamic cell manipulation (Figure 10(e)) and single-cell patterning (Figure
 1262 10(f)).



1263

1264 Figure 10. Examples of real-life medical applications of SSAW streaming, for both digital and
 1265 continuous acoustofluidics. **SSAW digital ones:** (a) A SSAW device with drop of glycine
 1266 solution for crystallization.³⁰⁴ Reproduced from CrystEngComm 20, 1245 (2018) with the
 1267 permission of The Royal Society of Chemistry. (b) SSAW device for cell and particle
 1268 separation by modification of the droplets contact angle.³⁰⁵ Reproduced with permission from
 1269 Sensors and Actuators A: Physical 326, 112731 (2021). Copyright 2021 Elsevier. (c) SSAW
 1270 device for the removal of molecules that are unbound to micromotors, realized for lowering
 1271 the detection limit of the cancer-related biomarker miRNA-21³⁰⁶. Reprinted with permission
 1272 from G. Celik Cogal, P.K. Das, G. Yurdabak Karaca, V.R. Bhethanabotla, and A. Uygun
 1273 Oksuz, ACS Appl. Bio Mater. 4, 7932 (2021). Copyright 2021 American Chemical Society.
 1274 **SSAW continuous ones:** (d) A taSSAW device for sorting of *E. coli* from human blood
 1275 samples.³⁰⁷ Reproduced with permission from J. Micromech. Microeng. 27 015031 (2017).
 1276 Copyright 2017 IOP Science. (e) Harmonic IDTs for harmonic SAWs generation, achieving
 1277 dynamic and selective particle manipulation³⁰⁸. Reproduced with permission from Nat. Mater.
 1278 21, 540–546 (2022). Copyright 2022 Springer Nature. (f) A two-dimensional SSAW device,
 1279 with four IDTs, for one cell per acoustic well patterning.³⁰⁹ D.J. Collins, B. Morahan, J.
 1280 Garcia-Bustos, C. Doerig, M. Plebanski, and A. Neild, Nat Commun 6, 8686, 2015; licensed
 1281 under Creative Commons Attribution (CC BY) license.

1282

1283 5.2.1. SSAW induced droplet streaming in digital acoustofluidics

1284 When SSAWs generated using a pair of IDTs actuate a sessile droplet, it results in symmetric
 1285 acoustic wave propagations and creates a strong acoustic streaming force inside droplet, even
 1286 though the droplet might not be easily moved. Therefore, SSAW induced streaming is
 1287 beneficial for stable mixing and jetting of sessile droplets. For example, SSAW mixing can

1288 increase the kinetic effect to influence the recrystallization process of metal organic
1289 frameworks (the best-known being HKUST-1 crystals)³¹⁰ and glycine³⁰⁴ with different
1290 morphologies and sizes in a droplet, as well as isolate sodium chloride crystals in a drying
1291 droplet³¹¹. This mixing effect has great potentials in drug delivery and/or release for
1292 pharmaceutical industry. The SSAW induced mixing allows for direct, safe and high efficiency
1293 mixing, facilitating the dynamic cell culture³¹², labelling of nanoparticles³¹³, or lowering the
1294 detection limit for biomarkers³⁰⁶. SSAW generated using a pair of small-aperture-straight-
1295 electrodes (SASE) in a vertical capillary tube has also been utilized for standardized and
1296 controllable droplet jetting³¹⁴. The SASE device has a higher energy density output
1297 performance and higher driving capability than large aperture SAW devices which ensures
1298 energy concentration and more standardized wave paths³¹⁴.

1299 Although droplet transport in liquid within channel is not as easily achieved with SSAWs, it
1300 can be achieved by SSAW induced streaming using a pair of straight IDTs in conjunction with
1301 anisotropic ratchet conveyors, which use hydrophilic patterns of background to control the
1302 directional movement of the droplet transport (Figure 11(a))³¹⁵. Additionally, this
1303 configuration can confine the droplet position to allow for nebulization controlled by the SAW
1304 frequency³¹⁵. Scattered SSAWs can be produced using pairs of opposing IDTs and nickel pillar
1305 type crystals to control the SAW field (Figure 11(b)). In a sessile droplet, the SSAW can
1306 simultaneously induce strong acoustic streaming localized on half a region and directional
1307 propagating longitudinal acoustic waves³¹⁶. This mechanism has been used for concentration
1308 and separation of 2 and 20 μm PS particles in a microliter droplet³¹⁶. SSAW based
1309 concentration and separation inside a sessile droplet may also be realized by adjusting the
1310 contact angle of the droplet³⁰⁵.

1311 **5.2.2. SSAW induced streaming in microchannel for acoustic tweezers in continuous** 1312 **acoustofluidics**

1313 The simplest way to generate SSAWs is by using a pair of IDTs. Two counter propagating
1314 waves interact, forming a time-averaged nodal and anti-nodal periodic patterning positions
1315 across the entire channel¹⁷⁴. Therefore, SSAWs can easily create one dimensional nodal lines
1316 inside channels or chambers³¹⁷ for applications such as separation of encapsulated cells³¹⁸,
1317 extracellular vesicles^{284,285} or CTCs^{286,287}. For example, tunable cell sorting of human white
1318 blood cells (WBC) (15 μm) and fluorescent PS beads (10 μm) was achieved using a pair of
1319 chirped IDT and a multi-channel sorting device³¹⁹. This was further developed by acoustically

1320 sorting different sizes such as platelets, RBCs and WBC ³²⁰. Tilted angle SSAWs ³²¹ (Figure
1321 11(c)) can be used to increase separation differences between similar sized particles, hence it
1322 can be used for cancer cell manipulation ³¹⁷ and separating exosomes from whole blood ³²².
1323 Phase modulation-based SSAW techniques are another advanced method to increase separation
1324 throughput as it uses multiple pressure nodes without the need to increase channel width ^{323–}
1325 ³²⁵.

1326 Multiple IDTs can be easily integrated for such applications, for example, two pairs of IDTs
1327 can be used to achieve multi-stage SAW concentration and separation (Figure 11(d)) ^{326–328}.
1328 The first stage is consisted of a pair of IDTs for particle/cell sorting by SSAWs. The second
1329 stage is consisted of an IDT, such as a straight IDT, SF-IDT or F-IDT to form TSAWs for
1330 particle/cell deflection ^{288,329,330}. Conventional SSAWs result in particle and cell patterning
1331 across the entire width of a microfluidic channel, preventing selective trapping, whereas
1332 applying nanosecond-scale pulses can generate localized time-averaged patterning regions for
1333 selective trapping ³³¹.

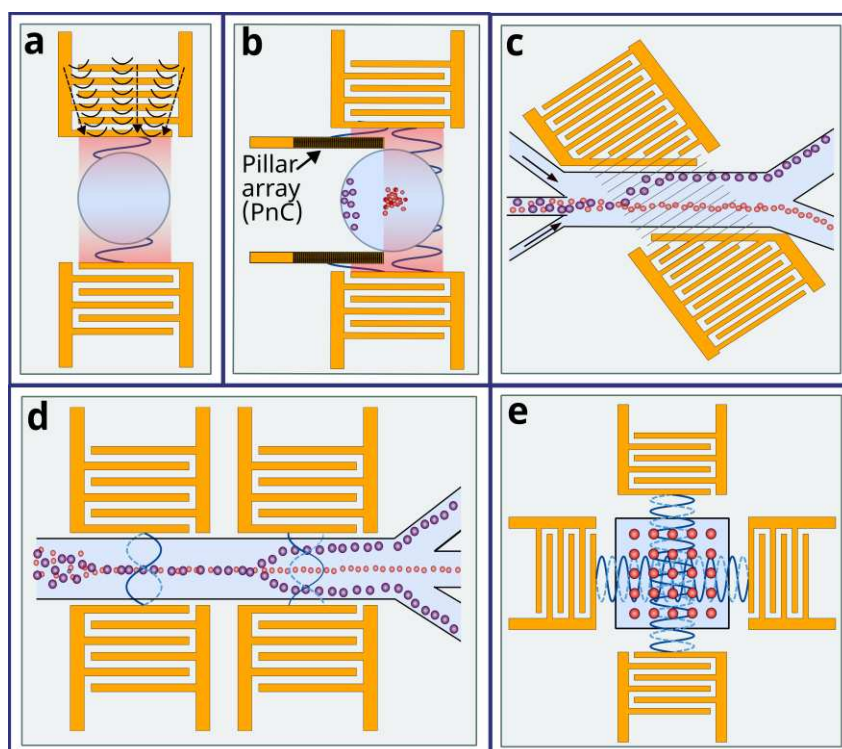
1334 Additional IDTs, for example, two orthogonal pairs of IDTs (Figure 11(e)), ^{27,332} can be used
1335 to form a 2D pattern of nodes and antinodes for particle manipulation ^{309,333,334}. The 3D spatial
1336 distribution of the cells, and preserve the viability and functionality of the patterned cells
1337 suitable for tissue engineering applications. In such an orthogonal pair IDT setup, intelligent
1338 modulation of harmonic waves can be used to generate time-effective Fourier-synthesized
1339 acoustic potential wells, allowing particles/cells in suspended fluids and acoustic lattices to be
1340 spatially controlled and reconfigured ³⁰⁸. Additionally, SSAW generated by SF-IDT can
1341 spatially localize cells encapsulated within a gelatibe methacryloyl hydrogel matrix ³³⁵. SSAWs
1342 allow particles and cells to be patterned into 3D spatial lines or crystal-lattice-like matrix
1343 patterns in chambers of millimeter height ³³⁶ (for example, such a chamber is large enough for
1344 entire organism manipulation of *Caenorhabditis elegans*) ¹⁴¹, or formation of multicellular
1345 spheroids ^{337,338}. These SSAW 3D patterns have also been effectively realized using alternative
1346 piezoelectric thin film SAW platform such as ZnO or AlN films, instead of LiNbO₃ ³³⁹.

1347 Acoustic tweezers with generated torque forces using SSAWs could be obtained using a
1348 temporal phase lag between the two standing waves, leading to a complex pressure field. The
1349 superimposed acoustic streaming induced fluid motion creates stable 3D trapping nodes within
1350 a chamber. This method allows for single cell manipulation ³⁴⁰ and controlled rotation and
1351 translation of spherical particles or living cells in a 3D format ³⁴¹. A wave number-spiral design

1352 for acoustic tweezers can enable frequency-based steering of SSAWs for simultaneous and
1353 independent control. This method only needs two multitone excitation signals which enables
1354 the resultant SAW wavefields to be dynamically reshaped without using complex and costly
1355 electronics¹⁵².

1356 SSAWs can also influence the fluid streaming patterns in a chamber. For example, the mixing
1357 performance with two opposing parallel straight IDTs (96.7%) is much higher than with one
1358 straight IDT (69.8%) as the same applied voltages (85 V_{p-p}) and flow rates (10 μl/min)³⁴². The
1359 mixing behavior induced by SSAW acoustic streaming can be beneficial in preventing particle
1360 deposition in a microchannel³⁴³, or generating microextraction functions for biochemical
1361 analysis applications^{344,345}.

1362 In brief, acoustic tweezers with functions for patterning and particle manipulation based on
1363 SSAWs have been a research hot topic in the acoustofluidic field, and have been
1364 comprehensively reviewed in many papers^{22,24,49,346–348}. Therefore, this paper will not discuss
1365 further. For these developments and readers should refer to the above or other review papers
1366 for more information.



1367
1368 Figure 11. SSAW induced droplet streaming in digital acoustofluidics and microchannel for
1369 acoustic tweezers in continuous acoustofluidics IDT device examples. (a) A pair of straight
1370 IDTs and anisotropic ratchet conveyors for controllable droplet transport³¹⁵. (b) A pair of
1371 straight IDTs and nickel pillar-type crystal arrays (PnC) which obstruct the lower half of SSAW
1372 to produce scattered SSAW for particle concentration and separation³¹⁶. (c) Tilted angle

1373 SSAW³¹⁷ and (d) Multi-stage SSAW using two pairs of straight IDTs for particle separation.
1374 (e) Two orthogonal pairs of IDTs for SSAW particle manipulation (acoustic tweezers).

1375

1376 **6. Summary and future prospects**

1377 This review aims to elucidate the underlying mechanisms, design methodology, techniques,
1378 and applications of acoustic streaming for various acoustofluidic applications. SAW
1379 technology is in high demand due to its function as both sensors and actuators in various
1380 disciplines. It offers efficient, non-invasive, and biocompatible devices that are valuable for
1381 biological research and clinical applications such as diagnosis and therapeutics, health
1382 monitoring, and biosampling/treatments. IDTs have their own developed design criteria
1383 whereby the IDT materials and geometries, as well as the piezoelectric material, can be
1384 changed, allowing for various functions of manipulation control for specific applications. Not
1385 only can the device be designed for a specific application, but also it is possible to design
1386 programmable features useful for microfluidic processing in applications such as on-chip
1387 bioassays, high throughput compound screening and biochemical synthesis. They can also
1388 achieve single droplet processing strategies that follow a digital logic rule. The highly sensitive
1389 and selective yet simple and low-cost nature of IDTs makes them suitable for lab-on-chip and
1390 point-of-care devices.

1391 Acoustic streaming generates regions of recirculation or pressure gradients that lead to rapid
1392 and localized motion, allowing it to manipulate particles, such as patterning, concentration, and
1393 separation. Such the manipulation is useful for applications such as CTC separation, single cell
1394 analysis and even submicron manipulation of exosomes. Acoustic streaming can also generate
1395 acoustic pressure or force to perform operations such as deformation, transportation, and
1396 manipulation of bulk fluid in a droplet format, namely jetting, nebulization or atomization,
1397 microscale streaming, and object rotation. This establishes advanced technologies, such as 3D
1398 bioprinting or rotational tweezing for 3D multispectral imaging and digital reconstruction of
1399 models.

1400 In brief, this review paper provides qualitative and quantitative descriptions of the acoustic
1401 streaming mechanism and recent developments. It presents a snapshot of its remarkable
1402 contributions to biomedical research and clinical science. Despite this review showing that
1403 much has been accomplished with acoustic streaming-based acoustofluidics, it is important to
1404 address that there is a huge amount of work to be done. Some major topics for future
1405 development are highlighted as follows.

1406 **Mechanisms, theory, and modelling**^{2,27,50} –

- 1407 • Analysis techniques need to be further improved. This is because the basic equations
1408 used in the analysis have borrowed directly from the classic derivations, which are
1409 convenient but might not be accurate for micro or nanoscale acoustofluidics.
- 1410 • There are specific topics which need to study, for example, nonlinearity, viscous,
1411 boundary, inertia, and temperature effects and strongly chaotic phenomena of the waves
1412 propagating inside the fluids and its effects on the fluid and particles movements and
1413 flow.
- 1414 • Studies need to be focused on improving computational modelling for acoustic
1415 streaming problems in three dimensions for mixed fluids, geometries, and frequency
1416 regimes, as well as the nonlinear interactions between the liquid and particles⁵⁰.
- 1417 • The large discrepancy in time and space domains between the driving SAW and the
1418 resulting liquid streaming which remains poorly understood. Hence challenges with
1419 numerical computational simulations as a very small time step and a very fine mesh are
1420 required to capture the SAW actuation of the liquid, but the resulting streaming occurs
1421 over a relatively large time scale and large spatial dimensions²⁷.
- 1422 • Biological effects of acoustic actuation should be studied at microscopic and
1423 nanoscopic length scales and at various time scales.
- 1424 • Effective nanofabrication and measurement techniques should be utilized to construct
1425 nanofluidic devices and study their nanoscale acoustofluidic behaviors.

1426 **Device and technique innovations** –

- 1427 • Various substrates and thin film materials, such as those for flexible or wearable ones,
1428 polymer-based or hybrid materials with tailored acoustic properties, or new functional
1429 platform (e.g., phononic crystals) should be explored for new applications.
- 1430 • Alternative materials such as electroactive polymer materials technologies apart from
1431 a piezoelectric material, or electrets (which have properties much like human muscle
1432 tissue) could be explored to design and transform energy between electrical and
1433 mechanical forms comparable to piezoelectric materials.

- 1434 • Disposable superstrates should also be investigated, such as a traditional Petri dish^{312,349}
1435 or multi-well plates³⁵⁰, which can make a single SAW-based device reusable and
1436 economical by exchanging the superstrates²⁷.
- 1437 • Alternate acoustic modes other than SAWs and BAWs could also be explored, which
1438 offer unique innovations²⁷, such as flexural waves^{351,352} (Wedge acoustic waves) with
1439 acoustic black holes³⁵³.
- 1440 • Improving heat management methods⁵⁰ is important as the heat can affect the sound
1441 velocity and hence the resonant frequency. Additionally, heating control is valuable as
1442 streaming relies on the acoustic wave being attenuated.

1443 **Standardization and commercialization –**

- 1444 • Characterization of the biological effects of the acoustic actuation with the specific
1445 frequencies and powers should be standardized so that biomedical researchers can
1446 ensure that this technology is suitable for their research or applications⁵⁰.
- 1447 • Open-source codes to compute the acoustic field generated by IDTs should be
1448 developed in designing and employing IDT devices for automation and precision
1449 control⁵⁰.
- 1450 • All-in-one acoustofluidic prototypes would be advantageous for biomedical research
1451 laboratories, which are not need access to external equipment or a high degree of user
1452 skills or training, integrated with modern technologies such as mobile phone, touch
1453 screen, and Bluetooth, internet⁴⁹.
- 1454 • Costs should be the key consideration for developing the future acoustofluidics devices.
1455 The end goal would be their commercialization, ideally with on-chip functionality
1456 without requiring extensive and costly external additional equipment such as power
1457 supplies, capillary pumps, lasers, and mass spectrometers - all of which at costs
1458 acceptable to manufacturers and consumers⁴⁸.

1459 **Acknowledgments**

1460 This work was financially supported by the International Exchange Grants from Royal Society
1461 [grant numbers of IEC/NSFC/170142; IEC/NSFC/201078], the UK Engineering and Physical
1462 Sciences Research Council (EPSRC) [grant numbers EP/P018998/1 and EP/P002803/1], UK
1463 Fluidic Network [EP/N032861/1] Special Interest Group of Acoustofluidics.

1464 **7. References**

- 1465 ¹American Scientific (n.d.).
- 1466 ²J. Friend and L.Y. Yeo, *Rev. Mod. Phys.* **83**, 647 (2011).
- 1467 ³A. Kundt, *Ann. Phys. Chem.* **203**, 497 (1866).
- 1468 ⁴V. Dvořák, *Annalen Der Physik* **233**, 42 (1876).
- 1469 ⁵A. Pavlic and J. Dual, *J. Fluid Mech.* **911**, A28 (2021).
- 1470 ⁶Lord Rayleigh, *Philosophical Transactions of the Royal Society of London* **175**, 1 (1884).
- 1471 ⁷*Physikalische Zeitschrift*. **Vol. 33**, (1932).
- 1472 ⁸P.J. Westervelt, *The Journal of the Acoustical Society of America* **25**, 60 (1953).
- 1473 ⁹W.L. Nyborg, *The Journal of the Acoustical Society of America* **25**, 68 (1953).
- 1474 ¹⁰Y. Gu, C. Chen, J. Rufo, C. Shen, Z. Wang, P.-H. Huang, H. Fu, P. Zhang, S.A. Cummer,
1475 Z. Tian, and T.J. Huang, *ACS Nano* **14**, 14635 (2020).
- 1476 ¹¹D.J. Collins, Z. Ma, J. Han, and Y. Ai, *Lab Chip* **17**, 91 (2016).
- 1477 ¹²G. Destgeer, H. Cho, B.H. Ha, J.H. Jung, J. Park, and H.J. Sung, *Lab Chip* **16**, 660 (2016).
- 1478 ¹³N. Zhang, J.P. Zuniga-Hertz, E.Y. Zhang, T. Gopesh, M.J. Fannon, J. Wang, Y. Wen, H.H.
1479 Patel, and J. Friend, *Lab Chip* **21**, 904 (2021).
- 1480 ¹⁴Y. Gu, C. Chen, Z. Mao, H. Bachman, R. Becker, J. Rufo, Z. Wang, P. Zhang, J. Mai, S.
1481 Yang, J. Zhang, S. Zhao, Y. Ouyang, D.T.W. Wong, Y. Sadovsky, and T.J. Huang, *Sci. Adv.*
1482 **7**, (2021).
- 1483 ¹⁵J. Zhou, P. Mukherjee, H. Gao, Q. Luan, and I. Papautsky, *APL Bioeng* **3**, 041504 (2019).
- 1484 ¹⁶C. Kumar, M. Hejazian, C. From, S. Saha, E. Sauret, Y. Gu, and N.-T. Nguyen, *Physics of*
1485 *Fluids* **31**, 063603 (2019).
- 1486 ¹⁷C. Zhao and C. Yang, *Adv Colloid Interface Sci* **201–202**, 94 (2013).
- 1487 ¹⁸A.C. Johnson and M.T. Bowser, *Lab Chip* **18**, 27 (2017).
- 1488 ¹⁹B.H. Lapizco-Encinas, *ELECTROPHORESIS* **40**, 358 (2019).
- 1489 ²⁰P. Paiè, T. Zandrini, R.M. Vázquez, R. Osellame, and F. Bragheri, *Micromachines (Basel)*
1490 **9**, E200 (2018).
- 1491 ²¹Y. Wang, Q. Zhang, Z. Zhu, F. Lin, J. Deng, G. Ku, S. Dong, S. Song, M.K. Alam, D. Liu,
1492 Z. Wang, and J. Bao, *Sci Adv* **3**, e1700555 (2017).
- 1493 ²²A. Ozcelik, J. Rufo, F. Guo, Y. Gu, P. Li, J. Lata, and T.J. Huang, *Nat Methods* **15**, 1021
1494 (2018).
- 1495 ²³M.-C.N. Le and Z.H. Fan, *Biomed Mater* **16**, 022005 (2021).
- 1496 ²⁴J. Novotny, A. Lenshof, and T. Laurell, *Electrophoresis* **43**, 804 (2022).
- 1497 ²⁵M.B. Mazalan, A.M. Noor, Y. Wahab, S. Yahud, and W.S.W.K. Zaman, *Micromachines*
1498 *(Basel)* **13**, 30 (2021).
- 1499 ²⁶S. Mohanty, I.S.M. Khalil, and S. Misra, *Proc Math Phys Eng Sci* **476**, 20200621 (2020).
- 1500 ²⁷X. Ding, P. Li, S.-C.S. Lin, Z.S. Stratton, N. Nama, F. Guo, D. Slotcavage, X. Mao, J. Shi,
1501 F. Costanzo, and T.J. Huang, *Lab Chip* **13**, 3626 (2013).
- 1502 ²⁸D. Mandal and S. Banerjee, *Sensors (Basel)* **22**, 820 (2022).
- 1503 ²⁹M.K. Tan, J.R. Friend, and L.Y. Yeo, *Phys. Rev. Lett.* **103**, 024501 (2009).
- 1504 ³⁰M. Jangi, J.T. Luo, R. Tao, J. Reboud, R. Wilson, J.M. Cooper, D. Gibson, and Y.Q. Fu,
1505 *International Journal of Multiphase Flow* **114**, 1 (2019).
- 1506 ³¹D.J. Collins, O. Manor, A. Winkler, H. Schmidt, J.R. Friend, and L.Y. Yeo, *Phys Rev E*
1507 *Stat Nonlin Soft Matter Phys* **86**, 056312 (2012).
- 1508 ³²C. Cortez-Jugo, A. Qi, A. Rajapaksa, J.R. Friend, and L.Y. Yeo, *Biomicrofluidics* **9**,
1509 (2015).
- 1510 ³³J. Wang, H. Hu, A. Ye, J. Chen, and P. Zhang, *Sensors and Actuators A: Physical* **238**, 1
1511 (2016).
- 1512 ³⁴J. Zhou, X. Tao, J. Luo, Y. Li, H. Jin, S. Dong, J. Luo, H. Duan, and Y. Fu, *Surface and*
1513 *Coatings Technology* **367**, 127 (2019).

1514 ³⁵ E. Galopin, M. Beaugeois, B. Pinchemel, J.-C. Camart, M. Bouazaoui, and V. Thomy,
1515 Biosensors and Bioelectronics **23**, 746 (2007).

1516 ³⁶ C. Chen, Y. Gu, J. Philippe, P. Zhang, H. Bachman, J. Zhang, J. Mai, J. Rufo, J.F. Rawls,
1517 E.E. Davis, N. Katsanis, and T.J. Huang, Nat Commun **12**, 1118 (2021).

1518 ³⁷ J. Zhang, S. Yang, C. Chen, J.H. Hartman, P.-H. Huang, L. Wang, Z. Tian, P. Zhang, D.
1519 Faulkenberry, J.N. Meyer, and T.J. Huang, Lab Chip **19**, 984 (2019).

1520 ³⁸ S. Marqus, L. Lee, T. Istivan, R.Y. Kyung Chang, C. Dekiwadia, H.-K. Chan, and L.Y.
1521 Yeo, European Journal of Pharmaceutics and Biopharmaceutics **151**, 181 (2020).

1522 ³⁹ Z. Gong, L. Huang, X. Tang, K. Chen, Z. Wu, L. Zhang, Y. Sun, Y. Xia, H. Chen, Y. Wei,
1523 F. Wang, and S. Guo, Advanced Healthcare Materials **10**, 2101312 (2021).

1524 ⁴⁰ Y. Wang, Q. Zhang, R. Tao, J. Xie, P. Canyelles-Pericas, H. Torun, J. Reboud, G. McHale,
1525 L.E. Dodd, X. Yang, J. Luo, Q. Wu, and Y. Fu, ACS Appl Mater Interfaces **13**, 16978
1526 (2021).

1527 ⁴¹ H. Lim, S.M. Back, H. Choi, and J. Nam, Lab Chip **20**, 120 (2019).

1528 ⁴² T. Inui, J. Mei, C. Imashiro, Y. Kurashina, J. Friend, and K. Takemura, Lab Chip (2021).

1529 ⁴³ J.H. Jung, G. Destgeer, J. Park, H. Ahmed, K. Park, and H.J. Sung, RSC Adv. **8**, 3206
1530 (2018).

1531 ⁴⁴ J. Nam, W.S. Jang, J. Kim, H. Lee, and C.S. Lim, Biosensors and Bioelectronics **142**,
1532 111496 (2019).

1533 ⁴⁵ P. Zhang, Sci Adv **6**, 0606, (2020).

1534 ⁴⁶ S. Zhang, Y. Wang, P. Onck, and J. den Toonder, Microfluid Nanofluid **24**, 24 (2020).

1535 ⁴⁷ W. Connacher, N. Zhang, A. Huang, J. Mei, S. Zhang, T. Gopesh, and J. Friend, Lab on a
1536 Chip **18**, 1952 (2018).

1537 ⁴⁸ L.Y. Yeo, H.-C. Chang, P.P.Y. Chan, and J.R. Friend, Small **7**, 12 (2011).

1538 ⁴⁹ P. Zhang, H. Bachman, A. Ozcelik, and T.J. Huang, Annu Rev Anal Chem (Palo Alto
1539 Calif) **13**, 17 (2020).

1540 ⁵⁰ J. Rufo, F. Cai, J. Friend, M. Wiklund, and T.J. Huang, Nat Rev Methods Primers **2**, 1
1541 (2022).

1542 ⁵¹ J. Rufo, P. Zhang, R. Zhong, L.P. Lee, and T.J. Huang, Nat Commun **13**, 3459 (2022).

1543 ⁵² C.K. Campbell, Proc. IEEE **77**, 1453 (1989).

1544 ⁵³ A.V. Mamishev, K. Sundara-Rajan, F. Yang, Y. Du, and M. Zahn, Proceedings of the
1545 IEEE **92**, 808 (2004).

1546 ⁵⁴ S. Datta, *Surface Acoustic Wave Devices* (Prentice-Hall, 1986).

1547 ⁵⁵ C.K. Campbell, *Surface Acoustic Wave Devices for Mobile and Communication*
1548 *Applications* (Academic Press, 1998).

1549 ⁵⁶ V. Plessky and L. Reindl, IEEE Trans. Ultrason. Ferroelectr. Fre. Control **57**, 654 (2010).

1550 ⁵⁷ Y.Q. Fu, J.K. Luo, N.T. Nguyen, A.J. Walton, A.J. Flewitt, X.T. Zu, Y. Li, G. McHale, A.
1551 Matthews, E. Iborra, H. Du, and W.I. Milne, Progress in Materials Science **89**, 31 (2017).

1552 ⁵⁸ M. Wu, K. Chen, S. Yang, Z. Wang, P.-H. Huang, J. Mai, Z.-Y. Li, and T.J. Huang, Lab
1553 Chip **18**, 3003 (2018).

1554 ⁵⁹ M. Wu, P.-H. Huang, R. Zhang, Z. Mao, C. Chen, G. Kemeny, P. Li, A.V. Lee, R.
1555 Gyanchandani, A.J. Armstrong, M. Dao, S. Suresh, and T.J. Huang, Small **14**, 1801131
1556 (2018).

1557 ⁶⁰ G. Zhang, *Bulk and Surface Acoustic Waves: Fundamentals, Devices, and Applications*
1558 (Jenny Stanford Publishing, New York, 2022).

1559 ⁶¹ Y.-Q. Fu, H.-F. Pang, H. Torun, R. Tao, G. McHale, J. Reboud, K. Tao, J. Zhou, J. Luo, D.
1560 Gibson, J. Luo, and P. Hu, Lab Chip **21**, 254 (2021).

1561 ⁶² J. Nam, H. Lim, and S. Shin, Korea-Aust. Rheol. J. **23**, 255 (2011).

1562 ⁶³ S. Song, Q. Wang, J. Zhou, and A. Riaud, Nanotechnology and Precision Engineering **5**,
1563 035001 (2022).

1564 ⁶⁴ M.P. Nair, A.J.T. Teo, and K.H.H. Li, *Micromachines* (Basel) **13**, 24 (2021).

1565 ⁶⁵ R. Fogel, J. Limson, and A.A. Seshia, *Essays Biochem* **60**, 101 (2016).

1566 ⁶⁶ K. Länge, *Sensors* (Basel) **19**, E5382 (2019).

1567 ⁶⁷ A. Mujahid and F.L. Dickert, *Sensors* (Basel) **17**, E2716 (2017).

1568 ⁶⁸ G. Destgeer, B.H. Ha, J.H. Jung, and H.J. Sung, *Lab Chip* **14**, 4665 (2014).

1569 ⁶⁹ D. Malocha, (2000).

1570 ⁷⁰ D.P. Morgans, *Surface Acoustic Wave Devices for Signal Processing* (Elsevier, 1991).

1571 ⁷¹ M. Feldmann and J. Henaff, (1989).

1572 ⁷² J.S. Bach and H. Bruus, *Phys. Rev. Lett.* **124**, 214501 (2020).

1573 ⁷³ H. Bruus, *Lab Chip* **12**, 20 (2012).

1574 ⁷⁴ J. Lei, P. Glynne-Jones, and M. Hill, *Microfluid Nanofluid* **21**, 23 (2017).

1575 ⁷⁵ S.S. Sadhal, *Lab Chip* **12**, 2292 (2012).

1576 ⁷⁶ S. Boluriaan and P.J. Morris, *International Journal of Aeroacoustics* **2**, 255 (2003).

1577 ⁷⁷ B.E. Rapp, in *Microfluidics: Modelling, Mechanics and Mathematics*, edited by B.E. Rapp (Elsevier, Oxford, 2017), pp. 243–263.

1578 ⁷⁸ L.K. Zarembo, in *High-Intensity Ultrasonic Fields*, edited by L.D. Rozenberg (Springer US, Boston, MA, 1971), pp. 135–199.

1581 ⁷⁹ M. Evander and J. Nilsson, *Lab Chip* **12**, 4667 (2012).

1582 ⁸⁰ M. Settnes and H. Bruus, *Phys. Rev. E* **85**, 016327 (2012).

1583 ⁸¹ H. Bruus, *Lab Chip* **12**, 1014 (2012).

1584 ⁸² S. Liu, Y. Yang, Z. Ni, X. Guo, L. Luo, J. Tu, D. Zhang, and J. Zhang, *Sensors* (Basel) **17**, 1664 (2017).

1585 ⁸³ R. Barnkob, P. Augustsson, T. Laurell, and H. Bruus, *Phys Rev E Stat Nonlin Soft Matter Phys* **86**, 056307 (2012).

1586 ⁸⁴ P. Glynne-Jones and M. Hill, *Lab Chip* **13**, 1003 (2013).

1589 ⁸⁵ J. Shi, H. Huang, Z. Stratton, Y. Huang, and T.J. Huang, *Lab Chip* **9**, 3354 (2009).

1590 ⁸⁶ M. Wiklund, R. Green, and M. Ohlin, *Lab Chip* **12**, 2438 (2012).

1591 ⁸⁷ S.J. Lighthill, *Journal of Sound and Vibration* **61**, 391 (1978).

1592 ⁸⁸ T. Laurell and A. Lenshof, *Microscale Acoustofluidics* (Royal Society of Chemistry, 2014).

1593 ⁸⁹ X. Luo, J. Cao, H. Gong, H. Yan, and L. He, *Ultrasonics Sonochemistry* **48**, 287 (2018).

1594 ⁹⁰ C. Devendran, T. Albrecht, J. Brenker, T. Alan, and A. Neild, *Lab Chip* **16**, 3756 (2016).

1595 ⁹¹ K. Sritharan, C.J. Strobl, M.F. Schneider, A. Wixforth, and Z. Guttenberg, *Appl. Phys. Lett.* **88**, 054102 (2006).

1597 ⁹² J.K. Luo, Y.Q. Fu, and W.I. Milne, *Modeling and Measurement Methods for Acoustic Waves and for Acoustic Microdevices* (2013).

1598 ⁹³ J. Li, M.H. Biroun, R. Tao, Y. Wang, H. Torun, N. Xu, M. Rahmati, Y. Li, D. Gibson, C. Fu, J. Luo, L. Dong, J. Xie, and Y. Fu, *J. Phys. D: Appl. Phys.* **53**, 355402 (2020).

1601 ⁹⁴ Z. Guttenberg, A. Rathgeber, S. Keller, J.O. Rädler, A. Wixforth, M. Kostur, M. Schindler, and P. Talkner, *Phys. Rev. E* **70**, 056311 (2004).

1603 ⁹⁵ R.M. Arzt, E. Salzmann, and K. Dransfeld, *Applied Physics Letters* **10**, 165 (1967).

1604 ⁹⁶ M.K. Tan, L.Y. Yeo, and J.R. Friend, *EPL* **87**, 47003 (2009).

1605 ⁹⁷ N. Riley, *Annual Review of Fluid Mechanics* **33**, 43 (2001).

1606 ⁹⁸ N. Nama, R. Barnkob, Z. Mao, C.J. Kähler, F. Costanzo, and T.J. Huang, *Lab Chip* **15**, 2700 (2015).

1607 ⁹⁹ A. Riaud, M. Baudoin, O. Bou Matar, J.-L. Thomas, and P. Brunet, *J. Fluid Mech.* **821**, 384 (2017).

1610 ¹⁰⁰ S. Sachs, M. Baloochi, C. Cierpka, and J. König, *Lab Chip* **22**, 2011 (2022).

1611 ¹⁰¹ T. Bui, V. Nguyen, S. Vollebregt, B. Morana, H. van Zeijl, T. Chu Duc, and P.M. Sarro, *Applied Surface Science* **426**, 253 (2017).

1612

1613 ¹⁰² M. Wu, A. Ozcelik, J. Rufo, Z. Wang, R. Fang, and T. Jun Huang, *Microsyst Nanoeng* **5**,
1614 (2019).

1615 ¹⁰³ G. Destgeer, J.H. Jung, J. Park, H. Ahmed, and H.J. Sung, *Anal. Chem.* **89**, 736 (2017).

1616 ¹⁰⁴ D.-T. Phan and G.-S. Chung, *Applied Surface Science* **257**, 8696 (2011).

1617 ¹⁰⁵ A. Winkler, R. Brünig, C. Faust, R. Weser, and H. Schmidt, *Sensors and Actuators A:*
1618 *Physical* **247**, 259 (2016).

1619 ¹⁰⁶ M.-I. Rocha-Gaso, Y. Jimenez, L.A. Francis, and A. Arnau, in (2013).

1620 ¹⁰⁷ J. Kirschner, in (2010).

1621 ¹⁰⁸ R. Weser, A. Winkler, M. Weihnacht, S. Menzel, and H. Schmidt, *Ultrasonics* **106**,
1622 106160 (2020).

1623 ¹⁰⁹ E. Ntagwirumugara, T. Gryba, V.Y. Zhang, E. Dogheche, and J.-E. Lefebvre, *IEEE*
1624 *Transactions on Ultrasonics, Ferroelectrics, and Frequency Control* **54**, 2011 (2007).

1625 ¹¹⁰ M. Akiyama, K. Nagao, N. Ueno, H. Tateyama, and T. Yamada, *Vacuum* **74**, 699 (2004).

1626 ¹¹¹ A. Vorobiev and S. Gevorgian, *IEEE Transactions on Ultrasonics, Ferroelectrics, and*
1627 *Frequency Control* **61**, 840 (2014).

1628 ¹¹² W. Soluch and E. Brzozowski, *IEEE Transactions on Electron Devices* **61**, 3395 (2014).

1629 ¹¹³ J. Chen, X. He, W. Wang, W. Xuan, J. Zhou, X. Wang, S.R. Dong, S. Garner, P. Cimo,
1630 and J.K. Luo, *Journal of Materials Chemistry C* **2**, 9109 (2014).

1631 ¹¹⁴ J. Zhou, X.Z. Wu, D.B. Xiao, M. Zhuo, H. Jin, J.K. Luo, and Y.Q. Fu, *Surface and*
1632 *Coatings Technology* **320**, 39 (2017).

1633 ¹¹⁵ V. Mišeikis, R.J. Shilton, M. Travagliati, M. Agostini, M. Cecchini, V. Piazza, and C.
1634 Coletti, *Nanotechnology* **32**, 375503 (2021).

1635 ¹¹⁶ J. Zhou, J. Zheng, X. Shi, Z. Chen, J. Wu, S. Xiong, J. Luo, S. Dong, H. Jin, H. Duan, and
1636 Y. Fu, *J. Electrochem. Soc.* **166**, B432 (2019).

1637 ¹¹⁷ Y. Yao and Y. Xue, *Sensors and Actuators B: Chemical* **222**, 755 (2016).

1638 ¹¹⁸ A.S. Mayorov, N. Hunter, W. Muchenje, C.D. Wood, M. Rosamond, E.H. Linfield, A.G.
1639 Davies, and J.E. Cunningham, *Applied Physics Letters* **104**, 083509 (2014).

1640 ¹¹⁹ D. Roshchupkin, L. Ortega, I. Zizak, O. Plotitsyna, V. Matveev, O. Kononenko, E.
1641 Emelin, A. Erko, K. Tynyshtykbayev, and D. Irzhak, *Journal of Applied Physics* **118**, 104901
1642 (2015).

1643 ¹²⁰ J. Zhou, X. Shi, D. Xiao, X. Wu, J. Zheng, J. Luo, M. Zhuo, X. Tao, H. Jin, S. Dong, R.
1644 Tao, H. Duan, and Y. Fu, *J. Micromech. Microeng.* **29**, 015006 (2019).

1645 ¹²¹ M. Darmawan and D. Byun, *Microfluidics and Nanofluidics* **18**, 1107 (2015).

1646 ¹²² Y.Q. Fu, L. Garcia-Gancedo, H.F. Pang, S. Porro, Y.W. Gu, J.K. Luo, X.T. Zu, F. Placido,
1647 J.I.B. Wilson, A.J. Flewitt, and W.I. Milne, *Biomicrofluidics* **6**, 24105 (2012).

1648 ¹²³ H. Jin, J. Zhou, X. He, W. Wang, H. Guo, S. Dong, D. Wang, Y. Xu, J. Geng, J.K. Luo,
1649 and W.I. Milne, *Sci Rep* **3**, 2140 (2013).

1650 ¹²⁴ D.-S. Lee, J. Luo, Y. Fu, W.I. Milne, N.-M. Park, S.H. Kim, M.Y. Jung, and S. Maeng, *J*
1651 *Nanosci Nanotechnol* **8**, 4626 (2008).

1652 ¹²⁵ C. Sun, F. Wu, Y. Fu, D.J. Wallis, R. Mikhaylov, F. Yuan, D. Liang, Z. Xie, H. Wang, R.
1653 Tao, M.H. Shen, J. Yang, W. Xun, Z. Wu, Z. Yang, H. Cang, and X. Yang, *Ultrasonics* **108**,
1654 106202 (2020).

1655 ¹²⁶ C. Sun, F. Wu, D.J. Wallis, M.H. Shen, F. Yuan, J. Yang, J. Wu, Z. Xie, D. Liang, H.
1656 Wang, R. Tickle, R. Mikhaylov, A. Clayton, Y. Zhou, Z. Wu, Y. Fu, W. Xun, and X. Yang,
1657 *IEEE Transactions on Electron Devices* **67**, 3355 (2020).

1658 ¹²⁷ S. Büyükköse, B. Vratzov, J. van der Veen, P.V. Santos, and W.G. van der Wiel, *Appl.*
1659 *Phys. Lett.* **102**, 013112 (2013).

1660 ¹²⁸ S. Büyükköse, B. Vratzov, D. Ataç, J. van der Veen, P.V. Santos, and W.G. van der Wiel,
1661 *Nanotechnology* **23**, 315303 (2012).

1662 ¹²⁹ J. Zhou, D. Zhang, Y. Liu, F. Zhuo, L. Qian, H. Li, Y.-Q. Fu, and H. Duan, *Engineering*
1663 S2095809922003575 (2022).

1664 ¹³⁰ R. Mikhaylov, F. Wu, H. Wang, A. Clayton, C. Sun, Z. Xie, D. Liang, Y. Dong, F. Yuan,
1665 D. Moschou, Z. Wu, M.H. Shen, J. Yang, Y. Fu, Z. Yang, C. Burton, R.J. Errington, M.
1666 Wiltshire, and X. Yang, *Lab Chip* **20**, 1807 (2020).

1667 ¹³¹ R. Mikhaylov, M.S. Martin, P. Dumcius, H. Wang, F. Wu, X. Zhang, V. Akhimien, C.
1668 Sun, A. Clayton, Y. Fu, L. Ye, Z. Dong, Z. Wu, and X. Yang, *J. Micromech. Microeng.* **31**,
1669 074003 (2021).

1670 ¹³² S. Zahertar, H. Torun, C. Sun, C. Markwell, Y. Dong, X. Yang, and Y. Fu, *Sensors* **22**,
1671 4344 (2022).

1672 ¹³³ Z. Ma, A.J.T. Teo, S.H. Tan, Y. Ai, and N.-T. Nguyen, *Micromachines (Basel)* **7**, (2016).

1673 ¹³⁴ A.R. Rezk, J.R. Friend, and L.Y. Yeo, *Lab Chip* **14**, 1802 (2014).

1674 ¹³⁵ R.P. Hodgson, M. Tan, L. Yeo, and J. Friend, *Appl. Phys. Lett.* **94**, 024102 (2009).

1675 ¹³⁶ C. Fu, K. Lee, K. Lee, S.S. Yang, and W. Wang, *Sensors and Actuators A: Physical* **218**,
1676 80 (2014).

1677 ¹³⁷ S. Lehtonen, V.P. Plessky, C.S. Hartmann, and M.M. Salomaa, *IEEE Transactions on*
1678 *Ultrasonics, Ferroelectrics, and Frequency Control* **51**, 1697 (2004).

1679 ¹³⁸ H. Nakamura, T. Yamada, T. Ishizaki, and K. Nishimura, *IEEE Transactions on*
1680 *Microwave Theory and Techniques* **49**, 761 (2001).

1681 ¹³⁹ M.M. de Lima Jr, F. Alsina, W. Seidel, and P.V. Santos, *Journal of Applied Physics* **94**,
1682 7848 (2003).

1683 ¹⁴⁰ T.-T. Wu, H.-T. Tang, Y.-Y. Chen, and P.-L. Liu, *IEEE Transactions on Ultrasonics,*
1684 *Ferroelectrics, and Frequency Control* **52**, 1384 (2005).

1685 ¹⁴¹ X. Ding, S.-C.S. Lin, B. Kiraly, H. Yue, S. Li, I.-K. Chiang, J. Shi, S.J. Benkovic, and T.J.
1686 Huang, *Proceedings of the National Academy of Sciences* **109**, 11105 (2012).

1687 ¹⁴² M. Lamothe, V. Plessky, J.-M. Friedt, T. Ostertag, and S. Ballandras, *Electronics Letters*
1688 **49**, 1576 (2013).

1689 ¹⁴³ V. Plessky and M. Lamothe, *Electronics Letters* **49**, 1503 (2013).

1690 ¹⁴⁴ T. Frommelt, M. Kostur, M. Wenzel-Schäfer, P. Talkner, P. Hänggi, and A. Wixforth,
1691 *Physical Review Letters* **100**, 034502 (2008).

1692 ¹⁴⁵ X. Ding, J. Shi, S.-C. Steven Lin, S. Yazdi, B. Kiraly, and T. Jun Huang, *Lab on a Chip*
1693 **12**, 2491 (2012).

1694 ¹⁴⁶ Y. Chen, X. Ding, S.-C. Steven Lin, S. Yang, P.-H. Huang, N. Nama, Y. Zhao, A.A.
1695 Nawaz, F. Guo, W. Wang, Y. Gu, T.E. Mallouk, and T.J. Huang, *ACS Nano* **7**, 3306 (2013).

1696 ¹⁴⁷ H. Mansoorzare and R. Abdolvand, in *2022 IEEE 35th International Conference on Micro*
1697 *Electro Mechanical Systems Conference (MEMS)* (2022), pp. 1014–1017.

1698 ¹⁴⁸ V. Laude, D. Gérard, N. Khelifaoui, C. Jerez-Hanckes, S. Benchabane, H. Moubchir, and
1699 A. Khelif, in (2007), pp. 2115–2118.

1700 ¹⁴⁹ S. Zaehring and N. Schwesinger, *Microsystem Technologies* **16**, 871 (2010).

1701 ¹⁵⁰ R. O’Rorke, A. Winkler, D. Collins, and Y. Ai, *RSC Adv.* **10**, 11582 (2020).

1702 ¹⁵¹ C. Pan, G. Xiao, Z. Feng, and W.-H. Liao, *Smart Mater. Struct.* **23**, 125029 (2014).

1703 ¹⁵² Z. Tian, S. Yang, P.-H. Huang, Z. Wang, P. Zhang, Y. Gu, H. Bachman, C. Chen, M. Wu,
1704 Y. Xie, and T.J. Huang, *Sci. Adv.* **5**, eaau6062 (2019).

1705 ¹⁵³ G.J. Xiao, C.L. Pan, Y.B. Liu, and Z.H. Feng, *Sensors and Actuators A: Physical* **227**, 1
1706 (2015).

1707 ¹⁵⁴ C.L. Pan, Y.T. Ma, Y.B. Liu, Q. Zhang, and Z.H. Feng, *Sensors and Actuators A: Physical*
1708 **148**, 250 (2008).

1709 ¹⁵⁵ S.V. Biryukov, G. Martin, and M. Weihnacht, *Appl. Phys. Lett.* **90**, 173503 (2007).

1710 ¹⁵⁶ P. Kang, Z. Tian, S. Yang, W. Yu, H. Zhu, H. Bachman, S. Zhao, P. Zhang, Z. Wang, R.
1711 Zhong, and T.J. Huang, *Lab Chip* **20**, 987 (2020).

1712 ¹⁵⁷ A. Riaud, M. Baudoin, J.-L. Thomas, and O. Bou Matar, *IEEE Transactions on*
1713 *Ultrasonics, Ferroelectrics, and Frequency Control* **63**, 1601 (2016).
1714 ¹⁵⁸ A. Riaud, J.-L. Thomas, E. Charron, A. Bussonnière, O. Bou Matar, and M. Baudoin,
1715 *Physical Review Applied* **4**, 034004 (2015).
1716 ¹⁵⁹ Z. Tian, *Sci Adv* **6**, 0494, (2020).
1717 ¹⁶⁰ M. Baudoin, J.-C. Gerbedoen, A. Riaud, O.B. Matar, N. Smagin, and J.-L. Thomas,
1718 *Science Advances* **5**, eaav1967 (2019).
1719 ¹⁶¹ T. Tsuji, R. Mihara, T. Saito, S. Hagihara, T. Oizumi, N. Takeda, T. Ohgi, T. Yanagisawa,
1720 S. Akao, N. Nakaso, and K. Yamanaka, *Materials Transactions* **55**, 1040 (2014).
1721 ¹⁶² M. Mańka, M. Rosiek, A. Martowicz, T. Stepinski, and T. Uhl, *Mechanical Systems and*
1722 *Signal Processing* **78**, 71 (2016).
1723 ¹⁶³ J. Zhu, N.W. Emanetoglu, Y. Lu, J.A. Kosinski, and R.A. Pastore, *IEEE Transactions on*
1724 *Ultrasonics, Ferroelectrics, and Frequency Control* **48**, 1383 (2001).
1725 ¹⁶⁴ M.M. de Lima and P.V. Santos, *Rep. Prog. Phys.* **68**, 1639 (2005).
1726 ¹⁶⁵ M.M. de Lima Jr, W. Seidel, H. Kostial, and P.V. Santos, *Journal of Applied Physics* **96**,
1727 3494 (2004).
1728 ¹⁶⁶ Q. Zhang, T. Han, G. Tang, J. Chen, and K. Hashimoto, in *2015 IEEE International*
1729 *Ultrasonics Symposium (IUS)* (2015), pp. 1–4.
1730 ¹⁶⁷ Q. Zhang, T. Han, J. Chen, W. Wang, and K. Hashimoto, *Diamond and Related Materials*
1731 **58**, 31 (2015).
1732 ¹⁶⁸ S.F. Hon, K.W. Kwok, H.L. Li, and H.Y. Ng, *Review of Scientific Instruments* **81**,
1733 065102 (2010).
1734 ¹⁶⁹ K.W. Kwok, S.F. Hon, and D. Lin, *Sensors and Actuators A: Physical* **168**, 168 (2011).
1735 ¹⁷⁰ C.-Y. Lee, W. Pang, H. Yu, and E.S. Kim, *Appl. Phys. Lett.* **93**, 034104 (2008).
1736 ¹⁷¹ K. Kalantar-Zadeh, D.A. Powell, W. Wlodarski, S. Ippolito, and K. Galatsis, *Sensors and*
1737 *Actuators B: Chemical* **91**, 303 (2003).
1738 ¹⁷² W.-C. Shih, H.-Y. Su, and M.-S. Wu, *Thin Solid Films* **517**, 3378 (2009).
1739 ¹⁷³ O. Legrani, O. Elmazria, S. Zhgoon, P. Pigeat, and A. Bartasyte, *IEEE Sensors Journal* **13**,
1740 487 (2013).
1741 ¹⁷⁴ A. Fakhfour, C. Devendran, A. Ahmed, J. Soria, and A. Neild, *Lab Chip* **18**, 3926 (2018).
1742 ¹⁷⁵ R.J. Shilton, M. Travaglati, F. Beltram, and M. Cecchini, *Advanced Materials* **26**, 4941
1743 (2014).
1744 ¹⁷⁶ Z. Wang, J. Rich, N. Hao, Y. Gu, C. Chen, S. Yang, P. Zhang, and T.J. Huang, *Microsyst*
1745 *Nanoeng* **8**, 1 (2022).
1746 ¹⁷⁷ S.P. Zhang, J. Lata, C. Chen, J. Mai, F. Guo, Z. Tian, L. Ren, Z. Mao, P.-H. Huang, P. Li,
1747 S. Yang, and T.J. Huang, *Nature Communications* **9**, 2928 (2018).
1748 ¹⁷⁸ Z. Ma, D.J. Collins, and Y. Ai, *Anal. Chem.* **88**, 5316 (2016).
1749 ¹⁷⁹ C. Sun, Y. Dong, J. Wei, M. Cai, D. Liang, Y. Fu, Y. Zhou, Y. Sui, F. Wu, R. Mikhaylov,
1750 H. Wang, F. Fan, Z. Xie, M. Stringer, Z. Yang, Z. Wu, L. Tian, and X. Yang, *Acta*
1751 *Biomaterialia* (2022).
1752 ¹⁸⁰ A.L. Zhang, Z.Q. Wu, and X.H. Xia, *Talanta* **84**, 293 (2011).
1753 ¹⁸¹ L.G. Schnitzler, S. Junger, D.M. Loy, E. Wagner, A. Wixforth, A. Hörner, U. Lächelt, and
1754 C. Westerhausen, *J. Phys. D: Appl. Phys.* **52**, 244002 (2019).
1755 ¹⁸² M.K. Tan, J.R. Friend, and L.Y. Yeo, *Lab Chip* **7**, 618 (2007).
1756 ¹⁸³ S.K.R.S. Sankaranarayanan, S. Cular, V.R. Bhethanabotla, and B. Joseph, *Phys. Rev. E*
1757 **77**, 066308 (2008).
1758 ¹⁸⁴ J. Liu, S. Li, and V.R. Bhethanabotla, *ACS Sens.* **3**, 222 (2018).
1759 ¹⁸⁵ Y. Li, Y.Q. Fu, S.D. Brodie, M. Alghane, and A.J. Walton, *Biomicrofluidics* **6**, 12812
1760 (2012).

1761 ¹⁸⁶ A.N. Darinskii, M. Weihnacht, and H. Schmidt, *Journal of Applied Physics* **123**, 014902
1762 (2018).

1763 ¹⁸⁷ M. Djukelic, A. Wixforth, and C. Westerhausen, *Biomicrofluidics* **11**, 024115 (2017).

1764 ¹⁸⁸ D. Peng, W. Tong, D.J. Collins, M.R. Ibbotson, S. Praver, and M. Stamp, *Frontiers in*
1765 *Neuroscience* **15**, 37 (2021).

1766 ¹⁸⁹ E.M. Kugler, K. Michel, D. Kirchenbüchler, G. Dreissen, A. Csiszár, R. Merkel, M.
1767 Schemann, and G. Mazzuoli-Weber, *Neuroscience* **372**, 213 (2018).

1768 ¹⁹⁰ R. Ravin, P.S. Blank, A. Steinkamp, S.M. Rappaport, N. Ravin, L. Bezrukov, H.
1769 Guerrero-Cazares, A. Quinones-Hinojosa, S.M. Bezrukov, and J. Zimmerberg, *PLoS One* **7**,
1770 e39421 (2012).

1771 ¹⁹¹ N. Sivanantha, C. Ma, D.J. Collins, M. Sesen, J. Brenker, R.L. Coppel, A. Neild, and T.
1772 Alan, *Appl. Phys. Lett.* **105**, 103704 (2014).

1773 ¹⁹² A.M. Jötten, S. Angermann, M.E.M. Stamp, D. Breyer, F.G. Strobl, A. Wixforth, and C.
1774 Westerhausen, *RSC Adv.* **9**, 543 (2018).

1775 ¹⁹³ U. Farooq, X. Liu, W. Zhou, M. Hassan, L. Niu, and L. Meng, *Sensors and Actuators B:*
1776 *Chemical* **345**, 130335 (2021).

1777 ¹⁹⁴ A. Bussonnière, Y. Miron, M. Baudoin, O. Bou Matar, M. Grandbois, P. Charette, and A.
1778 Renaudin, *Lab Chip* **14**, 3556 (2014).

1779 ¹⁹⁵ P. Gelin, Ö. Sardan Sukas, K. Hellemans, D. Maes, and W. De Malsche, *Chemical*
1780 *Engineering Journal* **369**, 370 (2019).

1781 ¹⁹⁶ P.R. Rogers, J.R. Friend, and L.Y. Yeo, *Lab Chip* **10**, 2979 (2010).

1782 ¹⁹⁷ H. Li, J.R. Friend, and L.Y. Yeo, *Biomed Microdevices* **9**, 647 (2007).

1783 ¹⁹⁸ R. Singh, S.K.R.S. Sankaranarayanan, and V.R. Bhethanabotla, *Journal of Applied*
1784 *Physics* **107**, 024503 (2010).

1785 ¹⁹⁹ J. Friend, L. Yeo, M. Tan, and R. Shilton, in *Proceedings - IEEE Ultrasonics Symposium*
1786 (IEEE, 2008), pp. 930–933.

1787 ²⁰⁰ R. Shilton, M.K. Tan, L.Y. Yeo, and J.R. Friend, *Journal of Applied Physics* **104**, (2008).

1788 ²⁰¹ Y. Bourquin, A. Syed, J. Reboud, L.C. Ranford-Cartwright, M.P. Barrett, and J.M.
1789 Cooper, *Angew Chem Int Ed Engl* **53**, 5587 (2014).

1790 ²⁰² W. Liang, F. Zhang, G. Yang, and Z. Wang, *Microfluidics and Nanofluidics* **21**, 2 (2017).

1791 ²⁰³ J.H. Jung, G. Destgeer, B. Ha, J. Park, and H.J. Sung, *Lab Chip* **16**, 3235 (2016).

1792 ²⁰⁴ S. Collignon, J. Friend, and L. Yeo, *Lab on a Chip* **15**, 1942 (2015).

1793 ²⁰⁵ Z. Guttenberg, H. Müller, H. Habermüller, A. Geisbauer, J. Pipper, J. Felbel, M.
1794 Kielpinski, J. Scriba, and A. Wixforth, *Lab on a Chip* **5**, 308 (2005).

1795 ²⁰⁶ J.-Y. Bao and A.-L. Zhang, *Ferroelectrics* **558**, 199 (2020).

1796 ²⁰⁷ A. Zhang, Y. Zha, and J. Zhang, *AIP Advances* **4**, 127144 (2014).

1797 ²⁰⁸ P. Brunet, M. Baudoin, O.B. Matar, and F. Zoueshtiagh, *Physical Review E - Statistical,*
1798 *Nonlinear, and Soft Matter Physics* **81**, (2010).

1799 ²⁰⁹ D. Beyssen, L. Le Brizoual, O. Elmazria, and P. Alnot, *Sensors and Actuators, B:*
1800 *Chemical* **118**, 380 (2006).

1801 ²¹⁰ M. Baudoin, P. Brunet, O.B. Matar, and E. Herth, *Applied Physics Letters* **100**, 154102
1802 (2012).

1803 ²¹¹ X.Y. Du, M.E. Swanwick, Y.Q. Fu, J.K. Luo, A.J. Flewitt, D.S. Lee, S. Maeng, and W.I.
1804 Milne, *Journal of Micromechanics and Microengineering* **19**, 035016 (2009).

1805 ²¹² J.T. Luo, N.R. Geraldi, J.H. Guan, G. McHale, G.G. Wells, and Y.Q. Fu, *Physical Review*
1806 *Applied* **7**, 014017 (2017).

1807 ²¹³ L. Wu, Z. Guo, and W. Liu, *Advances in Colloid and Interface Science* **308**, 102770
1808 (2022).

1809 ²¹⁴ Y. Wang, X. Tao, R. Tao, J. Zhou, Q. Zhang, D. Chen, H. Jin, S. Dong, J. Xie, and Y.Q.
1810 Fu, *Sensors and Actuators A: Physical* **306**, 111967 (2020).

1811 ²¹⁵ R. Tao, G. Mchale, J. Reboud, J.M. Cooper, H. Torun, J.T. Luo, J. Luo, X. Yang, J. Zhou,
1812 P. Canyelles-Pericas, Q. Wu, and Y. Fu, *Nano Letters* **20**, 3263 (2020).

1813 ²¹⁶ A.-L. Zhang and X.-H. Xia, *Chinese Journal of Analytical Chemistry* **39**, 765 (2011).

1814 ²¹⁷ Y. Ai and B.L. Marrone, *Microfluid Nanofluid* **13**, 715 (2012).

1815 ²¹⁸ A. Wixforth, C. Strobl, Ch. Gauer, A. Toegl, J. Scriba, and Z. v. Guttenberg, *Anal Bioanal*
1816 *Chem* **379**, 982 (2004).

1817 ²¹⁹ C. Chen, S.P. Zhang, Z. Mao, N. Nama, Y. Gu, P.-H. Huang, Y. Jing, X. Guo, F.
1818 Costanzo, and T.J. Huang, *Lab Chip* **18**, 3645 (2018).

1819 ²²⁰ D.S. Brodie, Y.Q. Fu, Y. Li, M. Alghane, R.L. Reuben, and A.J. Walton, *Appl. Phys. Lett.*
1820 **99**, 153704 (2011).

1821 ²²¹ C. Fu, A.J. Quan, J.T. Luo, H.F. Pang, Y.J. Guo, Q. Wu, W.P. Ng, X.T. Zu, and Y.Q. Fu,
1822 *Appl. Phys. Lett.* **110**, 173501 (2017).

1823 ²²² P.K. Bhattacharjee, A.G. McDonnell, R. Prabhakar, L.Y. Yeo, and J. Friend, *New Journal*
1824 *of Physics* **13**, (2011).

1825 ²²³ J.O. Castro, S. Ramesan, A.R. Rezk, and L.Y. Yeo, *Soft Matter* **14**, 5721 (2018).

1826 ²²⁴ R. Li, Z. Gong, Z. Wu, H. Chen, Y. Xia, Y. Liu, F. Wang, and S. Guo, *Nano Futures* **4**,
1827 045001 (2020).

1828 ²²⁵ R. Li, Z. Gong, K. Yi, W. Li, Y. Liu, F. Wang, and S. Guo, *ACS Appl. Bio Mater.* **3**, 6521
1829 (2020).

1830 ²²⁶ X. Wei, K. Chen, B. Cai, L. Rao, Z. Wang, Y. Sun, M. Yu, W. Liu, S. Guo, and X.-Z.
1831 Zhao, *ACS Appl. Mater. Interfaces* **11**, 41118 (2019).

1832 ²²⁷ Y. Xia, L.-X. Huang, H. Chen, J. Li, K.-K. Chen, H. Hu, F.-B. Wang, Z. Ding, and S.-S.
1833 Guo, *ACS Appl. Mater. Interfaces* **13**, 12950 (2021).

1834 ²²⁸ K. Chen, E. Jiang, X. Wei, Y. Xia, Z. Wu, Z. Gong, Z. Shang, and S. Guo, *Lab on a Chip*
1835 **21**, 1604 (2021).

1836 ²²⁹ D. Lee, N. Lee, G. Choi, and H.H. Cho, *Inventions* **3**, 38 (2018).

1837 ²³⁰ A.R. Rezk, J.K. Tan, and L.Y. Yeo, *Advanced Materials* **28**, 1970 (2016).

1838 ²³¹ A.R. Rezk, S. Ramesan, and L.Y. Yeo, *Lab Chip* **18**, 406 (2018).

1839 ²³² U. Demirci, *Journal of Microelectromechanical Systems* **15**, 957 (2006).

1840 ²³³ K. Chen, C. Sui, Y. Wu, Z. Ao, S.S. Guo, and F. Guo, *Nanotechnology* **30**, 084001
1841 (2018).

1842 ²³⁴ V. Laude, D. Gérard, N. Khelifaoui, C.F. Jerez-Hanckes, S. Benchabane, and A. Khelif,
1843 *Appl. Phys. Lett.* **92**, 094104 (2008).

1844 ²³⁵ J. Zhou, H.F. Pang, L. Garcia-Gancedo, E. Iborra, M. Clement, M. De Miguel-Ramos, H.
1845 Jin, J.K. Luo, S. Smith, S.R. Dong, D.M. Wang, and Y.Q. Fu, *Microfluidics and Nanofluidics*
1846 **18**, 537 (2015).

1847 ²³⁶ Y.J. Guo, H.B. Lv, Y.F. Li, X.L. He, J. Zhou, J.K. Luo, X.T. Zu, A.J. Walton, and Y.Q.
1848 Fu, *Journal of Applied Physics* **116**, (2014).

1849 ²³⁷ H.F. Pang, Y.Q. Fu, L. Garcia-Gancedo, S. Porro, J.K. Luo, F. Placido, J.I.B. Wilson, A.J.
1850 Flewitt, W.I. Milne, and X.T. Zu, *Microfluidics and Nanofluidics* **15**, 377 (2013).

1851 ²³⁸ J. Ho, M.K. Tan, D.B. Go, L.Y. Yeo, J.R. Friend, and H.-C. Chang, *Anal. Chem.* **83**, 3260
1852 (2011).

1853 ²³⁹ A. Qi, L.Y. Yeo, and J.R. Friend, *Physics of Fluids* **20**, 074103 (2008).

1854 ²⁴⁰ A. Rajapaksa, A. Qi, L.Y. Yeo, R. Coppel, and J.R. Friend, *Lab Chip* **14**, 1858 (2014).

1855 ²⁴¹ A. Qi, J.R. Friend, L.Y. Yeo, D.A.V. Morton, M.P. McIntosh, and L. Spiccia, *Lab Chip* **9**,
1856 2184 (2009).

1857 ²⁴² P.C.L. Kwok, A. McDonnell, P. Tang, C. Knight, E. McKay, S.P. Butler, A. Sivarajah, R.
1858 Quinn, L. Fincher, E. Browne, L.Y. Yeo, and H.-K. Chan, *International Journal of*
1859 *Pharmaceutics* **580**, 119196 (2020).

1860 ²⁴³ K.M. Ang, L.Y. Yeo, Y.M. Hung, and M.K. Tan, *Lab Chip* **16**, 3503 (2016).

1861 ²⁴⁴ K.M. Ang, L.Y. Yeo, J.R. Friend, Y.M. Hung, and M.K. Tan, *Journal of Aerosol Science*
1862 **79**, 48 (2015).

1863 ²⁴⁵ C. Westerhausen, L.G. Schnitzler, D. Wendel, R. Krzysztóń, U. Lächelt, E. Wagner, J.O.
1864 Rädler, and A. Wixforth, *Micromachines (Basel)* **7**, (2016).

1865 ²⁴⁶ A.M. Gracioso Martins, N.R. Glass, S. Harrison, A.R. Rezk, N.A. Porter, P.D. Carpenter,
1866 J. Du Plessis, J.R. Friend, and L.Y. Yeo, *Anal. Chem.* **86**, 10812 (2014).

1867 ²⁴⁷ G. Greco, M. Agostini, R. Shilton, M. Travagliati, G. Signore, and M. Cecchini, *Sensors*
1868 (Basel) **17**, (2017).

1869 ²⁴⁸ R.J. Shilton, L.Y. Yeo, and J.R. Friend, *Sensors and Actuators B: Chemical* **160**, 1565
1870 (2011).

1871 ²⁴⁹ H. Ahmed, J. Park, G. Destgeer, M. Afzal, and H.J. Sung, *Appl. Phys. Lett.* **114**, 043702
1872 (2019).

1873 ²⁵⁰ T.-T. Wu and I.-H. Chang, *Journal of Applied Physics* **98**, 024903 (2005).

1874 ²⁵¹ J.K. Luo, Y.Q. Fu, Y. Li, X.Y. Du, A.J. Flewitt, A.J. Walton, and W.I. Milne, *Journal of*
1875 *Micromechanics and Microengineering* **19**, 054001 (2009).

1876 ²⁵² Q. Zeng, F. Guo, L. Yao, H.W. Zhu, L. Zheng, Z.X. Guo, W. Liu, Y. Chen, S.S. Guo, and
1877 X.Z. Zhao, *Sensors and Actuators B: Chemical* **160**, 1552 (2011).

1878 ²⁵³ D. Ahmed, X. Mao, J. Shi, B.K. Juluri, and T.J. Huang, *Lab Chip* **9**, 2738 (2009).

1879 ²⁵⁴ D. Ahmed, C.Y. Chan, S.-C.S. Lin, H.S. Muddana, N. Nama, S.J. Benkovic, and T.J.
1880 Huang, *Lab Chip* **13**, 328 (2013).

1881 ²⁵⁵ S. Orbay, A. Ozcelik, J. Lata, M. Kaynak, M. Wu, and T.J. Huang, *J Micromech*
1882 *Microeng* **27**, 015008 (2017).

1883 ²⁵⁶ A. Ozcelik, D. Ahmed, Y. Xie, N. Nama, Z. Qu, A.A. Nawaz, and T.J. Huang, *Anal.*
1884 *Chem.* **86**, 5083 (2014).

1885 ²⁵⁷ N.F. Läubli, M.S. Gerlt, A. Wüthrich, R.T.M. Lewis, N. Shamsudhin, U. Kutay, D.
1886 Ahmed, J. Dual, and B.J. Nelson, *Anal. Chem.* **93**, 9760 (2021).

1887 ²⁵⁸ M. Ovchinnikov, J. Zhou, and S. Yalamanchili, *The Journal of the Acoustical Society of*
1888 *America* **136**, 22 (2014).

1889 ²⁵⁹ S.A. Endaylalu and W.-H. Tien, *Biomicrofluidics* **15**, 034102 (2021).

1890 ²⁶⁰ A. Doinikov, M. Gerlt, A. Pavlic, and J. Dual, *Microfluidics and Nanofluidics* **24**, 32
1891 (2020).

1892 ²⁶¹ N. Nama, P.-H. Huang, T.J. Huang, and F. Costanzo, *Biomicrofluidics* **10**, 024124 (2016).

1893 ²⁶² N. Nama, P.-H. Huang, T.J. Huang, and F. Costanzo, *Lab Chip* **14**, 2824 (2014).

1894 ²⁶³ C. Zhang, X. Guo, P. Brunet, M. Costalonga, and L. Royon, *Microfluid Nanofluid* **23**, 104
1895 (2019).

1896 ²⁶⁴ J. Boss and W. Poland, *Bulk Solids Handl* **6**, 1207 (1986).

1897 ²⁶⁵ P.-H. Huang, Y. Xie, D. Ahmed, J. Rufo, N. Nama, Y. Chen, C.Y. Chan, and T.J. Huang,
1898 *Lab on a Chip* **13**, 3847 (2013).

1899 ²⁶⁶ C. Zhang, X. Guo, L. Royon, and P. Brunet, *Phys Rev E* **102**, 043110 (2020).

1900 ²⁶⁷ S. Zhao, W. He, Z. Ma, P. Liu, P.-H. Huang, H. Bachman, L. Wang, S. Yang, Z. Tian, Z.
1901 Wang, Y. Gu, Z. Xie, and T.J. Huang, *Lab Chip* **19**, 941 (2019).

1902 ²⁶⁸ Z. Wang, P.-H. Huang, C. Chen, H. Bachman, S. Zhao, S. Yang, and T.J. Huang, *Lab*
1903 *Chip* **19**, 4021 (2019).

1904 ²⁶⁹ P.-H. Huang, N. Nama, Z. Mao, P. Li, J. Rufo, Y. Chen, Y. Xie, C.-H. Wei, L. Wang, and
1905 T.J. Huang, *Lab Chip* **14**, 4319 (2014).

1906 ²⁷⁰ A. Ozcelik, N. Nama, P.-H. Huang, M. Kaynak, M.R. McReynolds, W. Hanna-Rose, and
1907 T.J. Huang, *Small* **12**, 5120 (2016).

1908 ²⁷¹ L. Feng, B. Song, D. Zhang, Y. Jiang, and F. Arai, *Micromachines (Basel)* **9**, 596 (2018).

1909 ²⁷² L. Sun, T. Lehnert, M.A.M. Gijs, and S. Li, *Lab Chip* **22**, 4224 (2022).

1910 ²⁷³ L. Lin, H. Dang, R. Zhu, Y. Liu, and H. You, *Micromachines* **13**, 1439 (2022).

1911 ²⁷⁴ M. Zhou, D. Gao, Z. Yang, C. Zhou, Y. Tan, W. Wang, and Y. Jiang, *Talanta* **222**, 121480
1912 (2021).
1913 ²⁷⁵ T. Hayakawa, S. Sakuma, and F. Arai, *Microsyst Nanoeng* **1**, 1 (2015).
1914 ²⁷⁶ T. Hayakawa, S. Sakuma, T. Fukuhara, Y. Yokoyama, and F. Arai, *Micromachines* **5**, 681
1915 (2014).
1916 ²⁷⁷ X. Lu, A. Martin, F. Soto, P. Angsantikul, J. Li, C. Chen, Y. Liang, J. Hu, L. Zhang, and J.
1917 Wang, *Advanced Materials Technologies* **4**, 1800374 (2019).
1918 ²⁷⁸ H. Shen, K. Zhao, Z. Wang, X. Xu, J. Lu, W. Liu, and X. Lu, *Micromachines* **10**, 882
1919 (2019).
1920 ²⁷⁹ J. Nam and C.S. Lim, *Sensors and Actuators B: Chemical* **255**, 3434 (2018).
1921 ²⁸⁰ J. Nam, W.S. Jang, and C.S. Lim, *Sensors and Actuators B: Chemical* **258**, 991 (2018).
1922 ²⁸¹ M.S. Brugger, K. Baumgartner, S.C.F. Mauritz, S.C. Gerlach, F. Röder, C. Schlosser, R.
1923 Fluhner, A. Wixforth, and C. Westerhausen, *Proc Natl Acad Sci USA* **117**, 31603 (2020).
1924 ²⁸² D. Liao, F. Li, D. Lu, and P. Zhong, *Biochemical and Biophysical Research*
1925 *Communications* **518**, 541 (2019).
1926 ²⁸³ S. Ramesan, A.R. Rezk, P.M. Cevaal, C. Cortez-Jugo, J. Symons, and L.Y. Yeo, *ACS*
1927 *Appl. Bio Mater.* **4**, 2781 (2021).
1928 ²⁸⁴ M. Wu, C. Chen, Z. Wang, H. Bachman, Y. Ouyang, P.-H. Huang, Y. Sadovsky, and T.
1929 Jun Huang, *Lab on a Chip* **19**, 1174 (2019).
1930 ²⁸⁵ Z. Wang, H. Wang, R. Becker, J. Rufo, S. Yang, B.E. Mace, M. Wu, J. Zou, D.T.
1931 Laskowitz, and T.J. Huang, *Microsyst Nanoeng* **7**, 1 (2021).
1932 ²⁸⁶ P. Li, Z. Mao, Z. Peng, L. Zhou, Y. Chen, P.-H. Huang, C.I. Truica, J.J. Drabick, W.S. El-
1933 Deiry, M. Dao, S. Suresh, and T.J. Huang, *Proc Natl Acad Sci U S A* **112**, 4970 (2015).
1934 ²⁸⁷ R. Altay, M.K. Yapici, and A. Koşar, *Biosensors* **12**, 171 (2022).
1935 ²⁸⁸ K. Wang, W. Zhou, Z. Lin, F. Cai, F. Li, J. Wu, L. Meng, L. Niu, and H. Zheng, *Sensors*
1936 *and Actuators, B: Chemical* **258**, 1174 (2018).
1937 ²⁸⁹ J.W. Ng, C. Devendran, and A. Neild, *Lab Chip* **17**, (2017).
1938 ²⁹⁰ D.J. Collins, Z. Ma, and Y. Ai, *Anal. Chem.* **88**, 5513 (2016).
1939 ²⁹¹ D.J. Collins, B.L. Khoo, Z. Ma, A. Winkler, R. Weser, H. Schmidt, J. Han, and Y. Ai, *Lab*
1940 *Chip* **17**, 1769 (2017).
1941 ²⁹² Y. Zhou, Z. Ma, and Y. Ai, *RSC Adv.* **9**, 31186 (2019).
1942 ²⁹³ N.R. Glass, R.J. Shilton, P.P.Y. Chan, J.R. Friend, and L.Y. Yeo, *Small* **8**, 1881 (2012).
1943 ²⁹⁴ M.K. Tan, A. Siddiqi, and L.Y. Yeo, *Sci Rep* **7**, (2017).
1944 ²⁹⁵ Y. Wang, H. Pan, D. Mei, C. Xu, and W. Weng, *Lab Chip* **22**, 1149 (2022).
1945 ²⁹⁶ H. Zhu, P. Zhang, Z. Zhong, J. Xia, J. Rich, J. Mai, X. Su, Z. Tian, H. Bachman, J. Rufo,
1946 Y. Gu, P. Kang, K. Chakrabarty, T.P. Witelski, and T.J. Huang, *Science Advances* **7**,
1947 eabc7885 (2021).
1948 ²⁹⁷ J. Li, A. Crivoi, X. Peng, L. Shen, Y. Pu, Z. Fan, and S.A. Cummer, *Commun Phys* **4**, 1
1949 (2021).
1950 ²⁹⁸ J. Park, G. Destgeer, M. Afzal, and H.J. Sung, *Lab Chip* **20**, 3922 (2020).
1951 ²⁹⁹ V. Bussiere, A. Vigne, A. Link, J. McGrath, A. Srivastav, J.-C. Baret, and T. Franke,
1952 *Anal. Chem.* **91**, 13978 (2019).
1953 ³⁰⁰ A. Link, J.S. McGrath, M. Zaimagaoglu, and T. Franke, *Lab Chip* **22**, 193 (2022).
1954 ³⁰¹ P. Zhang, W. Wang, H. Fu, J. Rich, X. Su, H. Bachman, J. Xia, J. Zhang, S. Zhao, J.
1955 Zhou, and T.J. Huang, *Lab Chip* **20**, 4466 (2020).
1956 ³⁰² N. Zhang, A. Horesh, and J. Friend, *Advanced Science* **8**, 2100408 (2021).
1957 ³⁰³ M. Miansari and J.R. Friend, *Advanced Functional Materials* **26**, 7861 (2016).
1958 ³⁰⁴ C. Bai, C. Wang, T. Zheng, and Q. Hu, *CrystEngComm* **20**, 1245 (2018).
1959 ³⁰⁵ J.L. Han, H. Hu, Q.Y. Huang, and Y.L. Lei, *Sensors and Actuators A: Physical* **326**,
1960 112731 (2021).

1961 ³⁰⁶ G. Celik Cogal, P.K. Das, G. Yurdabak Karaca, V.R. Bhethanabotla, and A. Uygun
1962 Oksuz, *ACS Appl. Bio Mater.* **4**, 7932 (2021).
1963 ³⁰⁷ S. Li, F. Ma, H. Bachman, C.E. Cameron, X. Zeng, and T.J. Huang, *J. Micromech.*
1964 *Microeng.* **27**, 015031 (2016).
1965 ³⁰⁸ S. Yang, Z. Tian, Z. Wang, J. Rufo, P. Li, J. Mai, J. Xia, H. Bachman, P.-H. Huang, M.
1966 Wu, C. Chen, L.P. Lee, and T.J. Huang, *Nat. Mater.* **21**, 540 (2022).
1967 ³⁰⁹ D.J. Collins, B. Morahan, J. Garcia-Bustos, C. Doerig, M. Plebanski, and A. Neild, *Nat*
1968 *Commun* **6**, 8686 (2015).
1969 ³¹⁰ C. Xu, C. Wang, T. Zheng, Q. Hu, and C. Bai, *CrystEngComm* **20**, 7275 (2018).
1970 ³¹¹ Z. Tengfei, W. Chaohui, M. Baogang, and J. Zhuangde, *CrystEngComm* **18**, 6784 (2016).
1971 ³¹² G. Greco, M. Agostini, I. Tonazzini, D. Sallemi, S. Barone, and M. Cecchini, *Anal. Chem.*
1972 **90**, 7450 (2018).
1973 ³¹³ S. Sreejith, R. Kishor, A. Abbas, R. Thomas, T. Yeo, V.D. Ranjan, R. Vaidyanathan, Y.P.
1974 Seah, B. Xing, Z. Wang, L. Zeng, Y. Zheng, and C.T. Lim, *ACS Applied Materials &*
1975 *Interfaces* (2019).
1976 ³¹⁴ Y. Lei, H. Hu, J. Chen, and P. Zhang, *Actuators* **9**, 5 (2020).
1977 ³¹⁵ D. Sun, K. F. Böhringer, M. Sorensen, E. Nilsson, J. Scott Edgar, and D. R. Goodlett, *Lab*
1978 *on a Chip* **20**, 3269 (2020).
1979 ³¹⁶ J.-C. Hsu and Y.-D. Lin, *Sensors and Actuators A: Physical* **300**, 111651 (2019).
1980 ³¹⁷ F. Wu, M.H. Shen, J. Yang, H. Wang, R. Mikhaylov, A. Clayton, X. Qin, C. Sun, Z. Xie,
1981 M. Cai, J. Wei, D. Liang, F. Yuan, Z. Wu, Y.Q. (Richard) Fu, Z. Yang, X. Sun, L. Tian, and
1982 X. Yang, *IEEE Electron Device Letters* **PP**, 1 (2021).
1983 ³¹⁸ J. Nam, H. Lim, C. Kim, J. Yoon Kang, and S. Shin, *Biomicrofluidics* **6**, 024120 (2012).
1984 ³¹⁹ X. Ding, S.-C.S. Lin, M.I. Lapsley, S. Li, X. Guo, C.Y. Chan, I.-K. Chiang, L. Wang, J.P.
1985 McCoy, and T.J. Huang, *Lab Chip* **12**, 4228 (2012).
1986 ³²⁰ A. Shamloo and M. Boodaghi, *Ultrasonics* **84**, 234 (2018).
1987 ³²¹ S. Li, X. Ding, Z. Mao, Y. Chen, N. Nama, F. Guo, P. Li, L. Wang, C.E. Cameron, and
1988 T.J. Huang, *Lab Chip* **15**, 331 (2015).
1989 ³²² M. Wu, Y. Ouyang, Z. Wang, R. Zhang, P.-H. Huang, C. Chen, H. Li, P. Li, D. Quinn, M.
1990 Dao, S. Suresh, Y. Sadovsky, and T.J. Huang, *Proc Natl Acad Sci U S A* **114**, 10584 (2017).
1991 ³²³ M.C. Jo and R. Guldiken, *Sensors and Actuators A: Physical* **207**, 39 (2014).
1992 ³²⁴ G. Simon, M.A.B. Andrade, J. Reboud, J. Marques-Hueso, M.P.Y. Desmulliez, J.M.
1993 Cooper, M.O. Riehle, and A.L. Bernassau, *Biomicrofluidics* **11**, 054115 (2017).
1994 ³²⁵ J. Lee, C. Rhyou, B. Kang, and H. Lee, *J. Phys. D: Appl. Phys.* **50**, 165401 (2017).
1995 ³²⁶ C. Mu, Z. Zhang, M. Lin, Z. Dai, and X. Cao, *Sensors and Actuators B: Chemical* **215**, 77
1996 (2015).
1997 ³²⁷ M.C. Jo and R. Guldiken, in *2011 Annual International Conference of the IEEE*
1998 *Engineering in Medicine and Biology Society* (2011), pp. 7691–7694.
1999 ³²⁸ M.C. Jo and R. Guldiken, *Sensors and Actuators A: Physical* **187**, 22 (2012).
2000 ³²⁹ J.-C. Hsu, C.-H. Hsu, and Y.-W. Huang, *Micromachines* **10**, 52 (2019).
2001 ³³⁰ L. Ren, S. Yang, P. Zhang, Z. Qu, Z. Mao, P.-H. Huang, Y. Chen, M. Wu, L. Wang, P. Li,
2002 and T.J. Huang, *Small* **14**, 1801996 (2018).
2003 ³³¹ D.J. Collins, C. Devendran, Z. Ma, J.W. Ng, A. Neild, and Y. Ai, *Sci Adv* **2**, e1600089
2004 (2016).
2005 ³³² G. Feng, L. Peng, B.F. Jarrod, M. Zhangming, Z. Hong, L. Sixing, N. Nitesh, R.F. James,
2006 J.B. Stephen, and H. Tony Jun, *Proceedings of the National Academy of Sciences* **112**, 43
2007 (2015).
2008 ³³³ C. Devendran, N.R. Gunasekara, D.J. Collins, and A. Neild, *RSC Adv.* **6**, 5856 (2016).
2009 ³³⁴ T. Zheng, C. Wang, C. Xu, Q. Hu, and S. Wei, *Sensors and Actuators A: Physical* **284**,
2010 168 (2018).

2011 ³³⁵ S.M. Naseer, A. Manbachi, M. Samandari, P. Walch, Y. Gao, Y.S. Zhang, F. Davoudi, W.
2012 Wang, K. Abrinia, J.M. Cooper, A. Khademhosseini, and S.R. Shin, *Biofabrication* **9**, 015020
2013 (2017).
2014 ³³⁶ T.D. Nguyen, V.T. Tran, Y.Q. Fu, and H. Du, *Appl. Phys. Lett.* **112**, 213507 (2018).
2015 ³³⁷ B. Chen, Y. Wu, Z. Ao, H. Cai, A. Nunez, Y. Liu, J. Foley, K. Nephew, X. Lu, and F.
2016 Guo, *Lab Chip* **19**, 1755 (2019).
2017 ³³⁸ K. Chen, M. Wu, F. Guo, P. Li, C.Y. Chan, Z. Mao, S. Li, L. Ren, R. Zhang, and T.J.
2018 Huang, *Lab Chip* **16**, 2636 (2016).
2019 ³³⁹ X. Tao, T.D. Nguyen, H. Jin, R. Tao, J. Luo, X. Yang, H. Torun, J. Zhou, S. Huang, L.
2020 Shi, D. Gibson, M. Cooke, H. Du, S. Dong, J. Luo, and Y. Fu, *Sensors and Actuators B:*
2021 *Chemical* **299**, (2019).
2022 ³⁴⁰ F. Guo, Z. Mao, Y. Chen, Z. Xie, J.P. Lata, P. Li, L. Ren, J. Liu, J. Yang, M. Dao, S.
2023 Suresh, and T.J. Huang, *PNAS* **113**, 1522 (2016).
2024 ³⁴¹ I. Bernard, A.A. Doinikov, P. Marmottant, D. Rabaud, C. Poulain, and P. Thibault, *Lab*
2025 *Chip* **17**, 2470 (2017).
2026 ³⁴² M.C. Jo and R. Guldiken, *Sensors and Actuators A: Physical* **196**, 1 (2013).
2027 ³⁴³ Y. Sripitkiat and Y. Zhou, *Sensors* **17**, 106 (2017).
2028 ³⁴⁴ A. Zhang and Y. Zha, *J Sep Sci* **36**, 1085 (2013).
2029 ³⁴⁵ A.-L. Zhang and Y. Zha, *Chemical Engineering and Processing: Process Intensification*
2030 **62**, 145 (2012).
2031 ³⁴⁶ G. Destgeer and H.J. Sung, *Lab Chip* **15**, 2722 (2015).
2032 ³⁴⁷ A.G. Guex, N. Di Marzio, D. Eglin, M. Alini, and T. Serra, *Materials Today Bio* **10**,
2033 100110 (2021).
2034 ³⁴⁸ Y. Li, S. Cai, H. Shen, Y. Chen, Z. Ge, and W. Yang, *Biomicrofluidics* **16**, 031502
2035 (2022).
2036 ³⁴⁹ J. Mei, A. Vasan, U. Magaram, K. Takemura, S.H. Chalasani, and J. Friend, *Biomed*
2037 *Microdevices* **24**, 18 (2022).
2038 ³⁵⁰ P. Liu, Z. Tian, N. Hao, H. Bachman, P. Zhang, J. Hu, and T.J. Huang, *Lab Chip* **20**, 3399
2039 (2020).
2040 ³⁵¹ T. Peng, L. Li, M. Zhou, and F. Jiang, *Sensors* **22**, 1269 (2022).
2041 ³⁵² H. Bachman, Y. Gu, J. Rufo, S. Yang, Z. Tian, P.-H. Huang, L. Yu, and T.J. Huang, *Lab*
2042 *Chip* **20**, 1281 (2020).
2043 ³⁵³ P. Liu, Z. Tian, K. Yang, T.D. Naquin, N. Hao, H. Huang, J. Chen, Q. Ma, H. Bachman,
2044 P. Zhang, X. Xu, J. Hu, and T.J. Huang, *Science Advances* **8**, eabm2592 (2022).
2045